Final Technical Report

for

Office of Naval Research

The Jamie Whitten National Center for Physical Acoustics

The University of Mississippi

Final Technical Report

for

Office of Naval Research

Contract
N00014-92-J-1563

titled

NCPA Planning, Organization and Research FY 92

July 1994

NCPA Internal Tracking Number: SBS0794-1

National Center for Physical Acoustics
University of Mississippi
and Mississippi Resource Development Corporation

REPORT DOCUMENTATION PAGE

Form Approved
OMB No. 0704-0188

1. AGENCY USE ONLY (Leave blank)	2. REPORT DATE	3. REPORT TYPE AND DATES COVERED
	25 July 1994	Final Technical 01 Jan 92 - 31 Dec 92

4. TITLE AND SUBTITLE

Final Technical Report FY 92 (NCPA Acoustics Research)

5. FUNDING NUMBERS

N00014-92-J-1563

6. AUTHOR(S)

L.A. Crum, K.E. Gilbert, M.A. Breazeale, F.D. Shields

7. PERFORMING ORGANIZATION NAME(S) AND ADDRESS(ES)

Jamie Whitten National Center for Physical Acoustics
Coliseum Drive
University, MS 38677

8. PERFORMING ORGANIZATION REPORT NUMBER

SBS0725-1

9. SPONSORING/MONITORING AGENCY NAME(S) AND ADDRESS(ES)

Office of Naval Research
ONR 331
800 North Quincy Street
Arlington, VA 22217-5660

10. SPONSORING/MONITORING AGENCY REPORT NUMBER

11. SUPPLEMENTARY NOTES

12a. DISTRIBUTION/AVAILABILITY STATEMENT

Approved for public release: Distribution unlimited

12b. DISTRIBUTION CODE

13. ABSTRACT *(Maximum 200 words)*

This is a final technical report for the Mississippi Resource Development Corporation from the National Center for Physical Acoustics. Details of the individual projects are included in the attached technical narrative. A list of published papers and oral presentations is included.

14. SUBJECT TERMS

Ocean Acoustics, Acoustically Active Surfaces, Propagation Physics, Transducer Development, Graduate Fellowships

15. NUMBER OF PAGES

112

16. PRICE CODE

17. SECURITY CLASSIFICATION OF REPORT	18. SECURITY CLASSIFICATION OF THIS PAGE	19. SECURITY CLASSIFICATION OF ABSTRACT	20. LIMITATION OF ABSTRACT
unclassified	unclassified	unclassified	

TECHNICAL NARRATIVE

SUMMARY

During FY 92, work was performed in five project areas summarized briefly as follows. A more detailed account is provided in subsequent sections.

(a) The Role of Bubbles in Ocean Acoustics. Significant research progress was accomplished in the latest project period. This progress is documented in the format prescribed for reports to the Ocean Acoustics Program at ONR, and is appended. One detailed publication is also attached.

(b) Acoustically Active Surfaces. This research began in 1988 with an effort to develop smart acoustically active coatings using piezorubber and/or PVDF. The work with smart coatings has expanded to include three aspects. First concerns the development of actuators and sensors, especially those for use at low frequencies; the second concerns the study of different control algorithms; and the third involves the study of the coupling between the active surface and the medium. The work in these three areas is discussed in this report.

(c) Propagation Physics. This research addresses the physics of stochastic and deterministic sound propagation and scattering in the ocean. The principal investigator was not at the National Center for Physical Acoustics after January 1, 1992. However, during the first six months of 1992 the continuous-wave part of the research was completed and the results were written and submitted for publication in the Journal of the Acoustical Society of America. A preprint of the article serves here as the final report, as previously agreed in the proposal.

(d) Transducer Development. Most of the year was spent on transducer development and in completing the Ph.D. Dissertation of Dehua Huang; however, some of the time was spent in completing research supported in previous years under Navy Programs. These are included in this final report.

(e) Graduate Fellowships. The fellowship program was developed with the hope that outstanding undergraduates would be identified and attracted to the University of Mississippi for specialization in acoustics at the National Center for Physical Acoustics. We believe that this program has given more visibility to acoustics as a specialization in physics and engineering, and that visibility is in the best interests of the Navy. The report on the success of this program as well as the work of the five students supported during FY 92 follows.

The Role of Bubbles in Ocean Acoustics

The Role of Bubble Clouds in Low Frequency Scattering from the Ocean Surface

Principal Investigator: Lawrence A. Crum

Research Accomplished in 1992:

Significant research progress was accomplished in the latest project period. This progress is documented in the format proscribed for reports to the Ocean Acoustics Program at ONR, and is appended to this communication. One detailed publication is also attached.

Lawrence A. Crum
Ronald A. Roy

Papers Published in Refereed Journals

I. Articles

1. "The underwater sounds of precipitation," L.A. Crum, R.A. Roy and A. Prosperetti, Naval Research Reviews, **XLIV**, 2 (1992).

2. "Sonoluminescence and bubble dynamics for a single, stable, cavitation bubble," D.F. Gaitan, L.A. Crum, C.C. Church and R.A. Roy, J. Acoust. Soc. Am. **91**(6), 3166-3183, 1992.

3. "Low frequency scattering from submerged bubble clouds", R. Roy, W. Carey, M. Nicholas, J. Schindall and L. A. Crum, J. Acoust. Soc. Am. 2993 (1992).

4. "Acoustically forced oscillations of air bubbles in water: Experimental results", R. G. Holt and L. A. Crum, J. Acoust. Soc. Am.,**91**, 1924 (1992).

5. "Collective oscillations of a bubble cloud as a source of underwater ambient noise in the ocean", W. S. Yoon and L. A. Crum, J. Acoust. Soc. Korea, **10**, 47 (1991).

II. Proceedings

1. "Acoustic backscattering from a cylindrical bubble cloud in water", S. W. Yoon, K. J. Park, L. A. Crum and R. A. Roy, Proceedings: Western Pacific Acoustic Conference, IV, 462 (1991).

2. "Low frequency scattering from resonant bubble clouds", R. Roy, W. Carey, M. Nicholas, and L. Crum, Proceedings of 14th ICA, 2, C3-5, Beijing, China, August, (1992).

3. "Underwater acoustic backscatter from a cylindrical bubble cloud", S. W. Yoon, K. J. Park and L. A. Crum, Proceedings of the 14th ICA, **2**, C3-1,Beijing, China, August, (1992).

Lawrence A. Crum
Ronald A. Roy

Papers in Refereed Publications
(cont.)

4. "The acoustic emissions from bubble plumes generated by an impacting water jet", A. Kolaini, C. C. Church, R. A. Roy and L. A. Crum, Proceedings of the 14th ICA, 2, C3-4, Beijing, China, August, (1992)

5. "Enhancement of hydrodynamic flow noise radiation by the regulation of air bubbles in a turbulent water jet", M. S. Korman, R. A. Roy and L. A. Crum, Proceedings of the 14th ICA, 1, B6-1,Beijing, China, August, (1992).

Lawrence A. Crum
Ronald A. Roy

Papers Submitted to Refereed Journals

I. Articles

1. "Low frequency underwater sound generation by an impacting transient cylindrical water jet", A. Kolaini, R. Roy, L. Crum and Mao Yi, J. Acoust. Soc. Am., (submitted for publication).

2. "Bubble production by capillary-gravity waves", A. Kolaini, et al., J. Acoust. Soc. Am. (submitted for publication).

3. "The production of high-frequency ambient noise by capillary waves," R. A. Roy, A. R. Kolaini and L. A. Crum, In Natural Physical Sources of Underwater Sound, ed. by B. Kerman, Kluwer Acad. Pub., Dordrecht, Netherlands, in press.

4. "Collective oscillations in a bubble cloud," S. W. Yoon, K. J. Park, L. A. Crum, M. Nicholas, R. A. Roy, A. Prosperetti and N. Q. Lu, In Natural Physical Sources of Underwater Sound, ed. by B. Kerman, Kluwer Acad. Pub., Dordrecht, Netherlands, in press.

5. "Sound emissions by a laboratory bubble cloud", M. Nicholas, R. Roy, L. Crum, H. Oguz and A. Prosperetti, J. Acoust. Soc. Am., (submitted for publication).

II. Proceedings

1. "Sound scattering from microbubble distributions near the sea surface," W. Carey and R. A. Roy, Proceedings: The SACLANT Ocean Reverberation Symposium, Kluwer Acad., Dordrecht, Netherlands, in press.

2. "Low Frequency resonance backscatter from near-surface bubble clouds", L. A. Crum, J. A. Schindall, R. A. Roy, and W. M. Carey, Proceedings of the SACLANT Conference on Low Frequency Active Sonar (to be published).

Lawrence A. Crum
Ronald A. Roy

Books or Chapters

none

Lawrence A. Crum
Ronald A. Roy

Technical Reports

1. "Lake Seneca Bubble Scattering Quick Look", W. Carey and R. A. Roy, NUWC Tech. Report (in press).

Lawrence A. Crum
Ronald A. Roy

Invited Papers

1. "Low-frequency backscatter from dense submerged bubble clouds," R.A. Roy, W. Carey, M. Nicholas, L.A. Crum and J. Schindall, presented at the special session on *Acoustical Studies of Upper Ocean Processes* at the 123rd meeting of the Acoustical Society of America, Salt Lake City, UT, May, 1992.

2. "Laboratory experiments on bubble cloud oscillations," L.A. Crum, R.A. Roy, M. Nicholas and A. Kolaini, presented at the special session on *Acoustical Studies of Upper Ocean Processes* at the 123rd meeting of the Acoustical Society of America, Salt Lake City, UT, May 1992.

3. "Surface scattering from microbubble distributions near the sear surface," W. M. Carey, R. R. Goodman and R. A. Roy, presented at the SACLANT Ocean Reverberation Symposium, La Spezia, Italy, May 1992.

4. "The acoustic emissions from bubble plumes generated by an impacting transient water jet," A. R. Kolaini, C. C. Church, R. A. Roy and L. A. Crum, presented at the meeting of the 14th ICA, Beijing, China, September 1992.

5. "Low frequency scattering from resonant bubble clouds", R. Roy, W. Carey, M. Nicholas, and L. Crum, presented at the meeting of the 14th ICA, Beijing, China, August, (1992).

Lawrence A. Crum
Ronald A. Roy

Contributed Papers

1. "Air bubble interaction with a submerged axisymmetric water jet," S. M. Cordry, R. A. Roy and L. A. Crum, presented at the 122nd meeting of the Acoustical Society of America, Houston, TX, November, 1991.

2. "Sound velocity measurements in a bubble cloud," S. A. Cheyne and R. A. Roy, presented at the 122nd meeting of the Acoustical Society of America, Houston, TX, November, 1991.

3. "Collective oscillations in fresh and salt water bubble clouds," R. A. Roy, M. Nicholas, K. Markiewicz and L. A. Crum, presented at the 122nd meeting of the Acoustical Society of America, Houston, TX, November, 1991.

4. "Low-frequency acoustic scattering from a submerged bubble cloud," R. A. Roy, L. A. Crum, M. Nicholas, J. Schindall, W. A. Carey, W. A. Konrad, W. J. Marshall, E. C. Monahan and A. Prosperetti, presented at the 122nd meeting of the Acoustical Society of America, Houston, TX, November, 1991.

5. "Collective oscillations of a bubble cloud as a source of underwater ambient noise in the ocean," R. A. Roy, S. W. Yoon, M. Nicholas, K. J. Park and L. A. Crum, presented at Internoise 91, Sydney, Australia, November, 1991.

6. "Acoustic backscattering from a cylindrical bubble cloud in water," S. W. Yoon, K. J. Park, L. A. Crum, and R. A. Roy, presented at the Western Pacific Acoustic Conference IV, Sydney, Australia, November, 1991.

7. "A laboratory experiment on nonlinear coupling between surface and volume modes of a bubble," Y. Mao, L. A. Crum and R. A. Roy, presented at the 123nd meeting of the Acoustical Society of America, Salt Lake City, UT, May 1992.

Contributed Papers
(cont)

8. "Enhancement of hydrodynamic flow noise radiation by the regulation of air bubbles in a turbulent flow," M. S. Korman, R. A. Roy and L. A. Crum, presented at the 123nd meeting of the Acoustical Society of America, Salt Lake City, UT, May 1992.

9. "Acoustic emissions from toroidal bubbles", A. Kolaini, M. Nicholas and L. A. Crum, presented at the 123rd meeting of the Acoustical Society of America, Salt Lake City, UT, May, 1992.

10. "Acoustic characteristics of laboratory breaking waves", A. R. Kolaini and L. A. Crum, presented at the 124th meeting of the Acoustical Society of America, New Orleans, LA, October, 1992.

11. "Sound scattering from near-surface bubble clouds," J. Schindall, W. M. Carey, R. A. Roy, L. A. Crum and M. Nicholas, presented at the 124th meeting of the Acoustical Society of America, New Orleans, LA, October 1992.

12. "Acoustic phase velocity measurements in a bubbly liquid using a fiber optic laser Doppler velocimeter," S.A. Cheyne, C.T. Stebbings and R.A. Roy, presented at the 124th meeting of the Acoustical Society of America, New Orleans, LA, October 1992.

Lawrence A. Crum
Ronald A. Roy

Conferences Attended

1. Acoustical Society of America, Houston, TX, 4-8 November, 1991 (LAC, RAR)

2. Acoustical Society of America, Salt Lake City, UT, 11-15 May, 1992 (LAC, RAR)

3. ONR SRP Status Meeting, Victoria, BC, 19-21 May, 1992 (LAC)

4. SACLANT Symposium on Sea Surface Sound, La Spezia, Italy, 25-29 May, 1992 (LAC, RAR)

5. International Conference on Acoustics, Beijing, China, 7-15 September, 1992 (LAC)

Lawrence A. Crum
Ronald A. Roy

Patents Awarded

none

Lawrence A. Crum
Ronald A. Roy

Patent Applications

none

Lawrence A. Crum
Ronald A. Roy

Honors and Awards

- Ronald A. Roy was elected to Fellowship in the Acoustical Society of America.

- Lawrence A. Crum was awarded a Significant Alumni Achievement Award by Ohio University.

Graduate Students

Name: Christopher Hobbs

Citizenship: USA

Date of Graduation: August, 1992

Type of Thesis: Principally Experimental

Thesis Title: Propagation of Sound through a Bubble Screen

Thesis Objective: To determine the acoustical properties of bubble-filled geometrical shapes: Bubble screens are used in certain applications to "screen" the noise produced by naval vessels from radiating, by introducing a barrier that is nearly impenetrable to sound propagation. We determined that the screen itself may resonant, however, through the collective oscillations of the bubbles contained within the screen.

Name: Kenneth Markiewicz

Citizenship: USA

Date of Graduation: August, 1992

Type of Thesis: Principally experimental

Thesis Title: Collective Oscillations of Bubble Columns and Screens

Thesis Objective: To determine the collective-oscillation frequencies of specified geometries of bubble columns and screens: Clouds of bubbles can resonate at frequencies characteristic of the geometrical shape and acoustic properties of the cloud, which reduce the natural frequencies to values much below that of the individual bubble resonances. Mr. Schindall will study this problem and its application to surface scattering.

Name: Jeffrey Schindall

Citizenship: USA

Estimated Date of Graduation: May, 1995

Type of Thesis: Both experimental and theoretical

Thesis Title: Scattering from Bubble Clouds

Thesis Objective: To determine the scattering characteristics of bubble clouds: It has been demonstrated that bubble clouds can resonate at frequencies that are associated with their collective modes. These frequencies can be quite low and depend upon the total volume of air in the cloud and the geometrical shape. Thus, these objects can act as false target or be employed as decoys or for calibration of active sonars.

Graduate Students
(cont.)

Name: Yi Mao

Citizenship: PRC

Estimated Date of Graduation: August, 1993

Type of Thesis: Both theoretical and experimental

Thesis Title: Free oscillations of Gas Bubbles in Liquids

Thesis Objective: To determine the acoustical properties of gas bubbles at reduced pressures and elevated temperatures: It has been proposed that the surface waves on bubbles could nonlinearly couple into volume oscillations, thus converting a nonradiating energy source into a radiating one. This research is investigating the conditions under which this process is upheld.

Name: Sean Cordry

Citizenship: USA

Estimated Date of Graduation: May, 1994

Type of Thesis: Both theoretical and experimental

Thesis Title: Noise production by Bubble Fission and Fusion.

Thesis Objective: To determine the conditions under which bubbles coalesce and break up, and the noise emissions associated with this behavior. When bubbles are created in the ocean, they emit sound, and thus contribute to the ambient background; it is thought that adult bubbles are relatively silent. However, if the total energy of a bubble is changed by bubble fission or fusion, then they can radiate this additional energy. The conditions under which adult bubbles become noise are being examined.

Postgraduate Students

Name: Michael Nicholas

Citizenship: USA

Status: Completed project; now employed at NRL

Work Objective: To undertake a systematic study of collective oscillations of bubble clouds: The concept of collective oscillations of bubble clouds was not demonstrated until 1988, and has been examined principally since that time through the work of Dr. Nicholas.

Name: Ali Kolaini

Citizenship: Iran (currently has green card, and will soon be permanent resident)

Status: Completed project; now employed as a research scientist at NCPA

Work Objective: To undertake a systematic study of the noise produced by breaking waves. Dr. Kolaini supervised the construction of a unique laboratory facility in which breaking waves can be produced in an anechoic tank. His research has lead to a much more complete understanding of this important phenomenon.

Lawrence A. Crum
Ronald A. Roy

Transitions

1. Dr. William Carey, DARPA, (703) 696-2339: Dr. Carey has expressed an interest in applying the results of our studies of bubble cloud scattering to more applied projects involving the development of decoys and calibrated targets. An SBIR has been issued by DARPA and we are collaborating with Quest Integrated, Inc., to develop these decoys and targets.

2. Mr. Tom Warfield, ONT, (703) 696-5121; Mr. Warfield, a Program Manager at ONT, is planning to fund us to work with NRL to extend our scattering measurements of bubble clouds to a more general understanding of low frequency acoustic scattering from the sea surface. We will be working with Dr. Fred Erskine (202) 767-3149 and others in the NRL group to undertake these experiments in Exuma Sound later in 1993.

3. Dr. Maurice Sevik, DTRC, (410) 227-1335; Dr. Sevik, an Associate Director at David Taylor has expressed a keen interest in our studies of transmission through bubble screens. This facility pioneered the concept of bubble maskers and are interested in our discoveries of the low frequency emissions that might occur for these screens--due to collective oscillations. We are preparing a proposal for their consideration.

4. Dr. Michael Nicholas, NRL, (202) 767-3149; Dr. Nicholas was a Postdoctoral Research Associate under our direction and is now employed in the Underwater Acoustics Branch of NRL. He will be assisting in the analysis of the CST data and will likely transition insight gained in our laboratory from basic research studies relating to bubble cloud scattering directly to his more applied work at NRL.

5. Dr. Paul Hwang, Quest Integrated, Inc., (206) 872-9500; Dr. Hwang collaborated with us in the preparation of a SBIR proposal to DARPA in which calibrated acoustical targets and decoys are to be developed based on the theory of the collective oscillations of bubble clouds. Later phases of this work, if funded, will involve the construction of these targets for use in the fleet. This particular project demonstrates graphically how ideas and concepts developed in 6.1 research can be transitioned directly into the fleet within a very short time.

LOW FREQUENCY RESONANCE BACKSCATTER FROM NEAR-SURFACE BUBBLE CLOUDS

L. A. Crum, J. A. Schindall, and R. A. Roy
Applied Physics Laboratory
University of Washington, Seattle WA 98105 USA
and
W. M. Carey
Advanced Research Projects Agency
3701 N. Fairfax Drive
Arlington, VA 22203-1714 USA

Abstract

When active sonar systems are used to insonate the sea surface, anomalous scattering is observed in the form of enhanced backscatter, and more importantly, in the form of discrete, bright echoes. The most plausible explanation for these effects is the increased scattering resulting from the presence of bubble plumes and clouds, produced near the surface by breaking waves. This paper describes some preliminary calculations of the backscattered target strengths expected on the basis of resonance scattering from bubble clouds.

I. Introduction

In tests of low frequency active sonar systems, false targets have arisen when insonation of the sea surface is attempted, especially in circumstances of high sea state [Gauss *et al.*, 1992]. The origin of these false targets is still unclear, although the most likely candidates are assemblages of gas bubbles in an acoustically compact form. Bubble clouds are a common occurrence in the near surface of the ocean when breaking waves are present; these clouds are likely to result from bubble entrainment during wave breaking. Collections of bubbles in diffuse concentrations in the form of plumes have been observed at depths of several meters [Monahan, 1971; Thorpe, 1982; Farmer and Vagle, 1988], presumably drawn to these depths as a result of convective flows such as Langmuir circulation and thermal mixing [Thorpe, 1982]. Significant acoustic backscattering from the sea surface can result either from these small, relatively dense clouds that are near the surface, or from the larger, relatively diffuse plumes that can extend to greater depths.

It has been shown that the available surface scattering data [Chapman-Harris, 1962; Ogden and Erskine, 1992] can be accounted for in terms of either weak scattering (the well-known Born Approximation) from deep, diffuse bubble plumes generated by Langmuir circulation [MacDonald, 1991; Henyey, 1991], or by resonance scattering from higher void fraction clouds near the surface [Prosperetti and Sarkar, 1992]; it is the contention in this paper that the observed large target strength false echoes result principally from detatched bubble clouds; furthermore, we present in this paper the range of bubble cloud and environmental parameters that are likely to result in these bright targets.

2. Background

The attempts to characterize acoustic scattering from the ocean surface in the absence of bubble clouds, due to Bragg Scattering alone, have resulted in significant disagreement between the calculations [McDaniel, 1987] and the experimental data [Chapman and Harris, 1962; Ogden and Erskine, 1992]. Consequently, MacDonald [1991] and Henyey [1991] have used weak scattering theory (Born approximation) to obtain the surface backscatter in the presence of "tenuous" (void fractions less than, say, 10^{-3} %) bubble plumes of various configurations and orientations. Their calculations assume that the clouds are sufficiently diffuse so that multiple scattering can be ignored; consequently, the scattered sound energy is mostly specular. Their results indicate that if one wishes only to account for the average surface backscatter, then the tenuous bubble plumes generated by Langmuir circulation are sufficient. However, it is not yet clear whether these approaches can account for the presence of the "bright echoes" or "hot spots" observed in the critical sea tests and described by Gauss *et al.*, [1992]. Thorsos [1992] has examined the effect of a rough surface and noted that focusing from appropriate contours can significantly enhance the calculated backscatter from tenuous clouds. However, we shall follow a different approach and assume that there are concentrations of bubbles in the form of clouds that are of sufficient void fraction to lead to a resonance oscillation of the cloud itself, thus resulting in high target strengths at low frequencies.

These cloud oscillations are called "collective oscillations" and represent a type of acoustic backscatter that is fundamentally different from that described by Born-approximation, weak-scattering theory. Collective effects occur when the acoustic wavelength is considerably larger than the dimensions of the cloud and the resonance frequency of the individual bubbles comprising the cloud is much higher than the insonation frequency; thus, all the bubbles oscillate essentially in phase. Because the compressibility of the cloud is similar to that for a single gas bubble while the induced mass is associated with that of the entire cloud, the oscillation frequency can be quite low, and particularly, much lower than that of an individual gas bubble. An alternative but equivalent explanation is that because the phase speed in the bubbly mixture is greatly reduced (sometimes even below that for a pure gas), the oscillation frequency is correspondingly reduced.

2.1 Collective Oscillations

Carey and Browning, [1988] and Prosperetti [1988] independently suggested that bubble clouds whose geometrical dimensions were small with respect to a wavelength could behave as a compact scatterers. Evidence for the existence of collective oscillations have been firmly established by laboratory work [Yoon, *et al.*, 1991; Nicholas, *et al.*, 1992; Lu, *et al.*, 1991], and also by field experiments in a large fresh water lake [Roy, et al., 1992]. Furthermore, recent data by Farmer and Ding, [1992] on sources of ambient noise in the ocean provide strong support for the existence of low frequency emissions indicative of collective oscillations. If these clouds are observed to radiate at low frequencies by collective effects then it is likely that they would also act as effective scatterers of low frequency sound.

2.2 Preliminary Results

We have performed some preliminary experiments of the low frequency scattering characteristics of bubble clouds. The test plan and some initial results are described in a previous SACLANT Symposium report [Carey and Roy, 1993], and in a more widely distributed publication [Roy, et al., 1992]; they are shown for completeness in Fig. 1.

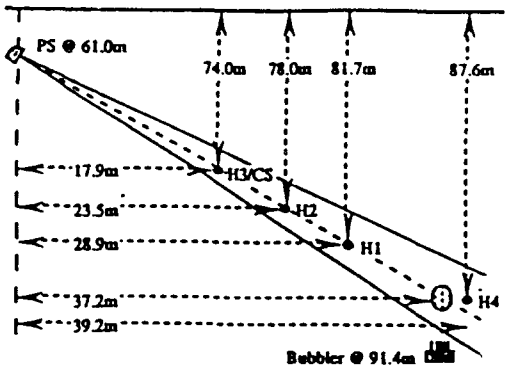

Fig. 1a. Test Plan for Seneca Lake scattering experiment.

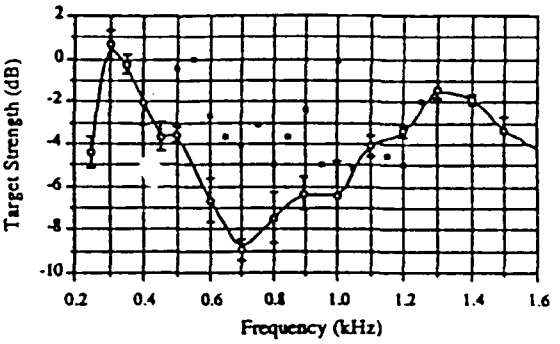

Fig. 1b. Low-frequency backscattering results.

The principal results of this experimental study can be summarized as follows:

• Artificially generated bubble clouds of ellipsoidal geometry and about 0.5 meter in diameter and 1.0 meter in length were created at a depth of about 90 meters in a fresh water lake. The clouds were insonified with both a directed beam (parametric array) and an omnidirectional conventional source over a frequency range from 200 Hz to approximately 14 kHz.

• Measurements of the target strength (TS) as a function of frequency show relative maxima at approximately 0.3 and 1.3 kHz, as well as several other (higher) frequencies. The amplitude of these peaks is quite large and indicative of resonance effects.

• The resonance frequencies of the individual bubbles comprising the clouds are on the order of 2-3 kHz, and are so much larger than the low frequency maximum that these low frequency peaks are most likely due to collective oscillation resonances. If the cloud is treated as an acoustically compact object with a velocity of sound significantly different than that of water, then the fundamental (monopole) resonance frequency depends solely upon its volume, and its effective acoustic impedance. Using a modified Minnaert formula, a calculated resonance frequency of about 324 Hz can be obtained for the lowest peak; this value compares favorably with the measured resonance of 310 Hz [Roy, et al., 1992; Carey and Roy, 1993].

• The target strength of these clouds insonified near resonance is on the order of 0 db. Thus, they represent bright targets and compact scatterers. Calculations of the target strength based on resonance scattering [Roy, et al., 1992; Carey and Roy, 1993] suggest values on this order.

The success of these preliminary studies has emboldened us to attempt a more systematic and detailed analysis of low frequency resonance scattering from near-surface bubble clouds; our progress along these lines is described in the sections to follow.

3. Approach

We follow the approach of Morse and Ingard [1968] in which we assume a plane wave incident on a compliant sphere of radius a_c surrounded by a continuous medium of density and sound speed ρ and c respectively. Likewise, we consider the sphere to be a homogeneous medium of density and sound speed ρ_ℓ and c_ℓ respectively. (It should be noted that the subscript "ℓ" refers to the bubbly mixture, not the pure liquid.) We shall assume that the target is illuminated by plane waves and that it radiates a spherically outgoing acoustic wave.

We shall also assume that the sphere (bubble cloud) is composed of many bubbles; thus, the medium is dispersive with effective density and wave number given by,

$$\rho_\ell = \beta\rho_{air} + (1-\beta)\rho$$
$$k_\ell^2 = k^2 + \frac{4\pi\omega^2 a\eta}{\omega_o^2 - \omega^2 + 2ib\omega}, \tag{1}$$

where $k = \omega / c$ is the wave number in the liquid, a is the radius of individual bubbles (considered to monodispersed in size), η is the number of bubbles per unit volume, ω_o is the resonance frequency of the bubbles, $\beta = 4\pi\eta a^3 / 3$ is the void fraction, and b is the damping constant [Commander and Prosperetti, 1989; Lu, *et al*, 1990]. For $\omega << \omega_o$, one can show that the real portion of the complex phase speed in the mixture is given by,

$$c_\ell^2 = \frac{\gamma P_\infty}{\frac{\gamma P_\infty}{c^2} + \beta\rho}. \tag{2}$$

Here, γ is the ratio of specific heats of the gas. It should be noted that for β not too small or P_∞ not too large, the low frequency phase speed in Eq. (2) reduces to the more familiar expression,

$$c_\ell = \sqrt{\frac{\gamma P_\infty}{\beta\rho}}. \tag{3}$$

For the scattering problem in an infinite medium we solve the Helmholtz equation subject to the boundary conditions of continuous pressure and normal velocity across the surface of the sphere.

$$\nabla^2 p_\omega + k^2 p_\omega = -f_\omega(\vec{r}). \tag{4}$$

We take the solution to be a superposition of incident plane wave and scattered waves:

$$p_\omega = p_i + p_s \quad \text{where } p_i = \vec{A} e^{-i\vec{k}\cdot\vec{r}}. \tag{5}$$

Morse and Ingard used an integral Green's function method to demonstrate that the solution for the exterior scattered wave in spherical coordinates is represented by an expansion in Legendre polynomials and spherical Hankel functions with appropriate coefficients,

$$p_s(r) = -\frac{1}{2}A\sum_{m=0}^{\infty} i^m(2m+1)(1+R_m)P_m(\cos\theta)h_m(kr)$$
$$\underset{r\to\infty}{\to} i\frac{A}{2k}\frac{e^{ikr}}{r}\sum_{m=0}^{\infty}(2m+1)(1+R_m)P_m(\cos\theta) \tag{6}$$

where the asymptotic form is given in the far field. The coefficient R_m satisfies the boundary conditions and describes the reflectivity of the sphere where,

$(1+R_m) = 2\dfrac{j_m'(ka_c)+i\beta_m j_m(ka_c)}{h_m'(ka_c)+i\beta_m h_m(ka_c)}$, and $\beta_m = i\dfrac{\rho c}{p_\ell c_\ell}\left[\dfrac{j_m'(k_\ell a_c)}{j_m(k_\ell a_c)}\right]$ is the specific

admittance of the surface. In this study we make use of the limiting form of c_ℓ given in Eq. (2) which is not a complex phase speed and hence does not take into account damping from the bubbles within the cloud.

We are primarily interested in the backscattering; hence, we take $\theta = \pi$. In the free-field, the TS is given by [Urick,1967],

$$TS_{ff} = 20\log\left|\frac{p_s}{p_i}\right|_{r=1m} \approx 10\log\left(\frac{I_s}{I_i}\right)_{r=1m} \tag{7}$$

Carey and Roy [1993] have shown that for small ka_c, the monopole term in Eq. (6) can be approximated by

$$\frac{p_s}{p_i} \approx i\frac{k^2a^3}{3r}\frac{\left(1-\frac{\rho c^2}{\rho_\ell c_\ell^2}\right)}{\left(1-\frac{\rho c^2}{\rho_\ell c_\ell^2}\frac{(ka_c)^2}{3}\right)-i\left(\frac{\rho c^2}{\rho_\ell c_\ell^2}\frac{(ka_c)^3}{3}\right)}. \tag{8}$$

At resonance, this leads to

$$\omega_c \approx \frac{1}{a_c}\sqrt{\frac{3\gamma P_\infty}{\beta\rho}}, \tag{9}$$

which is a modified form of Minnaert's equation for bubble resonance.

The above equations allow us to make some observations concerning the interdependence of some of the more important parameters, viz,

- The effective phase speed in the bubbly mixture increases with depth, for a fixed volume fraction β; likewise, for fixed a_c, the resonance frequency of the cloud, ω_c, also increases with depth.

- As β decreases/increases, both ω_c and c_ℓ increases/decreases (other parameters held fixed).

- As a_c decreases/increases, ω_c increases/decreases (other parameters held fixed).

Furthermore, we can also deduce how changes in some of these parameters affect the TS? At resonance, Eq(8) reduces to

$$\left|\frac{p_s}{p_i}\right|_{r=1m} \rightarrow \frac{c}{\omega_c}\left(\frac{\rho_t c_t^2}{\rho c^2} - 1\right). \tag{10}$$

Thus, as the resonance frequency decreases, or the void fraction becomes larger, or the size of the cloud increases, the TS increases.

We now turn to a determination of the TS for a variety of environmental and acoustic conditions. In our calculations, we choose to obtain the resonance frequencies by numerical methods. We will approximate Eq. (6) by truncating the series at the $m=0$ monopole term, since for the frequencies of interest in this paper, the wavelength of sound is many times greater than the bubble cloud radius and the higher order terms do not contribute to the lowest resonance.

To solve the problem of scattering from targets near the ocean surface we make use of the method of images; in Fig 2 below a diagram is shown of our approach.

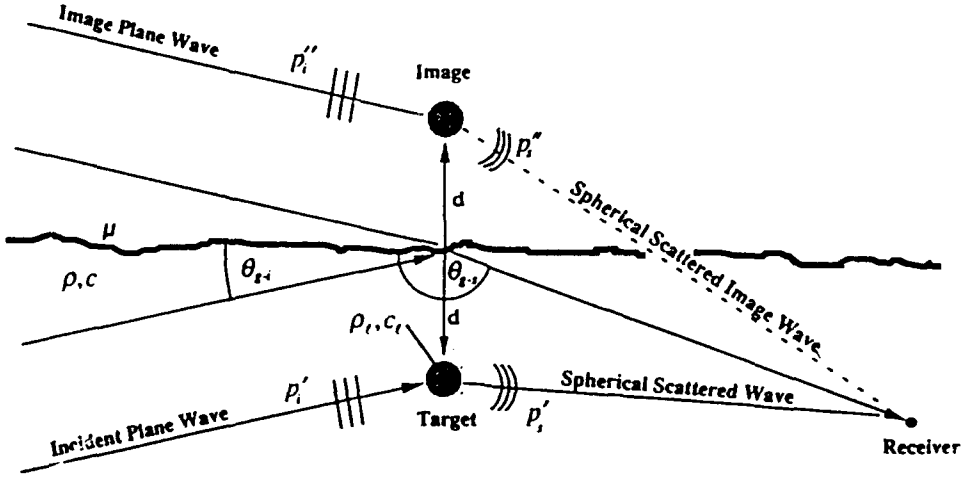

Fig. 2. Diagram of the theoretical model used in the determination of the scattered target strengths.

Here we treat the target as a point scatterer a distance d below a pressure release surface with reflectivity coefficient μ ($-1 < \mu < 0$). The reflection coefficient describes the roughness of the sea surface where $\mu = -1$ corresponds to a smooth pressure release surface and $\mu = 0$ corresponds to an extremely rough surface (effectively equivalent to an infinite medium); realistic sea states fall somewhere in between. Rather than relate μ to the frequency and wave-height, we have chosen to evaluate the TS at fixed values of μ in order to generalize the analysis. Using the method of images one obtains,

$$p_i = p_i' + p_i'' = p_i\left[e^{i(kx\cos\theta_g + kd\sin\theta_g)} + \mu e^{i(kx\cos\theta_g - kd\sin\theta_g)}\right] \tag{11a}$$

$$p_s = p_s' + p_s'' = \frac{p_s}{r}\left[e^{i(kx\cos\theta_g + kd\sin\theta_g)} + \mu e^{i(kx\cos\theta_g - kd\sin\theta_g)}\right], \tag{11b}$$

where θ_g is the surface grazing angle, and p_i and p_s are the magnitudes of the incident and scattered fields in the free-field. The single-primes indicate the fields neglecting the surface, the double-primes denote the image fields, and $|p_s|^2 = |P_i|^2 f^2$ is the response of the cloud to the incident plane wave, where $TS_{ff} = 10\log f^2$ is the target strength computed in a free field. After some algebra, we find that the TS for a bubble cloud near the sea surface is given by

$$TS = 20\log\left|\frac{p_s}{p_i}\right|_{r=1m} = TS_{ff} + 10\log\left\{1 + \mu^2 + 2\mu - 4\mu\sin^2\left(kd\sin\theta_g\right)\right\}^2 . \tag{12}$$

Clearly, when $\mu = 0$ the expression for TS yields the free-field target strength; for $\mu = -1$, and the source close to the surface, phase cancellation occurs, and the source behaves like a dipole.

If one considers the limiting from of Eq. (12), for kd<<1, one observes a dipole characteristic to the scattered field in which the scattered pressure scales with $(d/\lambda)^4 \sin^4\theta$, where λ is the acoustic wavelength. This equation suggests a complex acoustical behavior which can be briefly summarized as follows. High void-fraction clouds which generate significant TS's in the free field may not be acoustically important because these clouds tend to reside near the surface, and thus are subject to the mitigating effect of surface dipole cancellation. This effect is exacerbated by the fact that these large TS clouds tend to resonate at low frequencies (i.e. long wavelengths), and the proximity of the cloud to the surface is defined relative to the acoustic wavelength.

If one considers deeper scatterers, then one is necessarily limited (by oceanographic constraints) to the consideration of lower void-fraction clouds that will not have as pronounced a resonance scattering characteristic. Indeed, clouds in the deepest portion of the bubble layer, (order 10 m) are very tenuous and probably do not resonate at all. It seems likely that there are optimum combinations of cloud depth, cloud characteristics and frequency that produces significant backscatter target strengths (larger than, say -10 db). In the next section, using the equations determined above, we have explored a variety of conditions that could give rise to significant scattering TS's.

4. Results

We have generated a series of multidimensional figures to display the calculated target strengths of these bubble assemblages as a function of several relevant parameters. These figures are quite complex and require studious attention in order to fully grasp the principal implications of the data. The parameters shown in these figures with brief comments where appropriate are as follows: TS--the target strength, defined as in Eq. 12 above; β--the void fraction, defined above; d--the depth of the center of the bubble cloud below the ocean surface; θ_g--the grazing angle of the incident sound beam; a_c--bubble cloud radius; μ--a measure of the reflectivity of the surface: for $\mu = -1$, the surface is perfectly reflecting, for $\mu = 0$, the surface is at infinity and there is no reflection from the surface.

Consider Fig. 3, which is a four-dimensional plot of the target strength as a function of void fraction, cloud depth, and cloud resonance frequency. For this case, the grazing angle is shallow--10°--and the cloud radius is relatively large--0.5 m. We anticipate that this case would correspond to the insonation of a "bubble plume", formed from the convection of entrained gas bubbles to a considerable depth; however, this plume will be treated as a resonant, compact scatterer. We presume that the large bubbles have risen by gravitational forces to the surface, and that consequently the remaining bubbles, and particularly the void fraction, are both relatively small. The data shown in the lower right-hand-corner of Fig. 3 correspond to $\mu = -1$, which presumes a perfectly reflecting surface. Note that there is little scattering for small depths; in this case the cloud acts as a dipole scatterer, and thus for small grazing angles, the TS is very low. However, as the depth increases to a few meters, even for void fractions as low as 10^{-5}, relatively large TS's are observed. For example, at a depth of 5 m, and for a void fraction of 10^{-4}, the observed target strength is on the order of 0 db for an insonation frequency of 300 Hz.

With a value of $\mu = -1$, it is assumed that the surface is perfectly reflecting, a situation unlikely to be realized in a rough sea. The data shown in the upper left hand corner of this figure corresponds to value of $\mu = 0$, or for a surface so rough that no coherent energy is reflected. Note that in this case, there is little depth dependence--no phase cancellation from the reflecting surface--and this cloud is a high TS scatterer for all "depths". Perhaps a more reasonable representation of the surface effect is presented in the lower left-hand-corner, calculated for a value of $\mu = -0.5$, which thus corresponds to the intermediate case. It is seen from this figure, that TS's on the order of 0 db should be observed for plumes with void fractions above 10^{-4}, at depths between 2-6 m, and at insonation frequencies on the order of 300 Hz. As the void fraction falls below 10^{-5}, the backscattered intensity rapidly falls in magnitude.

Let us now compare and contrast these results for a relatively large, low void-fraction plume with the case shown in the next figure. Shown in Fig. 4 are plots for a bubble cloud of radius 0.1 m, and a grazing angle of 10° (as in Fig. 3). Consider again first the case for a perfect reflecting surface, as shown the lower right-hand-corner. This cloud is relatively small; thus, the monopole resonance frequency is rather high (of order 400 Hz near the surface). Consequently, it can produce a large backscattered TS even when it is within a few meters of the surface. Since we can presume that for such a small cloud, it is not unreasonable to expect a large void fraction, we shall consider values of β as high as 10^{-3}. Note that for the surface conditions of $\mu = -1$, TS's of 0 db can be expected only for clouds 3-4 meters below the surface.

Consider next, however, the conditions demonstrated in the upper left-hand-corner, in which the surface condition corresponds to a very rough surface--a more likely occurrence for large void fraction clouds. For this case, TS's of 0 db can be observed at any depth for a range of frequencies near 400 Hz. Again, if the more realistic case of $\mu = -0.5$ is considered (lower left), a TS of 0 db can be expected to occur for a cloud with a void fraction of 10^{-3}, a radius of 0.1 m, a frequency of 400 Hz, and at a depth of about 4 m.

Finally, let us consider Fig. 5, which summarizes the principal features of this report. Our field measurements at Lake Seneca [Roy, et al., 1992; Carey and Roy, 1993] demonstrated that TS's of approximately 0 db could be achieved for resonance oscillations of a bubble cloud, far removed from the surface, with a void fraction of about 10^{-3}, a radius of about 0.25 m and at an insonation frequency of about 300 Hz. Furthermore, Prosperetti and his students [Prosperetti, et al., 1993; Sarkar and Prosperetti, 1993] have demonstrated that bubble clouds of similar size and void fraction, when located very near the surface, could account for the Chapman-Harris, Ogden-Erskine surface acoustic backscatter when

Maximum TS as a function of depth and volume fraction

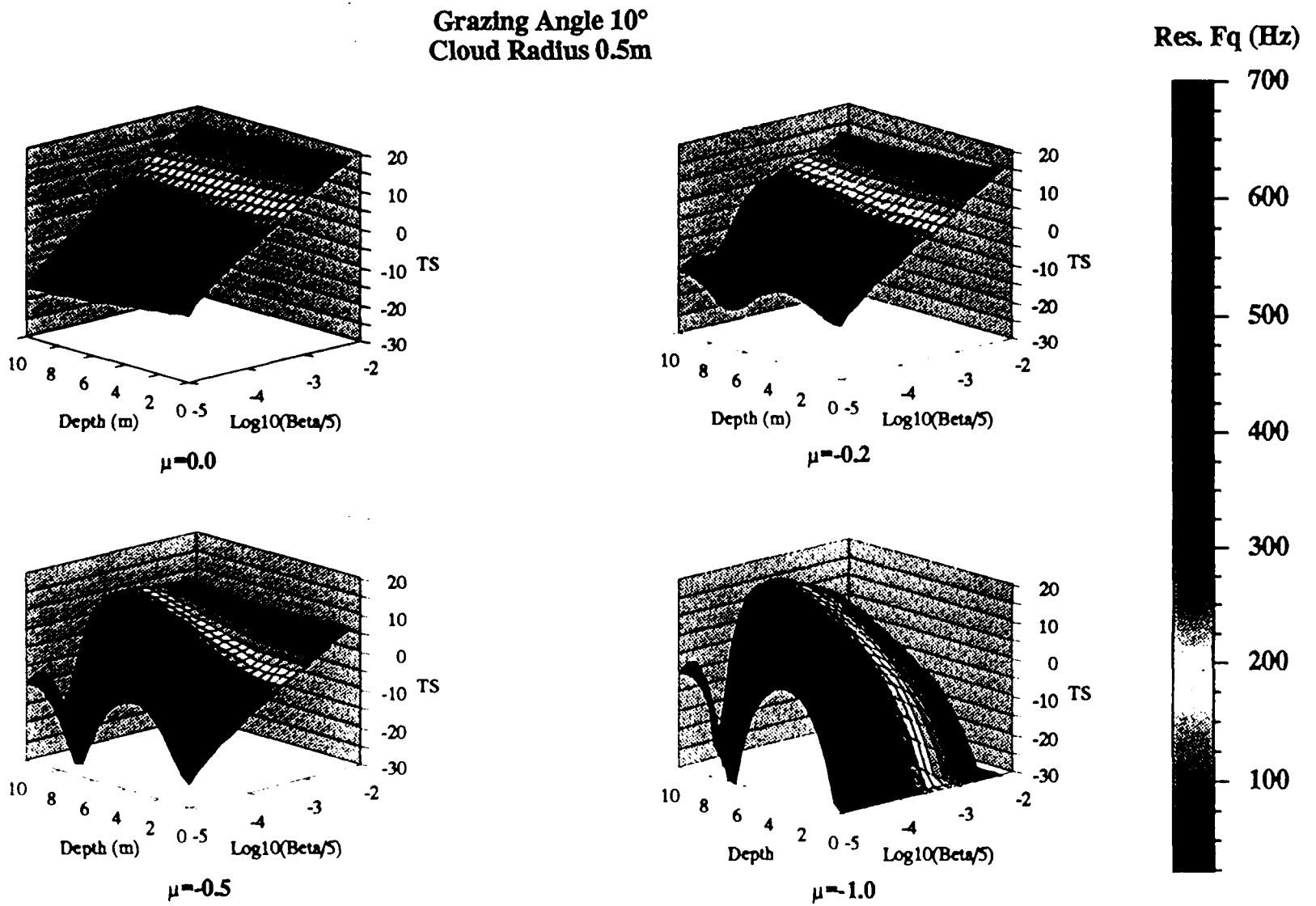

Fig. 3. Three dimensional plot of the calculated maximum target strength as a function of depth and volume fraction for a grazing angle of 10^0 and a cloud radius of 0.5 m. The frequency of the monopole resonance is shown via the color bar to the right; this figure demonstrates that these target strengths are thus obtained for a range of frequencies. The effect of the surface is described via a reflection coefficient, μ. When μ is -1, the surface is perfectly reflecting; when μ is 0, no reflection occurs.

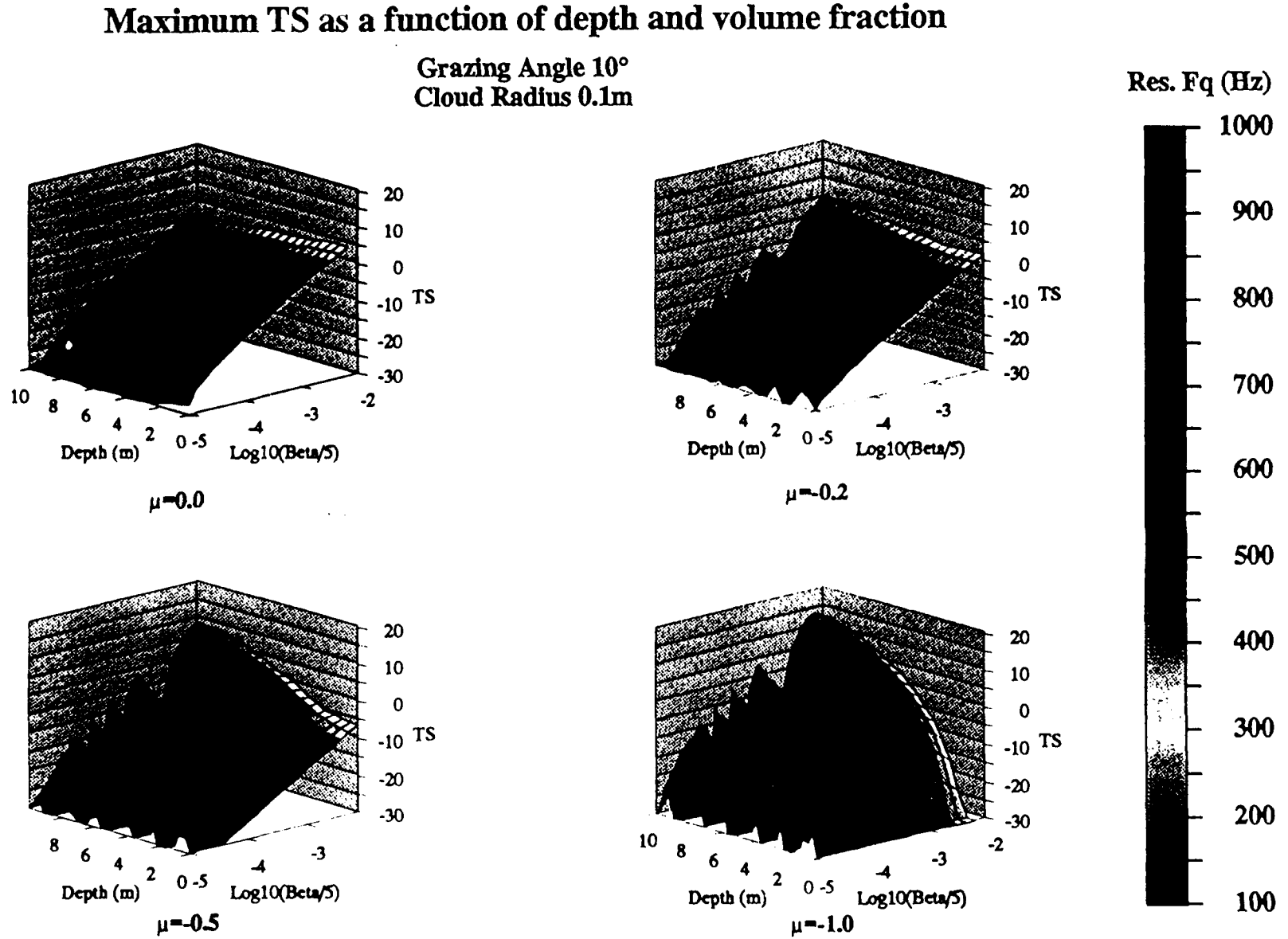

Fig. 4. Three dimensional plot of the calculated maximum target strength as a function of depth and volume fraction for a grazing angle of 10^0 and a cloud radius of 0.1 m. The frequency of the monopole resonance is shown via the color bar to the right. The effect of the surface is described via a reflection coefficient, μ. When μ is -1, the surface is perfectly reflecting; when μ is 0, no reflection occurs.

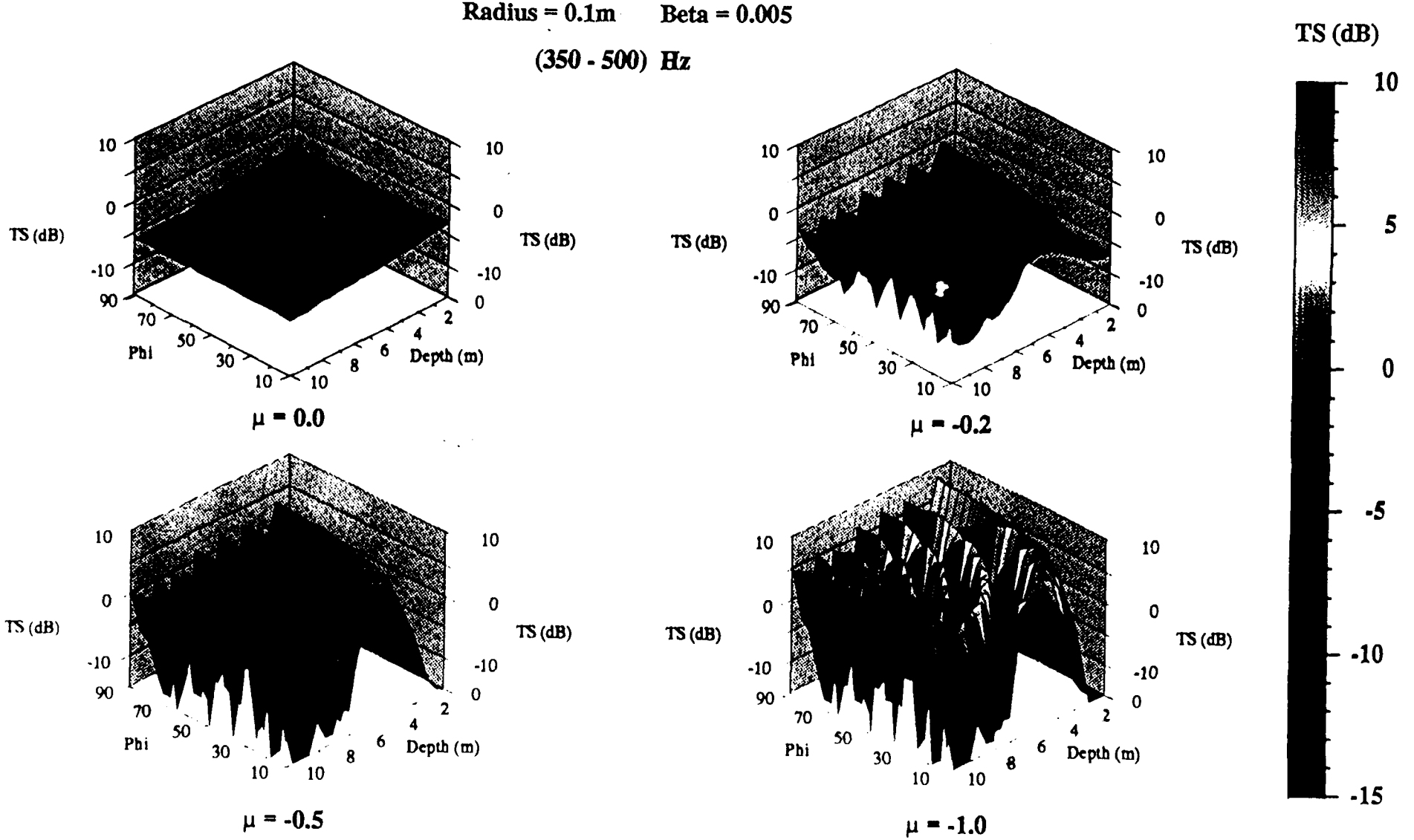

Fig. 5. Three dimensional plots showing calculations of the backscatter target strength at monopole resonance for a bubble cloud with a radius of 0.1 m and a void fraction of 0.5 %, as a function of cloud depth and grazing angle (phi). The range of resonance frequencies for this figure are from 350-500 Hz. The four different plots show the effect of the surface through the reflection coefficient, μ.

treated as resonant scatterers. We show now in Fig. 5 the expected individual resonance scattering characteristics of these clouds as a function of such parameters as grazing angle, depth below the surface, and surface conditions.

Shown in the lower right-hand corner of Fig. 5 is the predicted backscattered target strength for a bubble cloud at its monopole resonance (varying between 350-500 Hz), for a radius of 0.1 m, a void fraction of 0.5 %, and at a perfectly reflecting surface. Also shown in this figure are the cases for a free field (upper left) and for the intermediate case of a partially reflecting surface (lower left). Consider the plot in the lower left. This case represents our estimate of the conditions expected to give rise to false echoes in low-frequency, near-surface scattering. Note that one should expect echoes with TS's of 0 db for a wide range of grazing angles and cloud depths. Bright echoes (of order 0 db) can be expected to occur for grazing angles from 10-70°, and for cloud depths from near the surface to 10 meters. This figure indicates that the ocean surface is very rich with possibilities for bright echoes from resonant bubble clouds.

The conditions that lead to the production of bubble clouds (high winds and high sea states) also favor the generation of high scattering TS's. First of all, high sea state means that the ocean surface will be rough; thus, μ=-0.5 is not an unrealistic approximation; surface cancellation won't be as important except for very low frequencies. Secondly, stormy conditions usually imply an unstable water column, which is often upward refracting. Thus, the incident angles become steeper and the $\sin^4\theta$ dependence is no longer as important. These two effects tend to make far-field-like behavior much more pronounced.

Finally, we make note of the experiments of Lamarre and Melville [1992] who obtained measurements of the void fractions of ocean-generated bubble clouds in the open ocean off the coast of Delaware during the last week of February, 1991. Their data indicate that significant numbers of clouds are produced with void fractions on the order of 0.5 %; they remark that their data are consistent with their laboratory results and are several orders of magnitude higher than the often-reported *time-averaged* values [Farmer and Vagle, 1988].

Further experiments are required, however, to determine the precise acoustic and environmental conditions that give rise to these false echoes.

5.0 Summary

False targets can occur for low frequency sound scattering from the sea surface. It is unlikely that Bragg scattering from a rough surface is the source of these echoes; rather, bubble clouds or plumes resulting from breaking waves represent a more plausible explanation. We have shown that bubble clouds or plumes can act as resonant scatterers at low frequencies and generate target strengths as large as 0 db for a wide variety of conditions that are expected to occur in rough seas with wind-driven breaking waves. Future experiments are planned to determine more precisely the measured targets strengths in terms of the environmental conditions that would generate bubbles clouds of the required size, shape and void fraction to produce these false targets.

6.0 List of References

Carey, W. M. and Browning, D. , "Low-frequency ocean ambient noise: Measurement and theory," in *Sea Surface Sound,* B. R. Kerman Ed. (Kluwer, Boston) 361-376 (1988).

Carey, W. M., Fitzgerald, J. W., and Browning, D.G. , "Low frequency noise from breaking waves," in *Natural Physical Sources of Underwater Sound*, B. R. Kerman Ed. (Reidel, Dordrecht), to appear (1993).

Carey, W. M. and Roy, R. A., "Sound scattering from microbubble distributions near the sea surface," in *Proceedings of the SACLANT Reverberation Symposium* (Kluwer, Boston), to appear (1993).

Chapman, R. P. and Harris, J., "Surface backscattering strengths measured with explosive sound sources, "*J. Acoust. Soc. Am.* **34**, 1592-1597 (1962).

Commander, K. W. and Prosperetti, A. "Linear pressure waves in bubbly liquids: Comparison between theory and experiment," J. Acoust. Soc. Am. **85**, 732 (1989).

Farmer, D. M. and Ding, L., "Coherent acoustic radiation from breaking waves", *J. Acoust. Soc. Am.* **92**, 397 (1992).

Farmer, D. and Vagle, S., "On the determination of breaking wave distributions using ambient sound," *J. Geophys. Res.* **93**, 3591 (1988).

Gauss, R. C., Fialkiowski, J. M., and Soukup, R. J., "Low -frequency direct-path surface and volume scattering measured using narrowband and broadband pulses," *SACLANT Ocean Reverberation Symposium Proceedings* (to be published).

Henyey, F. S., "Acoustic scattering from oceanic microbubble plumes in the 100 Hz to 2 kHz region," *J. Acoust. Soc. Am.* **90**, 399-405 (1991).

Lamarre, E., and Melville, K., "Instrumentation for the measurement of void-fractions in breaking waves: Laboratory and field results", *IEEE J. Ocean Engr.* **17**, 204-215 (1992).

Lu, N.Q., Prosperetti, A. and Yoon, S.W., "Underwater noise emissions from bubble clouds," *IEEE J. Ocean Eng.* **15**, 275-281 (1990).

McDaniel, S. T. , "Vertical spatial coherence of backscatter from bubbles," *IEEE J. Ocean. Eng.* **OE-12**, 349-356 (1987).

McDonald, B. E., "Echoes from vertically striated subresonant bubble clouds: A model for ocean surface reverberation," *J. Acoust. Soc. Am.* **89**, 617-622. (1991).

Monahan, E. C., "Oceanic whitecaps," *J. Phys. Oceanogr.* **1**, 139-144 (1971).

Morse, P. M. and Ingard, K., Theoretical Acoustics, McGraw Hill Book Co., N. Y., 413-414 (1968).

Nicholas, M., Roy, R. A., Crum, L. A., Oguz, H. N. and Prosperetti, A., "Sound emissions by a laboratory bubble cloud," *J. Acoust. Soc. Am.*, submitted (1992).

Ogden, P.M. and Erskine, P.T., "An empirical prediction algorithm for low-frequency acoustic surface scattering strengths," Report NRL/FR/5160-92-9377, Naval Research Laboratory, Washington D.C. 20375-5000 (1992).

Prosperetti, A., "Bubble-related ambient noise in the ocean," *J. Acoust. Soc. Am.* **84**, 1042-1054 (1988).

Prosperetti, A., Lu, N.Q., and Kim, H. S., "Active and passive acoustic behavior of bubble clouds at the ocean surface," *J. Acoust. Soc. Am.* (in press) (1993).

Prosperetti, A. and Sarkar, K., "Enhanced backscattering from bubble cloud distributions on the ocean surface," *J. Acoust. Soc. Am.* **91**, 2315 (1992).

Roy, R.A., Carey, W., Nicholas, M., Schindall, J. and Crum, L.A., "Low-frequency scattering from submerged bubble clouds,' *J. Acoust. Soc. Am.* **92**, 2993-2996 (1992).

Sarkar, K. and Prosperetti, A., "Back-scattering of underwater noise by bubble clouds," *J. Acoust. Soc. Am.*, in press (1993).

Schindall, J., Carey, W. M., Roy, R. A., Crum, L. A., and Nicholas, M., "Sound scattering from near-surface bubble clouds", *J. Acoust. Soc. Am.*, **92**, 2392 (1992).

Thorpe, S. A., "On the clouds of bubbles formed by breaking wind-waves in deep water, and their role in air-sea gas transfer," *Phil. Trans. Roy. Soc.* London **A304**, 155-210 (1982).

Thorsos, E. I., "The effect of the rough air-sea interface on scattering from tenuous bubble clouds," J. Acoust. Soc. Am., **91**, 2317 (1992).

Urick, R. J., Principles of Underwater Sound for Engineers (McGraw-Hill, New York), Chap. 8, p. 188 (1967).

Yoon, S. W. , Crum, L. A., Prosperetti, A. and Lu, N. Q., "An investigation of the collective oscillations of a bubble cloud," *J. Acoust. Soc. Am.* **89**, 700-706 (1991).

7.0 Acknowledgment

We wish to acknowledge helpful discussions with A. Prosperetti and the financial support of the Office of Naval Research (Ocean Acoustics) and ARPA.

Acoustically Active Surfaces

Acoustically Active Surfaces and Active Noise and Vibration Control

Principal Investigator: F. Douglas Shields

Research Accomplished in 1992:

This research began in 1988 with an effort to develop smart acoustically active coatings using piezorubber and/or PVDF. Such smart surface coatings are constructed by combining a sensing layer with one or more actuating layers. The digital signal processing capability has been developed that enables the signal from a sensing transducing layer to be passed through a digital signal processor and applied to one or two actuating layers. With one actuator, it has been possible to control either transmission or reflection of plane waves. With two actuating layers it is possible to simultaneously control both reflection and transmission.

The work with smart coatings has expanded to include three aspects. First concerns the development of actuators and sensors, especially those for use at low frequencies; the second concerns the study of different control algorithms; and the third involves the study of the coupling between the active surface and the medium. This coupling can be complicated when the velocity of the surface becomes position dependent. The work is these three areas is discussed below.

The digital signal processors needed for the "smart" surface control are the same as those needed for active noise reducing headsets. About three years ago a research project was undertaken with the Navy Experimental Diving Unit in Panama City, Florida to develop such a head set for divers to use to reduce noise in a diving helmet.

A prototype headset with its digital control was delivered to the NEDU in February. Work was begun in February on an SBIR with the Army to develop an ANR stethoscope for use in helicopters and other noisy vehicles. This is also now in the prototype stage.

II. Summary of Work

Progress in the three areas of research with smart coatings funded by ONR is discussed in this section.

Sensor Development

Because of their limited thickness, active coatings are intrinsically insensitive at low frequencies. In 1991 NCPA developed panels consisting of transflexural capsules potted in a matrix of polyurethane. During the interval covered by this report, these panels were used to eliminate reflections from a pressure release surface in a water filled pulse echo tube 10 inches in diameter and 20 feet long at frequencies as low as 100 Hz. In order to predict the performance of such panels, the three port impedance matrix of these panels was measured experimentally using a Laser Doppler Velocimeter. Work was begun on a contract with The Sandia National Laboratory to collaborate in the development of transflexural capsules that could be used at great depths in the ocean. As part of that contract, the performance of a number of different capsules was measured as a function of pressure. An analytic expression was developed to calculate their performance and preliminary work was done on a finite element analysis of the unit.

Algorithm Development

The control of smart coatings at pressure release surfaces is especially susceptible to instability due to degenerative feedback from a pressure sensor. With a velocity sensor the feedback is nondegenerative. The pressure and velocity sensor reverse rolls at a rigid surface. This is one reason proposed for using a velocity sensor with a soft surface. However, a velocity sensor that does not alter the surface and has the needed sensitivity is very difficult to configure. During the period covered by this report, an analysis of the instability problems associated with various control algorithms was made and the results displayed on three dimensional plots of the reflection and transmission coefficients as a function of complex gain. A paper was prepared discussing these calculations and the results of some experimental work with multilayered

surfaces. This paper was ruled by ONR to contain sensitive material and it was, therefore, not published.

In the area of active noise control, innovative work was done in developing both frequency domain and time domain adaptive filters. Some of this work was described in a paper that was submitted for publication to the Journal of the Acoustical Society of America, but is still in the review process.

Coupling Between Active Surfaces and the Medium

To control reflections of plane waves that strike a plane surface obliquely requires a phased array of active surface elements. Tim Ruppel built such a surface as a part of his dissertation project. He made a plane surface with active strips and was able to drive these strips with a signal whose phase increased at a controlled rate. Using this surface he controlled reflections of plane waves from the surface and radiated plane waves at specified angles. This work was published and is referenced below. Additional work has been initiated to construct a square wave guide with inner walls that can be driven with a controllable phase shift so as to propagate waves with a controllable frequency and wave number on the inner wall.

A study has also been initiated by Dr. Lafleur of the propagation of different modes in a fluid filled tube with elastic walls.

Publications and Presentations

1. Daniel M. Warren, L. Dwynn Lafleur, and F. Douglas Shields, "Experimental determination of the three-part impedance matrix for an array of transflexural elements," J. Acoust. Soc. Am. 91, 2325 (1992). Abstract.
2. Daniel M. Warren, Dwynn Lafleur, and F. Douglas Shields, Theoretical model for the unimorph flexural disc transducer," J. Acoust. Soc. Am. 92, 2292 (1992). Abstract.
3. Timothy H. Ruppel, Lisa Lucks Mendel, and F. Douglas Shields, "Digital feedback suppression in open-ear hearing aids," J. Acoust. Soc. Am. 92, 2234 (1992). Abstract.

4. Timothy H. Ruppel and F. Douglas Shields, "Cancellation of air-borne plane waves obliquely incident upon a planar phased array of active surface elements," J. Acoust. Soc. Am. 93, 1970 (1993).

5. T.R. Harley, J.E. Hendrix, and K.T. Olree, "An adaptive feedback control for active noise cancellation in a headset," submitted to J. Acoust. Soc. Am., March 1993.

Student Support

Name: Timothy H. Ruppel

Degree: Ph.D.

Dissertation Title: Cancellation of air-borne plane waves obliquely incident upon a planar phased array of active surface elements

Date of Graduation: May 1992

Name: Daniel M. Warren

Degree: Ph.D.

Dissertation Title: The flexure of asymmetrically stacked piezoelectric laminated disks

Date of Graduation: August 1993

Name: Chris Lawrenson

Degree: Ph.D.

Tentative Dissertation Title: Propagation of sound in wave guides with active walls

Expected Date of Graduation: August 1995

Name: Keith Olree

Degree: Ph.D.

Tentative Dissertation Title: Active noise control in small enclosures

Expected Date of Graduation: August 1996

Name: Matt Miley

Degree: M.S.

Tentative Thesis Title: Acoustical transfer functions of conventional and electronic stethoscopes

Expected Date of Graduation: December 1993

Propagation Physics

Principal Investigator: Kenneth E. Gilbert

Research Accomplished in 1992:

Dr. Gilbert was not at the National Center of Physical Acoustics after January 1, 1992. However, the research described in the proposal was conducted during the first six months of the year. The continuous-wave part of the research was concluded and the results written up for publication in the Journal o. the Acoustical Society of America. A preprint of the article is attached and serves as the final report of this research effort.

ACCEPTED FOR PUBLICATION IN THE JOURNAL OF THE ACOUSTICAL SOCIETY OF AMERICA.

A STOCHASTIC MODEL FOR SCATTERING FROM THE NEAR-SURFACE OCEANIC BUBBLE LAYER [a)]

Kenneth E. Gilbert

Applied Research Laboratory and the Graduate Program in Acoustics
Pennsylvania State University, State College, PA 16804

RECEIVED:

PACS numbers: 43.30.Gv, 43.30.Zk

a) Presented in part at the 122nd meeting of the Acoustical Society of America [J. Acoust. Soc. Am. **90**, 2301 (A) (1991)].

ABSTRACT

A stochastic scattering model is derived in which the backscatter from the near-surface oceanic bubble layer is written directly in terms of an integral over the wavenumber spectrum ("power" spectrum) of the sound speed fluctuations in the layer. A factored form is given for the integral that allows the backscatter cross section per unit area to be expressed as the product of a "geometric factor" and an effective horizontal wavenumber spectrum. Because a power spectrum formulation is statistical, there are no assumptions about the geometry of the bubble layer. (E.g., hemispherical or cylindrical plumes are not assumed.) By dividing measured data for backscatter-vs-frequency by the geometric factor, we inverted scattering data from 12 different deep-ocean reverberation measurements and directly inferred the wavenumber spectrum of the sound speed in the bubble layer. For all 12 measurements, the inferred wavenumber spectrum is an inverse power law of the form $P(K)=AK^{-\beta}$ where A is a strength parameter, K is the horizontal wavenumber for a Fourier component of the sound-speed distribution, and the mean value of the spectral roll-off exponent β is $3.86 \pm .45$. The consistency in the inferred wavenumber spectrum strongly suggests that on scales of less than half an acoustic wavelength (5 to 10 m), the sound-speed structure in the bubble layer is governed by turbulence in the inertial subrange (Kolmogorov subrange) which has a universal value of $\beta = 11/3 = 3.67$ for fully developed isotropic turbulence. Using Von Karman's interpolation formula for Kolmogorov turbulence, together with oceanographically constrained input parameters, we computed theoretical backscatter cross sections and compared them with the empirical fit of Ogden and Erskine to Critical Sea Test data. It is shown that with no adjustable parameters, the stochastic scattering model gives a good account of the observed backscatter, as a function of both frequency and grazing angle.

INTRODUCTION

In the scattering of sound from the sea surface, a significant discrepancy exists between the observed measurements of backscatter and the values predicted by the classic theory of Bragg scattering from rough sea surfaces . At high sea states and low grazing angles, observed backscattering strengths are 10 to 100 times stronger than the strengths predicted by Bragg scattering theory applied to sea surfaces having realistic scales of roughness (McDaniel,1988, 1993; Ogden and Erskine, 1992). It is doubtful that the discrepancy can be removed by improvements to rough surface scattering theory or by adjustments to the known sea surface roughness spectra. Consequently it has been hypothesized that the observed high reverberation levels are due not to rough surface scattering but to scattering from the near-surface oceanic bubble layer which is created when air is entrained by breaking waves (Urick and Hoover,1956; McDaniel, 1988, 1993).

Since large bubbles rapidly rise to the surface, the bubble layer itself is composed primarily of clouds of very small bubbles ("microbubbles") that are distributed and mixed by downwelling currents and turbulence (Thorpe, 1982, 1984; Thorpe and Hall, 1983; Osborn, et al.,1992). The microbubbles are transported essentially passively until they finally go into solution, usually after many minutes (Thorpe, 1982; Thorpe and Hall, 1983). Although the microbubble layer has a low density of bubbles (air volume fractions of 10^{-5} or smaller), it nevertheless has a marked effect acoustically (Farmer and Vagle, 1989; Su,1992; Cartmill and Su, 1992; Su et al., 1993).

At low frequencies where the scattering is nonresonant ($f \lesssim 5$ kHz), the sound speed in the bubble layer can be considered to be the that of a water-bubble mixture. Small concentrations of bubbles significantly increase the compressibility of a water parcel without measurably changing its density. Since sound speed is inversely proportional to the square root of density times compressibilty, the sound speed in the bubble layer is decreased. For example, for a volume fraction of 10^{-5}, the speed of sound is reduced by about 170 m/s.

On records from upward-looking sonars, the distribution of bubbles in the layer appears to be random in space and time. (Thorpe,1982; Farmer and Vagle, 1989; Farmer, 1992; Commander, 1992). Thus the acoustic "picture" of the near-surface bubble layer is a region with a stochastic distribution of sound speed that is determined by upper ocean dynamic processes.

In this article we propose that the clouds of microbubbles discussed above are an important, and perhaps the primary, physical mechanism that controls the backscatter at low grazing angles and high sea states. Such a proposal has been made already by other workers (McDonald, 1991; Henyey 1991). In fact, the work described here was directly motivated by the original research of McDonald. Unlike previous workers, however, we do not assume the bubble layer to be a collection of plumes with a specified geometry such as cylinders or hemispheres. Rather, we more realistically consider the bubble layer to be a stochastic medium with certain statistical properties. With this picture of the bubble layer, the backscatter is viewed as Bragg scattering from the Fourier components of the sound-speed fluctuations created by the stochastic microbubble distribution. As is discussed below, this approach makes it possible to relate the backscatter directly to the wavenumber spectrum of the sound-speed fluctuations in the bubble layer, thereby connecting the backscatter to a realistic oceanographic process -- turbulence.

I. THEORETICAL FORMULATION

We want to calculate the backscatter from the near-surface microbubble layer under the assumption that the bubble distribution varies stochastically in space and time. To arrive at such a formulation we represent the bubble layer as an effective fluid continuum with a fluctuating sound speed that on the average is less than the sound speed in bubble-free water. We first outline the basic assumptions of the bubble-layer model. Then an expression is derived for the backscatter one obtains from the bubble layer model. Finally, we approximate the backscatter cross-section per unit area as the product of a "geometric factor" times the effective horizontal wavenumber spectrum for sound speed fluctuations in the bubble layer.

A. A Stochastic Bubble-Layer Model

When a wave breaks in the ocean, a wide spectrum of bubble sizes is generated. The larger bubbles rise to the surface rapidly, leaving behind a turbulent, smoke-like cloud of microbubbles with radii of 10-100 microns (Su and Cartmill, 1992; Su et al., 1993). Since the microbubbles may stay in the water for some time before dissolving, they can be transported downward by turbulent downwelling currents (Thorpe, 1982, 1984; Thorpe and Hall, 1983; Osborn, et al., 1992). Because of turbulence, the microbubble layer is a stochastic, inhomogeneous, time-dependent layer and, in high sea states, can extend as far as 20 m below the sea surface (Farmer, 1992).

As discussed in the Introduction, the effect of the microbubble layer on low-frequency sound is to "soften" the water so that the sound speed is lowered and the wavenumber is increased. Thus, in a continuum model, the square of the total wavenumber, k_{total}^2 , that appears in the wave equation can be written as the contribution from bubble-free water plus the contribution from the bubble distribution:

$$k_{total}^2 = k_0^2 + k_B^2 \qquad (1)$$

where $k_0^2 = \omega^2/c_0^2$ is the wavenumber for bubble-free seawater, and k_B^2 is the change due to bubbles. In terms of the bubble number density, n, the contribution of the microbubbles to the total wavenumber is

$$k_B^2 = 4\pi < t > n \qquad (2)$$

where $< t >$ is the average bubble scattering strength (Foldy, 1945; Carstensen and Foldy, 1947; Morse and Feshbach, 1953). At the frequencies we consider the micobubbles are nonresonant, and Eq.(2) reduces to the wavenumber one obtains using the sound-speed from simple mixture theory. Hence, for a small sound-speed change Δc due to bubbles, k_B^2 can be written as

$$k_B^2 = -\, 2k_0^2\, (\Delta c/c_o) \qquad (3)$$

where simple mixture theory gives $\Delta c/c_o \approx -\, 11{,}500\phi$, for a void fraction ϕ much less than one, (Urick,1975). In this article we keep in mind that k_B^2 is due to a distribution of discrete bubbles but always use a continuum model to represent the bubble layer and to calculate backscatter.

Because the microbubbles are distributed by turbulent diffusion, at any given time the bubble distribution is quite inhomogeneous. Although experimental measurements indicate that the average concentration of bubbles decays approximately exponentially with depth , it is clear from the uplooking sonar records (Thorpe, 1982; Farmer and Vagle, 1989; Farmer, 1992) and in-situ measurements (Su, 1992; Cartmill and Su, 1992, Su et al., 1993) that there are significant fluctuations about the average, both horizontally and vertically. Hence we write k_B^2 as the sum of an average value and a fluctuating part that depends stochastically on both depth and horizontal distance.

$$k_B^2 = <k_B^2(z)> \; + \delta k_B^2(\underline{r}) \qquad (4)$$

where $\langle k_B^2(z)\rangle = -2\,k_0^2\,[\langle \Delta c(z)\rangle / c_o)]$ is the average profile and $\delta k_B^2(\underset{\sim}{r})$ is the fluctuation about $\langle k_B^2(z)\rangle$. Because of bubble dissolution, both $\langle k_B^2(z)\rangle$ and $\delta k_B^2(\underset{\sim}{r})$ are observed to decrease with increasing depth (Su,1992; Cartmill and Su, 1992; Su et al., 1993).

For sound-speed fluctuations that are small relative to c_o we can write $\delta k_B^2(\underset{\sim}{r})$ as

$$\delta k_B^2(\underset{\sim}{r}) = -2k_0^2\,[\delta c(\underset{\sim}{r})/c_o] \tag{5}$$

where $\delta c(\underset{\sim}{r})$ is the fluctuation about the average sound speed. To account for the decrease in the bubble concentration with depth and the corresponding decrease in the size of fluctuations, we write the sound-speed fluctuation as the product of a monotonically decaying reference function $f_{ref}(z)$ and a fluctuation parameter $\varepsilon(\underset{\sim}{r})$: $\delta c(\underset{\sim}{r}) = f_{ref}(z)\varepsilon(\underset{\sim}{r})$. The reference function is chosen so that the standard deviation in sound speed fits measured values. We therefore let $f_{ref}(z) = \sigma_c(z)$, where $\sigma_c(z)$ is the measured rms sound-speed fluctuation with depth. The fluctuation parameter $\varepsilon(\underset{\sim}{r})$ is taken to represent an isotropic stationary stochastic process where the autocorrelation function $\langle \varepsilon(\underset{\sim}{r})\varepsilon(\underset{\sim}{r}')\rangle \equiv C(\underset{\sim}{r}-\underset{\sim}{r}')$ is normalized so that $C(0) = 1$. Conceptually, $\varepsilon(\underset{\sim}{r})$ accounts for the statistics of the fluid motion that transports the bubbles. As discussed later, the fluid motion statistics are directly related to the distribution statistics for "conservative passive additives" (Tartarski, 1961) that move with the fluid as infinite-lifetime tracer particles. The scaling function $\sigma_c(z)$ accounts for both the surface bubble concentration and the decay with depth due to the finite lifetimes of the microbubbles. Also any buoyancy effects are included implicitly in an empirically determined scaling function.

With the above formulation, we have

$$\delta k_B^2(\underset{\sim}{r}) = -2k_0^2\,[\sigma_c(z)/c_o]\varepsilon(\underset{\sim}{r}) \tag{6}$$

In the calculations presented later we will fit the measured values of $\sigma_c(z)$ with an exponential so that $\sigma_c(z) = \sigma_c(0)\exp(-z/L)$, where $\sigma_c(0)$ is the rms sound speed fluctuation at the surface and L is the e-folding distance. Thus, with the above exponential scaling of the fluctuations, we have finally

$$k_{total}^2 = k_0^2 + \langle k_B^2(z)\rangle - 2k_0^2 [\, \sigma_c(0)/c_o \,] e^{-z/L} \varepsilon(\underset{\sim}{r}) \tag{7}$$

The above expression for the total wavenumber is used in a wave equation to describe backscattering from the oceanic bubble layer.

B. Solution for the Backscattered Field

The wave equation to be solved for the acoustic pressure is given by

$$\nabla^2\Psi + k_{total}^2 \Psi = 0 \tag{8}$$

where the total field Ψ is the sum of the field in the absence of a bubble layer, Ψ_o , and the field, Ψ_s , scattered by the layer, i.e., $\Psi = \Psi_o + \Psi_s$.

The integral equation associated with the differential wave equation is the Lippmann-Schwinger equation (Rodberg and Thaler, 1967).

$$\Psi(\underset{\sim}{r}) = \Psi_0(\underset{\sim}{r}) + \frac{1}{4\pi}\int G_0(\underset{\sim}{r},\underset{\sim}{r}')\, k^2{}_B(\underset{\sim}{r}')\, \Psi(\underset{\sim}{r}')d^3\underset{\sim}{r}' \tag{9}$$

where the Green's function G_0 is the point source solution in the absence of a bubble layer and $k_B^2(\underset{\sim}{r}')$ denotes $\langle k_B^2(z')\rangle + \delta k_B^2(\underset{\sim}{r}')$. The average profile $\langle k_B^2(z')\rangle$ does not contribute to backscatter. Consequently, the backscattered field Ψ_s is given by

$$\Psi_s(\underset{\sim}{r}) = \frac{1}{4\pi}\int G_0(\underset{\sim}{r},\underset{\sim}{r}')\delta k^2{}_B(\underset{\sim}{r}')\Psi(\underset{\sim}{r}')d^3\underset{\sim}{r}' \tag{10}$$

For isospeed bubble-free water and a pressure-release boundary condition at a smooth sea surface we have for G_0:

$$G_0(\underset{\sim}{r},\underset{\sim}{r}') = \frac{e^{ik_0 R_+}}{R_+} - \frac{e^{ik_0 R_-}}{R_-} \tag{11}$$

The quantities R_+ and R_-, are defined as

$$R_\pm \equiv |\underset{\sim}{r} - \underset{\sim}{r}_\pm| \tag{12}$$

where with unit Cartesian vectors ($\hat{\underset{\sim}{1}}$, $\hat{\underset{\sim}{j}}$, $\hat{\underset{\sim}{k}}$) we have $\underset{\sim}{r}_\pm = \underset{\sim}{r}_h \pm z\,\hat{\underset{\sim}{k}}$, and $\underset{\sim}{r}_h = x\,\hat{\underset{\sim}{1}} + y\,\hat{\underset{\sim}{j}}$. Note that the vector $\underset{\sim}{r}_h$ is the horizontal component of the radius vector.

We are interested in the far field so we approximate G_0 as

$$G_0(\underset{\sim}{r},\underset{\sim}{r}') = -\frac{e^{ik_0 r}}{r}\, 2i \sin(k'_v z') e^{-i\underset{\sim}{k}'_h \cdot \underset{\sim}{r}'_h} \tag{13}$$

where $k'_v = k_0 \sin\theta$ and $\underset{\sim}{k}'_h = k_0 \cos\theta\, \hat{\underset{\sim}{k}}'_h$ are, respectively, the vertical wavenumber and vector horizontal wavenumber of the backscattered field.

For weak scattering from the bubble layer, the backscattered field makes only a small contribution to the total field. Hence in the integral in Eq.(10) we can use the first-order Born approximation, which approximates the total field in the bubble layer as the unscattered field, i.e., $\Psi \approx \Psi_o$. Taking Ψ_o to be a plane wave perfectly reflected from the surface we have

$$\begin{aligned} \Psi_o &= e^{i\underset{\sim}{k}_0 \cdot \underset{\sim}{r}_+} - e^{i\underset{\sim}{k}_0 \cdot \underset{\sim}{r}_-} \\ &= 2i \sin(k_v z)\, e^{i\underset{\sim}{k}_h \cdot \underset{\sim}{r}_h} \end{aligned} \tag{14}$$

where $k_v = -k_0 \sin\theta$ and $\underset{\sim}{k}_h = k_0 \cos\theta \, \hat{\underset{\sim}{k}}_h$ are, respectively, the vertical wavenumber and vector horizontal wavenumber of the unscattered field. With the results from Eqs.(13) and (14), the Born approximation for the backscattered field $\Psi_s(\underset{\sim}{r})$ is given by

$$\Psi_s(\underset{\sim}{r}) = \frac{e^{ik_0 r}}{\pi r} \int \sin(k'_v z') \sin(k_v z') \, \delta k^2_B(\underset{\sim}{r}') \, e^{i \underset{\sim}{q}_h \cdot \underset{\sim}{r}'_h} \, d^3\underset{\sim}{r}' \qquad (15)$$

where $k'_v = -k_v$, and $\underset{\sim}{q}_h = \underset{\sim}{k}_h - \underset{\sim}{k}'_h = 2\underset{\sim}{k}_h$.

The ensemble averaged backscattering cross-section is given by,

$$\sigma = < | f_{scat} |^2 > \qquad (16)$$

where the scattering amplitude f_{scat} is the coefficient of the spherical wave $\exp(ik_0 r)/r$ in Eq.(15):

$$f_{scat} = -\frac{1}{\pi} \int \sin^2(k_v z') \, \delta k^2_B(\underset{\sim}{r}') \, e^{i \underset{\sim}{q}_h \cdot \underset{\sim}{r}'_h} \, d^3\underset{\sim}{r}' \qquad (17)$$

Hence for backscattering we have,

$$\sigma = \left[\frac{4k_0^4 \sigma_c^2(0)}{\pi^2 c_0^2}\right] \int\int e^{i \underset{\sim}{q}_h \cdot (\underset{\sim}{r}''_h - \underset{\sim}{r}'_h)} g(k_v, z'') g^*(k_v, z') C(\underset{\sim}{r}'' - \underset{\sim}{r}') \, d^3\underset{\sim}{r}'' \, d^3\underset{\sim}{r}' \qquad (18)$$

where $g(k_v, z) \equiv \sin^2(k_v z) e^{-z/L}$ and, as discussed earlier, $C(\underset{\sim}{r}'' - \underset{\sim}{r}') = <\varepsilon(\underset{\sim}{r}'')\varepsilon(\underset{\sim}{r}')>$ is the autocorrelation function for the stochastic quantity $\varepsilon(\underset{\sim}{r})$ which represents the effects of turbulence and controls the variability in k_B^2. We now define $\underset{\sim}{r}'' - \underset{\sim}{r}'$ as $\underset{\sim}{S} = (\underset{\sim}{S}_h, S_v)$ and rewrite Eq. (18) as

$$\sigma = \left[\frac{4k_0^4 \sigma_c^2(0)}{\pi^2 c_0^2}\right] \int\int e^{i \underset{\sim}{q}_h \cdot (\underset{\sim}{r}''_h - \underset{\sim}{r}'_h)} g(k_v, z' + S_v) g^*(k_v, z') C(\underset{\sim}{S}_h, S_v) d^3\underset{\sim}{S} \, d^2\underset{\sim}{r}_h' dz' \qquad (19)$$

The integral over z' can be written as

$$\int g(k_v,z'+S_v)g^*(k_v,z')dz' = \frac{1}{2\pi}\int |\tilde{g}(k_v,q_v)|^2\, e^{iq_vS_v}dq_v \qquad (20)$$

where $\tilde{g}(k_v,q_v)$ is the Fourier transform of $g(k_v, z)$. Thus σ becomes

$$\sigma = \frac{1}{2\pi}\left[\frac{4k_o^4\sigma_c^2(0)}{\pi^2c_o^2}\right]\int |\tilde{g}(k_v,q_v)|^2\, \hat{C}(\underset{\sim}{q})\, dq_v\, d^2\underset{\sim}{r}_h' \qquad (21)$$

where the normalized wavenumber spectrum $\hat{C}(\underset{\sim}{q})$ is the Fourier transform of the normalized autocorrelation function , $C(\underset{\sim}{S})$:

$$\hat{C}(\underset{\sim}{q}) \equiv \int C(\underset{\sim}{S})\, e^{i\underset{\sim}{q}\cdot\underset{\sim}{S}}\, d^3\underset{\sim}{S}\ , \qquad (22)$$

and $\underset{\sim}{q} = (\underset{\sim}{q}_h, q_v)$. The full wavenumber spectrum for sound-speed fluctuations in the bubble layer is proportional to the normalized spectrum.

Experimentally, the quantity measured is the the cross section per unit area, $\hat{\sigma}$, where $\hat{\sigma}$ is related to σ by

$$\sigma = \int \hat{\sigma}\, d^2\underset{\sim}{r}_h' \qquad (23)$$

From Eqs. (23) and (21) we can see that $\hat{\sigma}$ is given by

$$\hat{\sigma} = \frac{1}{2\pi}\left[\frac{4k_o^4\sigma_c^2(0)}{\pi^2c_o^2}\right]\int |\tilde{g}(k_v,q_v)|^2\, \hat{C}(\underset{\sim}{q})\, dq_v \qquad (24)$$

We want to use Eq.(24) and surface backscatter measurements to estimate the horizontal wavenumber spectrum (i.e., power spectrum) of sound-speed fluctuations in the bubble layer. Consequently, we would like to have an expression for $\hat{\sigma}$ that is factored into the product of a "geometric factor" times the power spectrum. To obtain a factored form we must make some approximations to the integral in Eq.(24).

C. Factored Form for the Scattering Cross Section

As indicated in Eq.(24), computing $\hat{\theta}$ requires a weighted integration over $\hat{C}(\underset{\sim}{q})$ with $|\tilde{g}(k_v,q_v)|^2$ as the weighting function. We assume that the fluctuations are separately isotropic horizontally and isotropic vertically so that we can write $\hat{C}(\underset{\sim}{q})$ as a function of q_h^2 and q_v^2: $\hat{C}(\underset{\sim}{q}) \equiv \hat{C}(q_h^2, q_v^2)$. If, over the range of integration, $\hat{C}(\underset{\sim}{q})$ is a smooth function of q_v^2 (such as a power law), then in Eq.(24) we can expand $\hat{C}(\underset{\sim}{q})$ in a Taylor series in q_v^2. We expand $\hat{C}(q_h^2, q_v^2)$ about some as yet unspecified average value $\langle q_v^2 \rangle$:

$$\hat{C}(q_h^2, q_v^2) = \hat{C}(q_h^2, \langle q_v^2 \rangle) + \frac{\partial \hat{C}}{\partial q_v^2} (q_v^2 - \langle q_v^2 \rangle) + \frac{1}{2} \frac{\partial^2 \hat{C}}{\partial (q_v^2)^2} (q_v^2 - \langle q_v^2 \rangle)^2 + \ldots \qquad (25)$$

The second term vanishes if we define $\langle q_v^2 \rangle$ to be the average value of q_v^2 over the integration interval : $\langle q_v^2 \rangle \equiv I_1/I_2$, where

$$I_1 = \int_{-\infty}^{\infty} q_v^2 \, |\tilde{g}(k_v,q_v)|^2 dq_v = -2\pi \int_{-\infty}^{\infty} g(k_v,z) \frac{\partial^2}{\partial z^2} \, g(k_v,z) dz \qquad (26)$$

$$I_2 = \int_{-\infty}^{\infty} |\tilde{g}(k_v,q_v)|^2 dq_v = 2\pi \int_{-\infty}^{\infty} |g(k_v,z)|^2 dz \qquad (27)$$

Evaluating the integrals I_1 and I_2 and simplifying yields,

$$\langle q_v^2 \rangle = \frac{1}{3L^2} (1 + 4 k_v^2 L^2) \qquad (28)$$

Keeping the first two terms in the Taylor series expansion and evaluating the integral over q_v, gives us an approximation for $\hat{\theta}$ that is in factored form:

$$\hat{\theta} \approx \frac{1}{2\pi} \left[\frac{4 k_o^4 \sigma_c^2(0)}{\pi^2 c_o^2} \right] \left[\int |\tilde{g}(k_v,q_v)|^2 \, dq_v \right] \hat{C}(q_h^2, \langle q_v^2 \rangle) \qquad (29)$$

$$= \frac{3L}{4\pi^2}\left[\frac{k_0^4\sigma_c^2(0)}{c_0^2}\right]\frac{4k_v^4L^4}{(1+4k_v^2L^2)(1+k_v^2L^2)}\hat{C}(q_h^2, \langle q_v^2\rangle)$$

where the result in Eq.(27) has been used to evaluate the integral over q_v. Note that the approximation in Eq.(29) is equivalent to approximating the average value of a function f(x) as $\langle f\rangle \approx f(\langle x\rangle)$. We have tested the approximation in Eq.(29) by comparing with an exact numerical evaluation of the integral. For small grazing angles and a power-law spectrum of the form $\hat{C}(q_h^2,q_v^2) = A/(Bq_h^2 + Cq_v^2)^{\beta/2}$, where A, B, and C are constants, the approximation agrees very well with an exact numerical evaluation of the integral.

We now define the effective horizontal wavenumber spectrum for sound-speed fluctuations in the bubble layer as

$$P(q_h) \equiv \sigma_c^2(0)\hat{C}(q_h^2, \langle q_v^2\rangle) \tag{30}$$

where $\sigma_c^2(0)$ is the rms sound-speed fluctuation at z=0. We further define a "geometric factor" F

$$F \equiv \frac{3L}{4\pi^2}\frac{k_0^4}{c_0^2}\left[\frac{4k_v^4L^4}{(1+4k_v^2L^2)(1+k_v^2L^2)}\right] \tag{31}$$

With the P and F defined as given above, we have

$$\vartheta = F\,P(q_h) \tag{32}$$

Very little is presently known about the wavenumber spectrum for sound-speed fluctuations in the oceanic bubble layer. In the next section we use Eq.(32) to "invert" measured backscatter data and obtain empirical results for $P(q_h)$.

II. THE WAVENUMBER SPECTRUM FOR SOUND-SPEED FLUCTUATIONS IN THE BUBBLE LAYER

The stochastic model discussed above has been used to invert surface backscatter data from 12 different deep-ocean measurements. As will be shown, all the measurements yield an inverse power-law wavenumber spectrum that is consistent with turbulent diffusion of microbubbles by inertial subrange turbulence (Kolmogorov turbulence). Hence in this section we propose that the wavenumber spectrum for sound-speed fluctuations in the bubble layer can be described by the Kolmogorov spectrum, which is proportional to $K^{-11/3}$, where K is the wavenumber for a Fourier component of the sound-speed distribution. In the next section (Section III) we use the spectrum to make predictions for scattering from the bubble layer.

A. Analysis of Reverberation Data

Figure 1 shows some typical results obtained from deep-ocean reverberation experiments for scattering versus frequency at a fixed grazing angle. (Chapman and Harris, 1962; Chapman and Scott 1964; Percy, 1970; Brown et al., 1966). To use the data to estimate the horizontal wavenumber spectrum $P(q_h)$ as a function of q_h, we convert the measured backscatter strength, BS (in decibels), to a scattering cross section per unit area, $\hat{\sigma}$, and divide by the geometric factor F as indicated in Eq.(33) below:

$$P(q_h) = \hat{\sigma}_{meas} / F \tag{33}$$

where the measured cross section $\hat{\sigma}_{meas}$ is related to the backscatter strength BS by $BS = 10\log_{10}(\hat{\sigma}_{meas})$.

By plotting $\log_{10} P(q_h)$ versus $\log_{10}(q_h)$ from the measured data, we observed that, for all cases examined, the wavenumber spectrum is well represented by a power law of the form $Aq_h^{-\beta}$, where A is a strength parameter and β is a spectral roll-off exponent.

Numerical values for the quantities A and β were obtained from a least-squares fit for each data set. As examples, the estimated wavenumber spectra for four of the data sets in Fig. 1 are shown in Fig. 2. The horizontal axis in Fig.2 is the logarithm (base 10) of q_h, and the vertical axis is the logarithm (base 10) of the estimated wavenumber spectrum, P. In determining the optimum least-squares fit, the e-folding depth was varied about L =1.5 to further improve the fit. Since there was little improvement, in all four cases in Fig. 2 we have used an e-folding depth of L=1.5 m, a value that is consistent with oceanographic measurements (Thorpe, 1982; Farmer and Vagle ,1989; Su 1992; Cartmill and Su, 1992; Su et al., 1993).

The procedure described above for inferring $P(q_h)$ was used to analyze reverberation data for surface backscatter for a total of 12 different measurements, for windspeeds ranging from approximately 15 kts to over 30 kts. In Fig. 3 we show the inferred values for the spectral exponent β as a function of windspeed for the 12 measurements (Chapman and Harris, 1962; Chapman and Scott 1964; Percy, 1970; Brown et al., 1966; Jin et. al, 1989).

In a given experiment the strength parameter A (and hence the rms sound-speed fluctuation $\sigma_c(0)$) generally increases dramatically and sytematically with windspeed. However, in the examination of the 12 measurements, we found that, between different experiments, the correlation of the strength parameter A with windspeed was poor. Hence a plot of the strength parameter A versus windspeed for the 12 measurements gives little insight and consequently is not presented.

Although the strength parameter A depends strongly on windspeed, the spectral exponent β appears to have little windspeed dependence. The mean value of β from the 12 least-squares fits is $\beta = 3.86$, and the standard deviation is .45.

One can understand the origin of the apparent universal value $\beta = 3.86$ from a simple analysis of the geometric factor F and an inspection of plots of ∂ versus frequency at a fixed grazing angle (E.g., Fig. 1). At a grazing angle of 20^o , for example,

and frequencies above a few kilohertz, the vertical wavelength is on the order of the e-folding distance ("thickness") of the bubble layer. Consequently, the quantity $k_v^2 L^2$ in the geometric factor is much greater than 1, so that the frequency dependence in the geometric factor comes solely from the k_o^4 factor (See Eq.(31)). Thus at frequencies above a few kilohertz, the geometric factor F varies as frequency to the fourth power. From inspection of plots of δ versus frequency at a fixed grazing angle, we can see that δ varies weakly with frequency for frequencies above a few kilohertz. For δ to depend weakly on frequency, the exponent in the wavenumber spectrum $P(q_h)$ must almost cancel the fourth power frequency dependence in the geometric factor. Therefore we can directly infer from the weak frequency dependence of δ that β is slightly less than 4 . Since δ apparently always has weak dependence on frequency above a few kilohertz, the data directly imply a nearly universal value for β that is slightly less than 4.

The consistency of the value of β for the 12 measurements suggested to us that, at the scales probed by the backscattered waves (1/2 the acoustic wavelength), the distribution of microbubbles is governed by a model-independent mechanism such as small-scale turbulence. In the discussion below we present evidence for the turbulence hypothesis.

B. Kolmogorov Turbulence and the Distribution of Microbubbles

Langmuire (1938), in his original studies of the near-surface circulation that now bears his name, noted that "...although the motion was very slow it was very turbulent." In recent years, Thorpe (1982) has made comprehensive observations of the turbulent nature of Langmuire circulation and emphasized its role in the turbulent diffusion of microbubbles (Thorpe 1982, 1984). Very recently, Osborn et al. (1992) simultaneously measured both the turbulence and acoustic scattering associated with bubble plumes and concluded that turbulence is a dominant feature of the plumes. From a simplistic viewpoint, the bubble-cloud records from upward-looking high-frequency sonars, which are often remarkably similar to clouds in the atmosphere, visually suggest the turbulent nature of the

currents that transport microbubbles (Thorpe, 1982; Farmer and Vagle, 1989; Farmer, 1992).

Because, at small scales, turbulence has some universal characteristics, we seek here to establish a connection between the empirical value of $\beta = 3.86$ and small-scale turbulence. We first present some basic background information in order to make our reasoning easier to follow.

In turbulent fluids, steady-state small-scale turbulence is governed by an energy cascade process that leads to model-independent structure at small length scales where the fluid has "forgotten" the details of the driving mechanism that supplies the energy (Landau and Lifshitz, 1959; Tatarski, 1961). These length scales are commonly known as the "inertial subrange" (Hinze, 1959; Neumann and Pierson, 1966; Grant et al. 1962; Grant et al., 1968; Embleton and Daigle, 1991). Kolmogorov has shown that the velocity structure of such turbulence has a three-dimensional wavenumber spectrum proportional to $K^{-11/3} = K^{-3.67}$, regardless of the intensity of the turbulence (Tatarski, 1961) . Further, Obukhov and others have studied the the concentration distribution of "passive additives" such as heat (or, in our case, microbubbles) that are mixed by Kolmogorov turbulence (Tatarski,1961; Corrsin, 1951). Obukhov was the first to show that, given sufficient time, the concentration distribution acquires the same spectrum as the turbulence itself (Tatarski, 1961).

In the ocean mixed layer, Obukhov's prediction is strongly supported by measurements of near-surface temperature fluctuations (Whitmarsh, et al., 1957; Voorhis and Perkins, 1966; Grant, et al., 1968) which clearly show the characteristics of turbulent mixing by inertial subrange turbulence. Whitmarsh, et al., for example, have shown that the "structure function" for the temperature fluctuations $< [T(\underset{\sim}{r_2}) - T(\underset{\sim}{r_1})]^2 >$ closely follows Kolmogorov's well - known "2/3 law" which states that for inertial subrange turbulence the structure function varies as $\rho^{2/3}$, where $\rho = |\underset{\sim}{r_2} - \underset{\sim}{r_1}|$ is the separation between two measurement points. In wavenumber space the 2/3 law corresponds to a

three-dimensional wavenumber spectrum that varies as $K^{-11/3}$ (Tatarski, 1961). Thus four pieces of information -- direct observations with high-frequency sonars, Kolmogorov/Obukhov theory, temperature fluctuation measurements, and the acoustic analysis presented here -- have led us to hypothesize that, except for the monotonic decay with depth due to dissolution, the microbubble distribution, like the distributions for turbulence and temperature, can be represented by the $K^{-11/3}$ spectrum associated with inertial subrange turbulence.

The inverse power law $K^{-11/3}$ proposed by Kolmogorov is not valid at all scales but only in the inertial subrange, $2\pi/L_o << K << 2\pi/l_o$, where L_o is the scale of the largest eddies ("outer scale") and l_o is the scale for the smallest eddies ("inner" scale) where energy is dissipated by viscosity. The complete turbulence spectrum is often approximated with an analytic expression due to Von Karman (Clifford, 1978). The normalized Von Karman spectrum varies as $K^{-11/3}$ in the inertial subrange and by construction has a three-dimensional integral of unity in wavenumber space. To make backscatter predictions from first principles without a direct measurement of the strength parameter A, one must use some expression such as the Von Karman spectrum that can be normalized in wavenumber space. Although often used in the atmospheric community, the Von Karman spectrum is only one of a many possible choices for a convenient integrable expression and has no deep physical significance.

For our purposes, it is convenient to generalize the spectral exponent in the Von Karman spectrum and set the inner scale to zero. With a general spectral exponent β and with $l_o = 0$, the normalized Von Karman spectrum is

$$\hat{C}(K) = N(\beta)\ (8\pi^{3/2}\ K_o^{-3})(1 + K^2/K_o^2)^{-\beta/2} \qquad (34)$$

where $K_o = 2\pi/L_o$, and $N(\beta) = \Gamma(\beta/2)/\ \Gamma(\beta/2-3/2)$, is the ratio of two gamma functions. In the inertial subrange we have $K/K_o >> 1$. Hence we have

$$\hat{C}(K) = N(\beta)\ (8\pi^{3/2}\ K_o^{-3})(K/K_o)^{-\beta}, \qquad K/K_o >> 1 \qquad (35)$$

Langmuire observed that, in Lake George, the downwelling currents were consistently confined to the mixed layer (Langmuire, 1938). Therefore, in the ocean, when a mixed layer is present, we expect L_o to be on the order of the mixed layer depth, or roughly 50 m to 100 m. This estimate is consistent with existing oceanographic measurements of horizontal bubble layer structure (Commander, 1992; Henyey et al., 1992). To get some idea of the size of $\hat{C}(K)$ for such outer scale values, we can consider the special case $\beta = 4$, for which $\hat{C}(K)$ can be simply evaluated. For $\beta = 4$ and $L_o = 100$ m, we have

$$\hat{C}(K) = (16\pi^2 / L_o)K^{-4}$$

$$\approx 1.6\ K^{-4} \qquad (36)$$

Any value of β that is close to 4 gives a similar numerical coefficient for $K^{-\beta}$.

The complete wavenumber spectrum for sound-speed fluctuations is $\sigma_c^2(0)$ times the normalized spectrum $\hat{C}(K)$. Hence, using the result in Eq.(36), we have for the strength parameter A (the coefficient of $K^{-\beta}$ inferred from reverberation data) the value $A \approx 1.6\sigma_c^2(0)$. From Fig. 2, it can be seen that for windspeeds in the range of 20 kts to 30 kts, the inferred values of $\log_{10}A$ (i.e., the y-intercept) are in the range 3.5 to 5.2. We can therefore infer $\sigma_c(0)$ to be in the range of 44 m/s to 315 m/s, which corresponds to rms void fraction fluctuations of order 10^{-6} to 10^{-5}.

The results for $\sigma_c(0)$ inferred from backscatter data are consistent with the in-situ measurements of Su (1992) and Cartmill and Su (1992). Using acoustic measurements of bubble sizes, they infer values for $\sigma_c(0)$ for a 30 kt wind that are in the range 150 m/s to 200 m/s, or approximately ten percent of the speed of sound in bubble-free water. Preliminary direct travel-time measurements of sound speed recently reported by Lamarre

and Melville (1993) for moderate sea states (winds less than 20 kt) also suggest near-surface sound speed fluctuations on the order of ten percent. Farmer and Vagle (1989), in contrast, have estimated near-surface average sound speed reductions of about 1 per cent. If we assume that the fluctuations in sound speed are on the same order of magnitude as the average sound-speed reduction, then our inferred value for $\sigma_c(0)$ and the measured values of Su, Cartmill and Su, and Lamarre and Melville are all significantly larger than the value inferred from the data of Farmer and Vagle. In the backscatter predictions in this article we use data for $\sigma_c(z)$ provided by Su (1992) since they are the only in-situ measurements presently available for high sea states.

It should be noted that although the Von Karman spectrum used here is isotropic at all scales, isotropy is a plausible approximation only in the inertial subrange. Even in the inertial subrange, measurements of temperature fluctuations show a clear departure from isotropy (Whitmarsh, et al., 1957). Fortunately, it is easy to generalize the scattering model to account for anisotropy in the normalized wavenumber spectrum $\hat{C}(\mathbf{K})$. For low grazing angle backscatter, the primary anisotropy, the vertical/horizontal anisotropy, affects only the normalization of the spectrum and not the spectral exponent β . To account for vertical/horizontal anisotropy , we simply multiply the normalized wavenumber spectrum for isotropic turbulence by a factor L_v/L_h , where L_v and L_h are, respectively, the outer scales associated with vertical and horizontal turbulence structure. Without oceanographic measurements of L_v and L_h , however, any attempt to theoretically account for anisotropy would be pure conjecture. Hence, in this article, we normalize the spectrum under the assumption of isotropy ($L_v = L_h = L_o$) realizing that such an assumption is crude at best. Ideally we would like to have a direct measurement of the spectrum, but, currently, no measurements exist.

C. RMS Sound-Speed Fluctuations Versus Depth

To complete the statistical description of the bubble layer, we need an estimate of the rms sound-speed fluctuation as a function of depth. As discussed in Section I, we use an exponential fitting function of the form $\sigma_c(z) = \sigma_c(0)e^{-z/L}$, an approximation that is consistent with observed bubble distributions (Thorpe, 1982 ; Farmer and Vagle, 1989; Su, 1992; Su et al., 1993). For the backscatter predictions in a 30-kt wind presented in the next section, the function $\sigma_c(z)$ was fitted to the rms sound-speed measurements of Su (1992) from a measurement site in the Northeast Pacific in winter conditions. A least-squares fit to the measured values of σ_c versus depth gives an rms sound-speed fluctuation at the surface of $\sigma_c(0) = 207$ m/s and an e-folding distance of L=1.95. In the next section, the fitted values for $\sigma_c(0)$ and L, together with the above result for $\hat{C}(K)$ are used in Eqs.(30)-(32) to compute the backscatter cross section.

III. COMPARISON OF BACKSCATTER PREDICTIONS WITH EXPERIMENT

In the previous section we proposed a wavenumber spectrum for use in a stochastic scattering model. In this section we use the proposed spectrum and the stochastic scattering model to make predictions for backscatter from the oceanic bubble layer. We compare the predictions with the experimental results reported by Ogden and Erskine (1992) for the Critical Sea Tests (CST). The purpose of the comparison is to show that with oceanographically constrained parameters (no "adjustable" parameters) the stochastic model can give a good account of the measured backscatter as function of both frequency and angle.

We consider two sets of calculations. The first set uses the empirically determined value of $\beta = 3.86$ and the second uses the Kolmogorov value for the inertial subrange, $\beta = 11/3 = 3.67$. In both calculations we use the normalized Von Karman spectrum with an outer scale of $L_0 = 106$ m, which was the average mixed layer depth for a 30 kt wind during the CST-7 experiment (Farmer, 1992). As discussed in the previous section, the rms sound-speed fluctuation profile was fitted to measured data of Su (1992) for a 30 kt wind.

Figure 4 compares the predicted scattering strength-vs-grazing angle at several frequencies with the Ogden-Erskine empirical fits to CST data. Since at very low frequencies, surface scattering can be the dominant scattering mechanism, we have for completeness included two theoretical curves, one that includes both bubble layer scattering and rough surface scattering(solid line), and one with only bubble layer scattering(dashed line). The rough surface contribution is from Thorsos (1990) and is added incoherently to the bubble-layer contribution. Figure 5 shows the backscatter as a function of the frequency for several different fixed grazing angles. Since the solid and dashed lines in Figs. 4 and 5 overlay except at very low frequencies, we can see that the main scattering contribution is from the bubble layer.

Figures 6 and 7 are the same as Figs 4 and 5 except the Kolmogorov value of $\beta=11/3=3.67$ was used instead of $\beta=3.86$. With $\beta=3.67$ the agreement with the CST data is not quite as good as with $\beta=3.86$, but nevertheless is satisfactory and shows that Kolmogorov's theory for inertial subrange turbulence is consistent with the observed backscatter.

IV. SUMMARY AND CONCLUSIONS

A stochastic scattering model based on the wavenumber spectrum for sound-speed fluctuations in the oceanic bubble layer has been derived. The model was used to analyze data from 12 different measurements of surface backscatter. From the analysis it was found that the effective horizontal wavenumber spectrum for sound-speed fluctuations in the bubble layer is an inverse power law of the form $P(K)=AK^{-\beta}$, where A is a strength parameter, K is the horizontal wavenumber, and the mean value of the spectral roll-off exponent is $\beta = 3.86 \pm .45$. The universal character of β suggests that the small-scale structure of the microbubble distribution (scales < 5 - 10 m) is governed by turbulent mixing due to turbulence in the inertial subrange. Moreover, using a spectrum based on the notion of inertial subrange turbulence and observed oceanographic parameters, good agreement was obtained with measurements from the Critical Sea Test surface backscatter experiments.

Although the stochastic scattering model , with no adjustable parameters, gives good agreement with surface backscatter data, there nevertheless is a need for further oceanographic measurements to establish the physical validity of the model. Since the backscatter depends on the square of the rms sound-speed fluctuation, the most important experiment is a direct sound-speed measurement to confirm the measurements of Su (1992) where $\sigma_c(z)$ was inferred indirectly from acoustic estimates of the bubble size distribution. The next most important measurement is to determine whether or not an inertial subrange actually exists in the spectrum of the sound-speed fluctuations. Establishing that β is exactly 11/3 is not as important as determining whether the bubble distribution is systematically controlled by small-scale turbulence. In fact, since the value 11/3 applies to fully developed isotropic turbulence, it would not be surprising if the effective value for β in the bubble layer were not exactly 11/3. Finally, an important and hopefully possible task would be to relate the observed wavenumber spectrum for sound-speed fluctuations in the

bubble layer to environmental parameters such as windspeed, air/sea temperatures, and sea state. To accomplish such a task would require that the wavenumber spectrum and the associated environmental parameters be measured under a variety of conditions so that predictive models could be tested.

We have presented evidence that scattering from microbubbles in the near-surface bubble layer is as strong as any other surface scattering mechanism, but we have not shown that it is the sole mechanism. If, for example, scattering from dense, near-surface bubble plumes under breaking waves were equally strong, the cross-section would be raised by 3 dB, an amount that is within the experimental error in the measurements. Thus, until more definitive measurements are made, the stochastic model presented here must be viewed as one of a number of mechanisms that can contribute significantly to surface backscatter.

ACKNOWLEDGMENTS

I thank Dr. R.R. Goodman for encouragement and for many enjoyable and useful discussions. I am grateful to Dr. M.Y. Su for providing data on sound-speed fluctuations in the bubble layer. In the first part of the investigation I was ably assisted by Mr. Lintao Wang at the National Center for Physical Acoustics. For valuable assistance in completing the research, I thank Mr. Tim Kulbago and Ms. Lucy Ameling of the Graduate Program in Acoustics, Pennsylvania State University. Funding for the work was provided by the Office of Naval Research.

REFERENCES

Brown, J.R., Scrimger, J.A. and Turner, R.G. (**1962**). "Reverberation from the ocean surface," Pacific Naval Laboratory, Esquimalt, B.C., Canada, Technical Memorandom 66-8.

Carstensen, E.L., and Foldy, L.L.(**1947**). "Propagation of sound through a liquid containing bubbles," J. Acoust. Soc. Am. **19**, 481-501.

Cartmill, J., and M.Y. Su (**1992**). " Characteristics of near-surface, low-frequency sound speeds," J. Acoust. Soc. Am. **92**, 2348 (A).

Chapman, R.P., and J.H. Harris (**1962**). "Surface backscattering strengths measured with explosive sound sources," J. Acoust. Soc. Am. **34**, 1592-1597 .

Chapman, R.P., and Scott, H.D. (**1964**). "Surface backscattering strengths measured over an extended range of frequencies and grazing angles," J. Acoust. Soc. Am. **36**, 1735-1737 .

Clifford, S.F. (**1978**). "The Classical Theory of Wave Propagation in a Turbulent Medium," in *Laser Beam Propagation in the Atmosphere*, edited by J.W. Strohbehn (Springer-Verlag, New York).

Commander, K.W. (**1992**). "High-frequency surface scattering phenomena in high sea states," J. Acoust. Soc. Am. **91**, 2319 (A)

Corrsin, S., (**1951**)."On the spectrum of isotropic temperature fluctuations in an isotropic turbulence," J. of Applied Physics, **22**, 469-473.

Embleton, T.F.W. and G.A. Daigle, G.A. (**1991**). "Atmospheric Propagation," in Aeroacoustics of Flight Vehicles: Theroy and Practice, edited by H.H. Hubbard (NASA Langley Research Center, Hampton, VA [NASA Ref. Pub. 1258, Vol. 2; also WRDC Tech. Rep. 90-3052 , Chap. 12].

Farmer, D.M., and Vagle, S. (**1989**). "Waveguide propagation of ambient sound in the ocean surface bubble layer," J. Acoust. Soc. Am. **86**, 1897-1908 .

Farmer, D.M., (**1992**). Cruise Report, CSS John P. Tully, 17February to 6March, 1992, Institute of Ocean Sciences, Sidney, B.C. Canada.

Foldy, L.L., (**1945**). "The multiple scattering of waves," Physical Review, **47**, 107-119.

Grant, H.L., Hughes. B.A., Vogel, W.M., and Moillet, A. (**1968**)." The spectrum of temperature fluctuations in turbulent flow," J. Fluid Mech., **34**, 423-442.

Grant, H.L., Stewart, R.W., and Moillet, A. (**1962**). "Turbulence spectra from a tidal channel," J. Fluid Mech., **12** , 241-263.

Hinze, J.O., (**1959**). *Turbulence*, (McGraw-Hill, New York)

Henyey, F.S., (**1991**). "Acoustic scattering from ocean microbubble plumes in the 100 Hz to 2 kHz region." J.Acoust. Soc. Am. **90**, 399-405.

Henyey, F.S., Farmer, D.M., and Vagle, S. (**1992**) "Using acoustic scattering (high frequency) to predict acoustic scattering (low frequency)," J. Acoust. Soc. Am. **91**, 2314 (A).

Jin, G., Li, Y.,Yang, Y., Li, Z.,Wu, X., and Liu, L. (**1989**)."Deep ocean reverberation measurement in the south China Sea," Technical Acoustics Vol. 8, No. 1, pp 8-11. (in Chinese)

Lamarre, E., and Melville, W.K. (**1993**). "Direct measurements of sound speed in the oceanic surface bubbly layer," J. Acoust. Soc. Am., **93**, 2379 (A)

Landau, L.D., and Lifshitz, E.M. (**1959**). *Fluid Mechanics*, (Addison-Wesley, Reading)

Langmuir, I. (**1938**). "Surface motion of water induced by wind," Science vol. 87 no. 2250, 119-123 .

McDaniel, S.T. (**1988**). "High-frequency scattering from the sea-surface: Recent Progress," J. Acoust. Soc. Am. Suppl. 1 **84**, S121.

McDaniel, S.T. (**1993**) "Sea surface reverberation: A review," submitted to J. Acoust. Soc. Am. .

McDonald, B.E. (**1991**). "Echoes from vertically striated subresonant bubbles clouds: A model for ocean surface reverberation," J. Acoust. Soc. Am. **89**, 617-622 .

Morse, P.M., and Feshbach, H. (**1953**). *Methods of Theoretical Physics*, (McGraw-Hill, New York) pp1501-1502

Neumann, G., and Pierson Jr., W.J. (**1966**). "Principles of Physical Oceanography," (Prentice-Hall, Inc., Englewood, N.J.).

Ogden, P.M., and Erskine, F.T. (**1992**)"An empirical prediction algorithm for low-frequency acoustic surface scattering strengths," Naval Research Laboratory Report NRL/FR/5160-92-9377.

Osborn, T., Farmer, D. M., Vagle S., Thorpe, S.A., and Cure, M. (**1992**). "Measurements of bubble plumes and turbulence from a submarine, Atmosphere-Ocean 30 (3), 419-440.

Percy, J.L. (**1970**). "Surface backscattering strengths from several FASOR II deep-water stations," Naval Undersea Research and Development Center Technical Publication NUC TP 185.

Rodberg, L.S., and Thaler, R.M. (**1967**). *Introduction to the Quantum Theory of Scattering*, (Academic Press, New York).

Su, M.Y. (**1992**). personal communication.

Su, M.Y., and Cartmill, J.(**1992**). "Generation and dispersion of near-surface bubble densities," J. Acoust. Soc. Am., **92**, 2348 (A)

Su, M.Y., Burge, R., and Cartmill, J. (**1993**). "Measurement of near-surface microbubble density during SWADE," J. Geophysic. Res.: Oceans. (to appear)

Tatarski, V.I. (**1961**). *Wave Propagation in A Turbulent Medium*, (McGraw-Hill, New York)

Thorpe, S. A. (**1982**). "On the clouds of bubbles formed by breaking windwaves in deep water, and their role in air-sea gas transfer," Philos. Trans. R. Soc. London A 304, 155-210.

Thorpe, S.A., and Hall, A. J. (**1983**)."The characteristics of breaking waves, bubble clouds, and near-surface currents observed using side-scan sonar," Continental Shelf Research **1**, 353-384.

Thorpe, S.A. (**1984**). "The effect of Languir circulation on the distribution of submerged bubbles caused by breaking wind waves," J. Fluid Mech. **142**, 151-170.

Thorsos, E. I. (**1990**). "Acoustic scattering from a 'Pierson-Moskowitz' sea surface," J. coust. Soc. Am. **88**, 335-349.

.ĸ, R.J. (**1975**). *Principles of Underwater Sound,* 2nd Edition, (McGraw-Hill, New ..ork) p. 224.

Urick, R.J., and Hoover, R.M.(**1956**). "Backscattering of sound from the sea surface: its measurement causes, and application to the prediction of reverberation levels," J. Acoust. Soc. Am. **28**, 1038-1042.

Voorhis, A.D., and Perkins, H.T. (**1966**). "The spatial spectrum of short-wave temperature fluctuations in the near-surface thermocline," Deep-Sea Research 13, 641-654.

Whitmarsh, D.C., Skudrzyk, E., and Urick, R. (**1957**). "Forward scattering of sound in the sea and its correlation with temperature microstructure," J. Acoust. Soc. Am. **29**, 1124-1143 (1957).

FIGURE CAPTIONS

Fig. 1. Backscatter strength versus frequency for a grazing angle of 20°. Note the common weak dependence on frequency at frequencies above a few kilohertz.

Fig. 2. Horizonal wavenumber spectra for sound-speed fluctuations in the bubble layer. The spectra were inferred from the backscatter versus frequency curves in Fig. 1. The form of the spectra is $P(q_h) = A\, q_h^{-\beta}$ where A is a strength parameter and β is a spectral roll-off exponent. The quantity q_h is $2k_h$, where k_h is the horizontal wavenumber.

Fig. 3. The spectral roll-off exponent β versus windspeed for 12 different backscatter measurements. There appears to be little dependence on windspeed. The approximately constant value of $\beta = 3.86$, is a result of the weak frequency dependence seen in Fig. 1. The nearly universal value of β suggests that the wavenumber spectrum of sound-speed fluctuations in the bubble layer is governed by a model-independent mechanism such as inertial subrange turbulence (Kolmogorov turbulence) for which $\beta = 11/3 = 3.67$ for fully developed isotropic turbulence.

Fig. 4. Scattering strength versus grazing angle at several fixed frequencies using the empirical value of β=3.86. The dashed line is backscatter just from the bubble layer. The solid line is the incoherent sum of bubble layer scattering and rough surface scattering. The diamonds are the Ogden-Erskine empirical fit to the Critical Sea Test data.

Fig. 5. Same as Fig. 4 except that the grazing angles are fixed and the frequency is varied.

Fig. 6. Same as Fig. 4 except the Kolmogorov value of $\beta = 11/3 = 3.67$ is used.

Fig. 7. Same as Fig. 4 except the grazing angles are fixed and the frequency is varied. Also the Kolmogorov value of $\beta = 11/3 = 3.67$ is used.

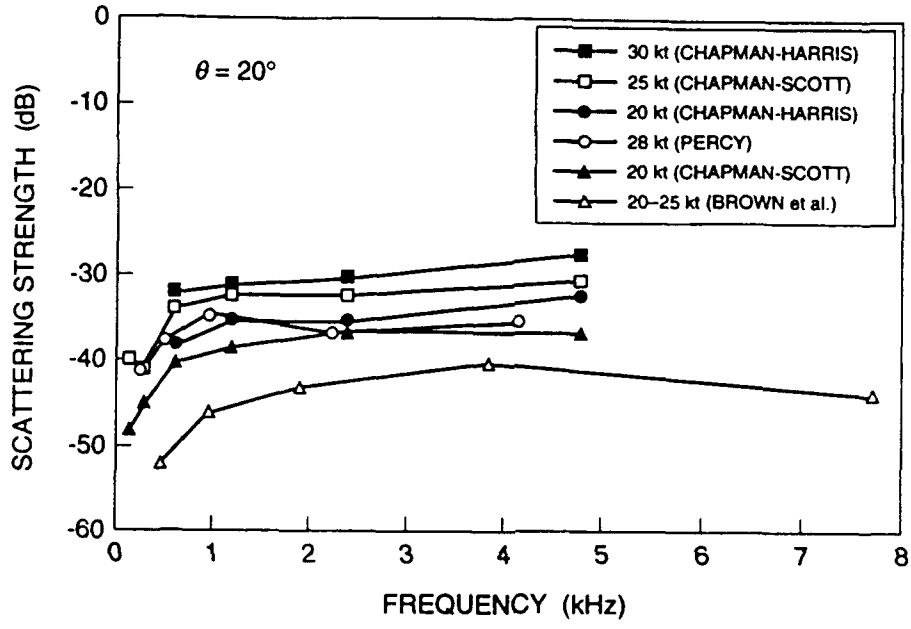
θ = 20°
30 kt (CHAPMAN-HARRIS)
25 kt (CHAPMAN-SCOTT)
20 kt (CHAPMAN-HARRIS)
28 kt (PERCY)
20 kt (CHAPMAN-SCOTT)
20–25 kt (BROWN et al.)
SCATTERING STRENGTH (dB)
0
-10
-20
-30
-40
-50
-60
0
1
2
3
4
5
6
7
8
FREQUENCY (kHz)

Fig. 1

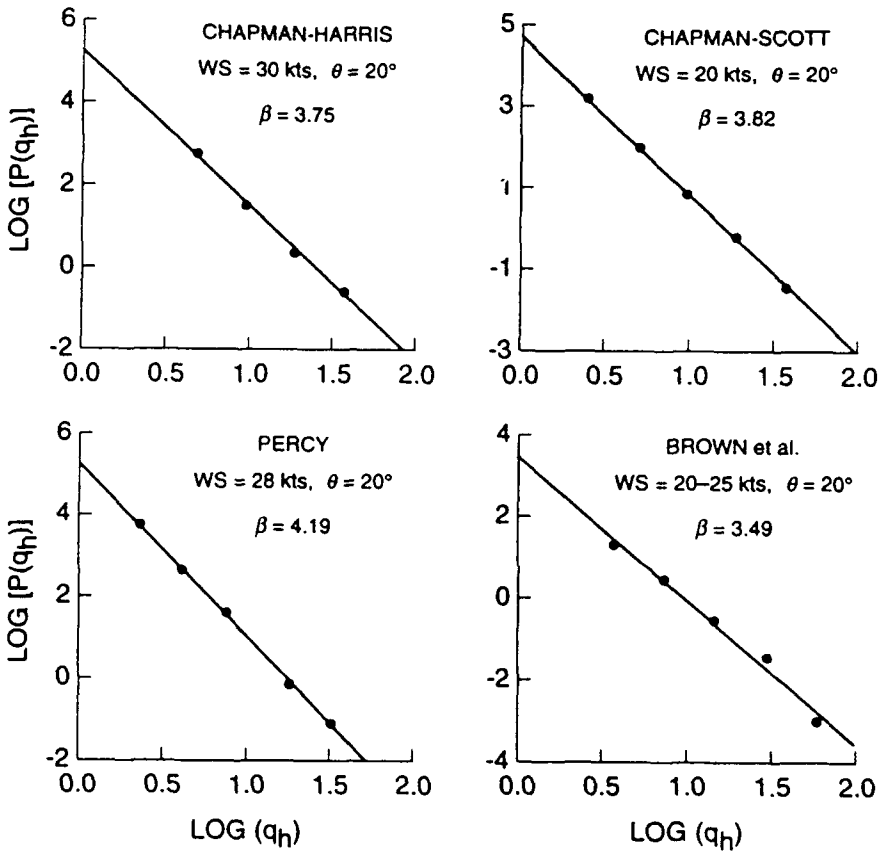
CHAPMAN-HARRIS
WS = 30 kts, θ = 20°
β = 3.75
CHAPMAN-SCOTT
WS = 20 kts, θ = 20°
β = 3.82
PERCY
WS = 28 kts, θ = 20°
β = 4.19
BROWN et al.
WS = 20–25 kts, θ = 20°
β = 3.49
LOG [P(qh)]
LOG (qh)

Fig. 2

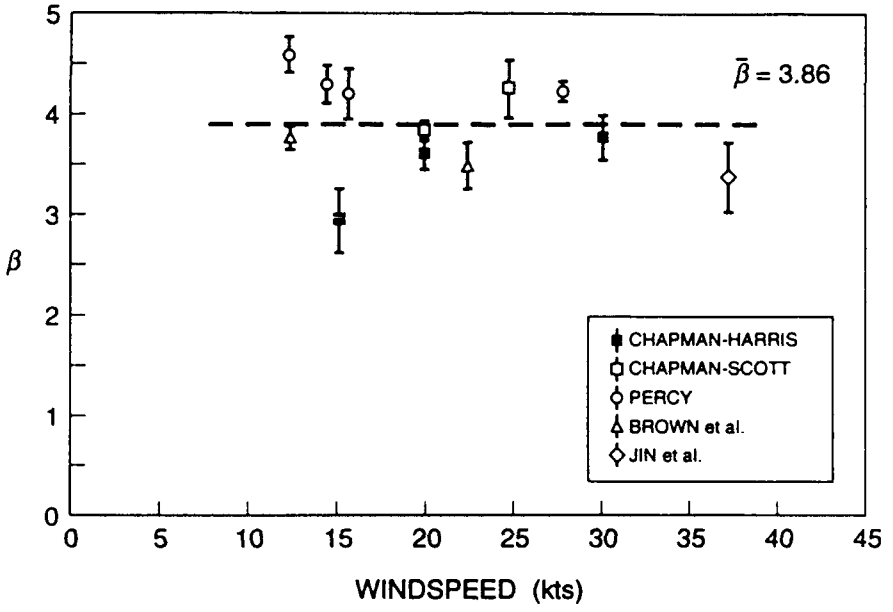
$\bar{\beta}$ = 3.86
β
CHAPMAN-HARRIS
CHAPMAN-SCOTT
PERCY
BROWN et al.
JIN et al.
0
1
2
3
4
5
0
5
10
15
20
25
30
35
40
45
WINDSPEED (kts)

Fig. 3

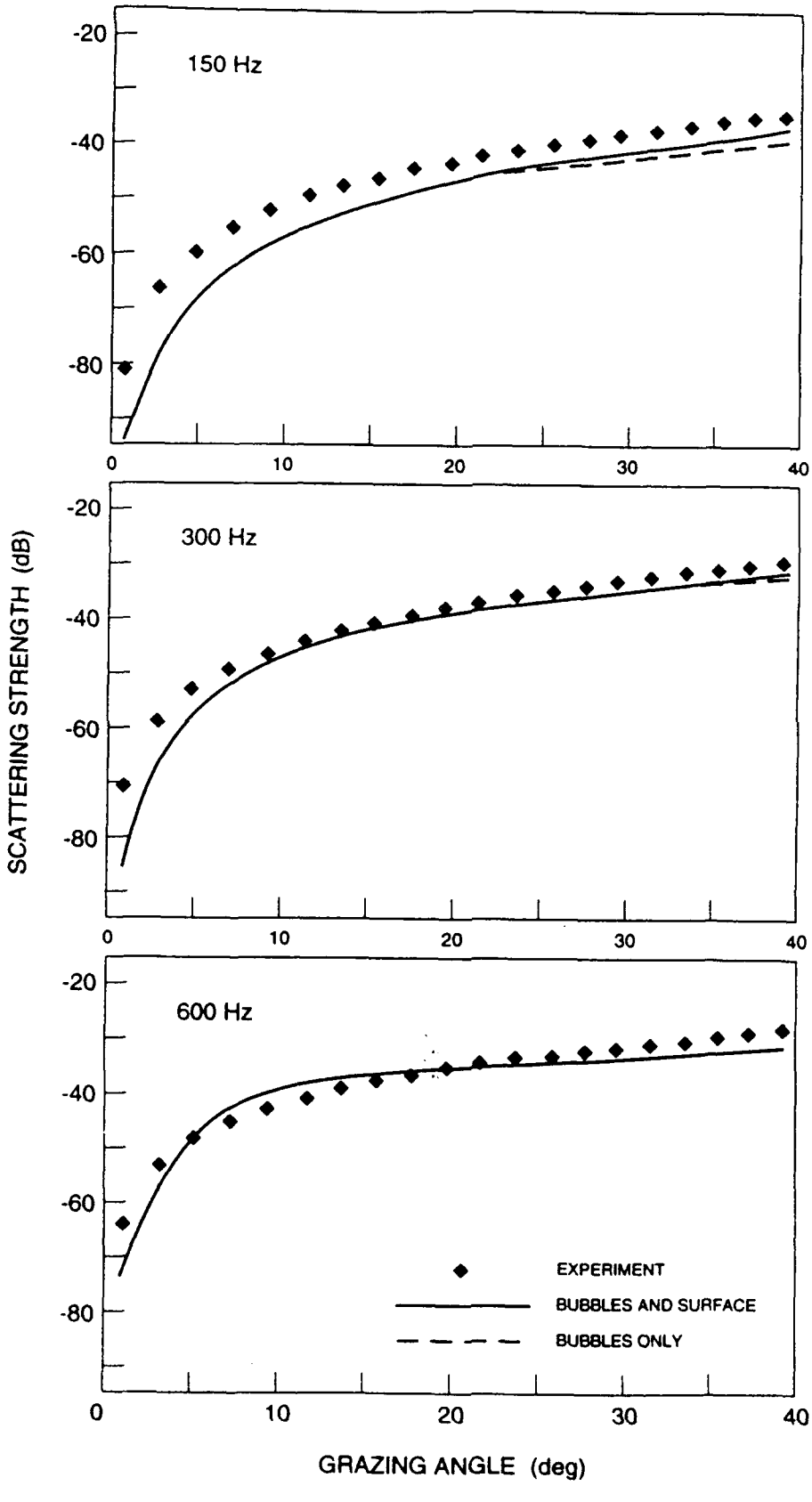
150 Hz
300 Hz
600 Hz
-20
-40
-60
-80
0
10
20
30
40
SCATTERING STRENGTH (dB)
GRAZING ANGLE (deg)
EXPERIMENT
BUBBLES AND SURFACE
BUBBLES ONLY

Fig 4

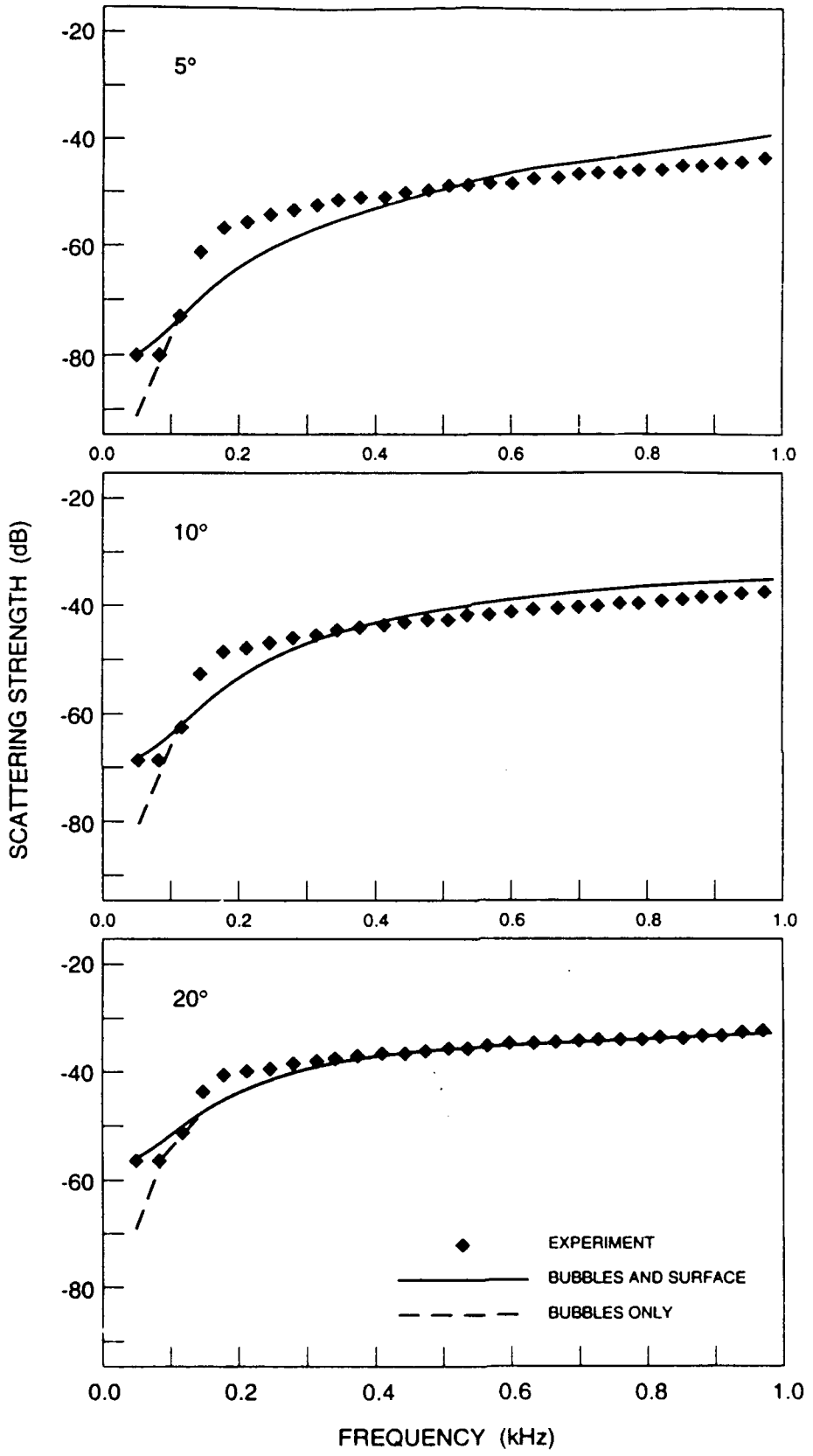
5°
10°
20°
-20
-40
-60
-80
0.0
0.2
0.4
0.6
0.8
1.0
SCATTERING STRENGTH (dB)
FREQUENCY (kHz)
EXPERIMENT
BUBBLES AND SURFACE
BUBBLES ONLY

Fig. 5

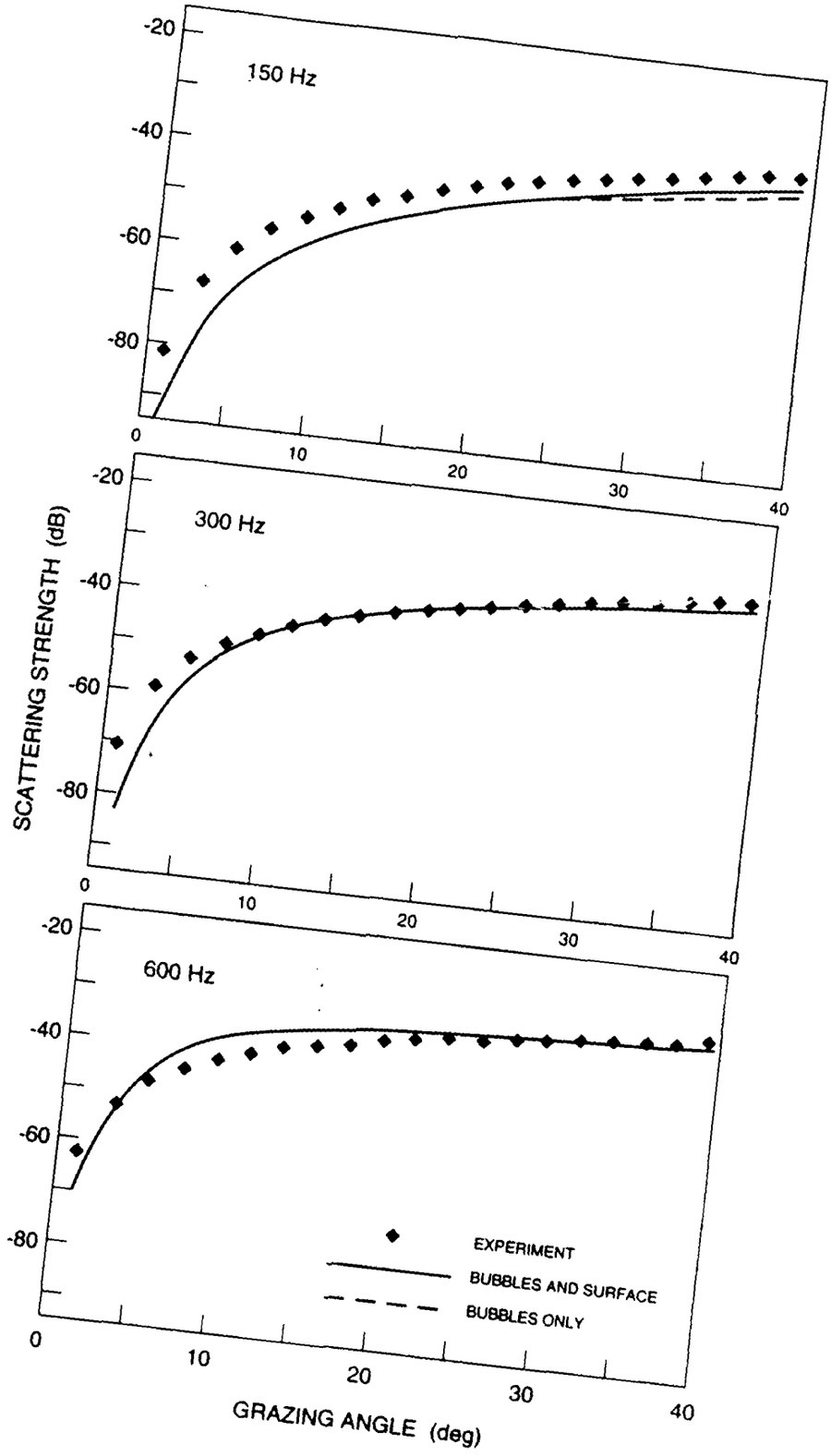

(ARL) KEG-304-07-md

Fig. 6

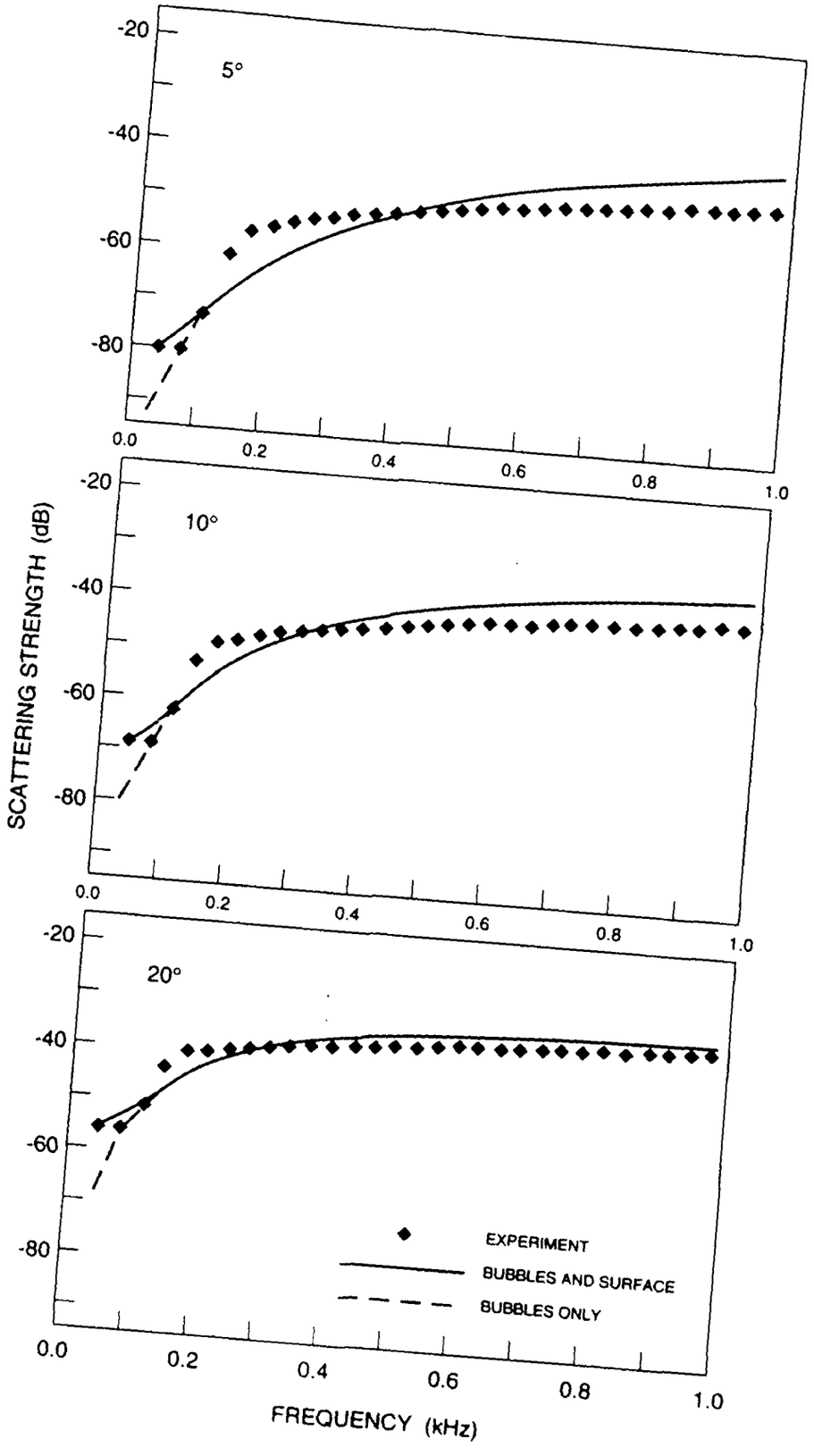

(ARL) KEG-304-06-md

Fig. 7

Transducer Development

Principal Investigator: M. A. Breazeale

Research Accomplished in 1992:

Most of the year was spent on transducer development and in completing the Ph.D. Dissertation of Dehua Huang; however, some of the time was spent in completing research supported in previous years under Navy Programs. These will be included in this Final Technical Report.

Ph.D. Dissertation of Dehua Huang. The Ph.D. Dissertation "Gaussian finite element method for description of underwater sound diffraction," was completed in August 1992. The dissertation describes a new method for solving diffraction problems. The method is based on the use of Gaussian diffraction theory. The Rayleigh integral is used to prove the core of Gaussian theory: the diffraction field of a Gaussian radiator also is described by a Gaussian function. The parabolic approximation used by previous authors is not necessary to this proof. Comparison of the Gaussian beam expansion and Fourier series expansion reveals that the Gaussian expansion is a more general and more powerful technique.

The method combines the Gaussian beam superposition technique [Wen and Breazeale, J. Acoust. Soc. Am. **83**, 1752-1756 (1988)] and the Finite element solution to the parabolic equation [Huang, J. Acoust. Soc. Am. **84**, 1405-1413 (1988)]. Computer modeling shows that the new method is capable of solving for the sound field even in an inhomogeneous medium, whether the source is a Gaussian source or a distributed source. It can be used for horizontally layered interfaces or irregular interfaces. Calculated results are compared with experimental results by use of a recently designed an improved Gaussian transducer in a laboratory water tank. In addition, the power of the Gaussian Finite element method is demonstrated by comparing numerical results with experimental results from use of a piston transducer in a water tank. A publication detailing these results is in preparation.

Patent Application. A patent application has been filed to cover the advances made in the fabrication of a Gaussian transducer. The patent in the names of Dehua Huang and M. A. Breazeale has been filed by Airmar Technology Corporation, current employer of Dehua Huang, on December 8, 1992. It is anticipated that a number of licenses will be issued for various applications of the Gaussian principle to different situations.

Elastic Nonlinearities in Single Crystal Gallium Arsenide. Experimental investigation of single crystal gallium arsenide nonlinearity has been completed and the results have been published. Gallium arsenide is a technologically important crystal whose nonlinearity had not been investigated. The harmonic generation technique is ideally suited for measurement of a set of third order elastic constants of this material, and the variation of ultrasound velocity with applied hydrostatic pressure completes the set of six third order elastic constants. By using a modification of the Keating theory for cubic lattice solids we were able to obtain a complete set of third order elastic constants between 77K and 300K.

Nonlinear Techniques for Nondestructive Evaluation of Composites. A new investigation has been opened up with the use of nonlinear techniques to investigate composites and heat damage in composites. Since very little scientific information is available about the physical behavior of composites, it is highly desirable that new techniques, such as the harmonic generation technique, be applied to collection of data on composites. It also desirable to use more standard techniques to collect data on composites. Tentative measurements have been made of the behavior of composites. Tentative measurements have been made of the behavior of composites. We find that the velocity in the basal plane is approximately one-third of that in the axial direction. Thus, composites are highly anisotropic the behavior of composites; however, it is clear that primitive cells in composites are not hexagonal. Thus, much is to be learned about the linear and the nonlinear physical properties of composites.

Publications:

1. "Elastic Nonlinearities in Single Crystal Gallium Arsenide Between 77 and 300^{o}K", M. A. Breazeale, D. Joharapurkar and D. Gerlich, in Proceedings of 14th International Congress on Acoustics, Vol. 1A, Li Peizi, Ed., Academia Sinica, Paper A1-1 (1992).
2. "Nonlinear Acoustics and How She Grew", M. A. Breazeale, in Review of Progress in Quantitative Nondestructive Evaluation, Vol. 11B, D. O. Thompson and D. E. Chimenti, eds., Plenum Press, New York, pp. 2015-2023 (1992).
3. "Temperature Dependence of Elastic Nonlinearities in Single Crystal Gallium Arsenide," D. Joharapurkar, D. Gerlich and M. A. Breazeale, Journal of Applied Physics, 72, 2202-2208 (1992).
4. "Electric Potential in Piezoelectric Medium and its Influence on Measurement of the Ultrasonic Nonlinearity Parameter," W. Jiang, G. Du and M. A. Breazeale, in Proceedings of 14th International Congress on Acoustics, Vol. 1A, Li Peizi, ed., Academia Sinica, Paper A1-5 (1992).
5. "Nonlinear Techniques for Nondestructive Evaluation of Composites," M. A. Breazeale, in Proceedings of Conference on Characterization and NDE of Heat Damage in Graphite Epoxy Composites, Orlando, FL, April 27-28, 1993.

ELASTIC NONLINEARITIES IN SINGLE CRYSTAL GALLIUM ARSENIDE BETWEEN 77 AND 300 K

M. A. BREAZEALE, D. N. JOHARAPURKAR AND D. GERLICH

National Center for Physical Acoustics, Coliseum Drive, University, MS 38677, USA

Third order elastic (TOE) constants are necessary to a fundamental description of many physical properties of solids resulting from lattice nonlinearity. The properties in question include thermal expansion, heat conduction, temperature dependence of the specific heat, temperature and pressure dependence of the elastic constants, difference between the adiabatic and isothermal elastic constants, phonon viscosity, thermal attenuation of acoustic waves, shock deformation of materials, acoustically induced static stress and strain, etc. Previously[1,2] we have shown that measurement of ultrasonic harmonic generation gives information about combinations of TOE constants from helium temperatures to at least 350° K. Since no single technique gives all six TOE constants of cubic crystals it was necessary to introduce a second technique in order to plot all six of the TOE constants of the semiconductor Gallium Arsenide (GaAs) over a wide temperature range. The purpose of this report is to describe the technique used because it makes optimum use of theory and experiment to arrive at data which would not be available otherwise. The technique should be applicable without modification to the evaluation of all TOE constants of all zincblende structure compounds. The data on GaAs verify its validity.

Measurement of Harmonic Generation

The propagation of a finite amplitude ultrasonic wave along the three principal directions in a cubic lattice is described by

$$\rho_0 \frac{\partial^2 U}{\partial t^2} = K_2 \frac{\partial^2 U}{\partial a^2} + (3K_2 + K_3) \frac{\partial U}{\partial a} \frac{\partial^2 U}{\partial a^2} . \qquad (1)$$

Assuming an initially sinusoidal wave allows one to write a solution in the form

$$U = A_1 \sin(ka - \omega t) + A_2 \cos 2(ka - \omega t) + \ldots \qquad (2)$$

where

$$A_2 = -\left[3 + \frac{K_3}{K_2}\right] A_1^2 k^2 x . \qquad (3)$$

Defining the nonlinearity parameter

$$\beta = -\left[3 + \frac{K_3}{K_2}\right] \qquad (4)$$

allows one to write the nonlinearity parameters in terms of measured quantities

$$\beta = \frac{A_2}{A_1^2 k^2 x} . \qquad (5)$$

where $k = \frac{2\pi}{\lambda}$ is the propagation constant and x is the sample length. In terms of TOE constants the nonlinearity parameters along the principal directions are

$$\beta_{100} = -\left[3 + \frac{C_{111}}{C_{11}}\right]$$

$$\beta_{110} = -\left[3 + \frac{C_{111} + 3C_{112} + 12C_{166}}{2(C_{11} + C_{12} + 2C_{44})}\right] \qquad (6\ a,b,c)$$

$$\beta_{111} = -\left[3 + \frac{C_{111} + 6C_{112} + 12C_{144} + 24C_{166} + 2C_{123} + 16C_{456}}{3(C_{11} + 2C_{12} + 4C_{44})}\right]$$

By measuring the amplitudes A_2, A_1, the frequency (from which k can be calculated), and the sample length x in the principal directions one can evaluate the nonlinearity parameters. The results for GaAs are shown in Fig. 1 plotted between 77° K and room temperature.

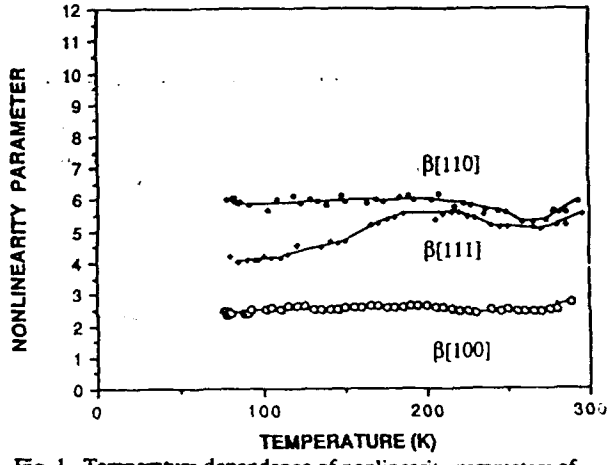

Fig. 1. Temperature dependence of nonlinearity parameters of GaAs.

To evaluate the individual TOE constants from these data, additional information is needed. The Keating[3] theory is a three-parameter theory from which one can calculate all six TOE constants. Thus, in principle these data plus the Keating theory would be sufficient to isolate all six TOE constants of GaAs. We chose to provide additional experimental data, however.

Measurement of Pressure Variation of Sound Velocity

The most accurate evaluation of TOE constants of cubic crystals at room temperature appears to come from the combination of harmonic generation data with those taken by use of pressure variation of ultrasonic wave velocity.[4] A pressure bomb was used to take pressure variation data at room temperature with the same GaAs samples. A plot of the normalized frequency (essentially sound velocity) as a function of pressure is given in Fig. 2. The curves all are straight lines except for the longitudinal wave in the [111] direction (labelled [111],[111] in Fig. 2). The slopes of these curves can be used to calculate combinations of TOE constants at room temperature.

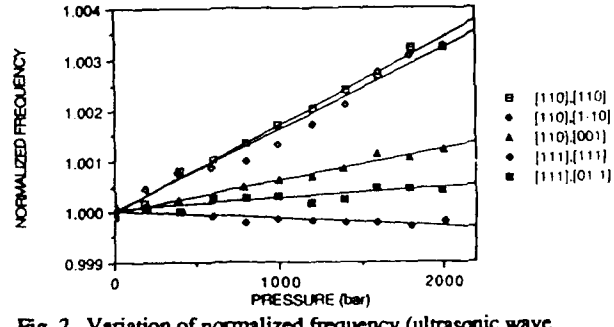

Fig. 2. Variation of normalized frequency (ultrasonic wave velocity) with pressure in GaAs.

Results

The results of the two sets of measurements can be combined to isolate all six TOE constants at room temperature. The results have been evaluated for GaAs and compared with room temperature values of other researchers. Having these values one now is able to use the Keating model along with the harmonic generation data to calculate the temperature dependence of each TOE constant. Results of the values of all six TOE constants of GaAs between room temperature and liquid nitrogen temperature are given in Figs. 3 and 4 in which the curves are least squares fits of the data with a fifth order polynomial. Most of the

TOE constants are linear functions of temperature; however, both C_{112} and C_{123} exhibit remarkable temperature variations and emphasize the importance of being able to measure these fundamental parameters over a range of temperatures.

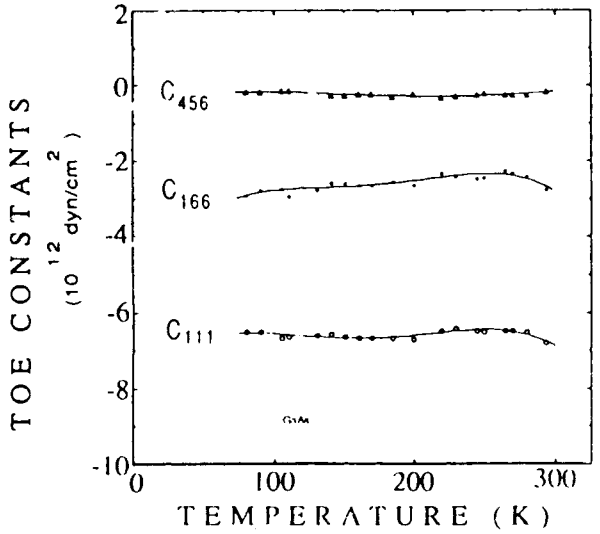

Fig. 3. Temperature dependence of TOE constants C_{111}, C_{166} and C_{456}.

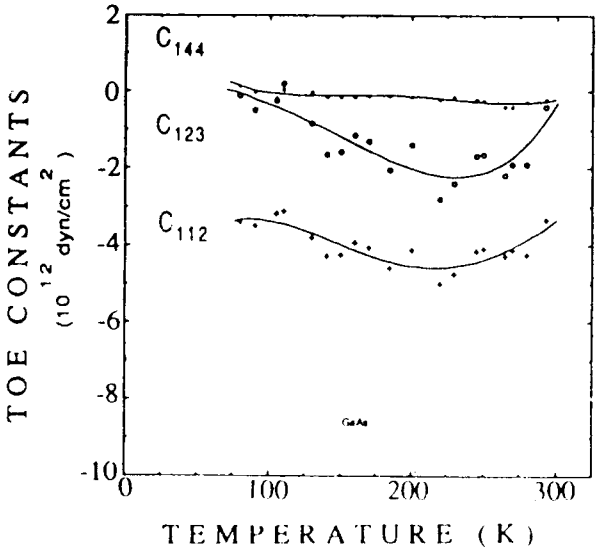

Fig. 4. Temperature dependence of C_{112}, C_{123} and C_{144}.

Cauchy Relations

Although the Cauchy relations usually are evaluated for the second order elastic constants (from the sound velocity), they also can be evaluated for the TOE constants as well. If all lattice interactions are of the central force type, and each atom is a center of symmetry, then all elastic constants should obey the Cauchy relations. For the TOE constants the Cauchy relations are

$$C_{112} = C_{155} \quad (7)$$

$$C_{123} = C_{144} = C_{456} \quad (8)$$

If in addition the short range repulsive interaction is the dominant one, there are the so-called "strong" Cauchy relations

$$C_{111} = 2C_{112} = 2C_{155} \quad (9)$$

$$C_{123} = C_{144} = C_{456} = 0 \quad (10)$$

We have examined the strong Cauchy relations over the available temperature range by comparing the measured quantities $C_{112} + 4C_{155}$ and $C_{123} + 6C_{144} + 8C_{456}$ with $\frac{5}{2}C_{111}$ and find that there is a tendency for better agreement with the TOE constant Cauchy relations as 0K is approached. Since both the Keating model and the Cauchy relations strictly should apply only at 0K, this may indicated that the lattice interaction in GaAs is basically of the central type, and the deviations from the Cauchy relations are caused by thermal effects. An analogous observation has been made for germanium and silicon.[1]

Summary

All six TOE constants of GaAs have been evaluated between room temperature and liquid nitrogen temperatures. Two of the TOE constants, C_{112} and C_{123}, exhibit considerable variation, (at least a factor of 10 for C_{123}). The other four are almost linear functions of temperature.

The technique we have used can be applied directly to evaluation of the TOE constants of all zincblende structure compounds. Other structures or samples in which interstitials or dislocations are prominent require further analysis.

References

1. M.A. Breazeale and Jacob Philip, in Physical Acoustics, W.P. Mason and R.N. Thurston, eds., Vol. XVII, Academic Press, New York, pp. 1-60 (1984).
2. Wenwu Cao, Gerhard R. Barsch, Wenhua Jiang, and M.A. Breazeale, Phys. Rev. B38, 10244-10254 (1988).
3. P.N. Keating, Phys. Rev. 145,, 637 (1964); Phys. Rev. 149, 674 (1966).
4. M.A. Breazeale, Jacob Philip, A. Zarembowitch, M. Fischer and Y. Gesland, J. Sound and Vibration 88, 133-140 (1983).

Acknowledgement

Research supported in part by the University of Mississippi and by the U.S. Navy. M. A. Breazeale is on assignment from the University of Tennessee; present addresses: D. Joharapurkar, Department of Physics, Sindhu Mahavidyalaya, Nagpur 4400017, INDIA ; D. Gerlich, School of Physics and Astronomy, Raymond and Beverly Sackler Faculty of Exact Science, Tel Aviv University, Tel Aviv 69978, ISRAEL.

NONLINEAR ACOUSTICS AND HOW SHE GREW

M. A. Breazeale

National Center for Physical Acoustics
University of Mississippi
University, MS 38677

INTRODUCTION

When I was asked to review the progress in nonlinear acoustics I realized that considerable progress recently has been made even in a relatively restricted field, the nonlinear acoustics of solids. For example, there recently was a correlation of the nonlinearity parameter in zincblende structure crystals with interatomic potential functions.[1] Later a generalization[2] showed that in essentially all symmetries of crystalline solids one finds that the nonlinearity parameter depends exclusively on the Born-Mayer hardness parameter, meaning that in all crystalline solids the magnitude of the nonlinearity parameter is largely determined by the shape of the interatomic potential function. Furthermore, with crystalline solids having a larger nonlinearity parameter one finds an increasingly important zero-point energy contribution.[2] The nonlinearity parameter also has been correlated with the Anderson-Grüneisen parameter in solids[3] and temperature dependence of the third order elastic constants of NaCl-structure alkalide halide crystals.[4] Of more technological interest is the fact that the nonlinearity parameter has been correlated with the ultimate yield strength of isotropic solids[5] and with hardness in steels.[2] Nowadays the magnitude of the nonlinearity parameters of such inhomogeneous substances as muscle tissue[6], PZT ceramics[7] and high T_c superconductors[8] such as $YBa_2Cu_3O_{7-\delta}$, are being measured. Results on some of these materials form the substance of this report.

With the wide-ranging investigations to be reported, one tends to give the impression that there has been randomness in the development of nonlinear acoustics, that it "just grew" as my title implies. The truth is that it did. Nonlinear acoustics just grew. As early as 1660, Hooke discovered that we could get reasonable results just by ignoring nonlinearity. Subsequently, more subtle observations required a nonlinear theory. In this case there still was the desire to "keep things simple" and use only a linear theory. Whether or not the "linearization" worked depended on the detail desired in the agreement between experiment and theory. At that time the understanding of nonlinearity was not sufficient to allow one to predict where and how it would be encountered. This is the reason for the lack of systematic development. Early on, scientists did not understand that the nonlinear theory is the more fundamental one. Having become enlightened, some scientists now are developing a systematic approach to nonlinearity, but many of the developments have been random, analogous to the way Topsy in Uncle Tom's Cabin "just grew." Harriet Beecher Stowe wrote Uncle Tom's Cabin[9] in Stowe House near Bowdoin College, so it is appropriate that I quote directly from her description of Topsy so we can have a mental picture of how Topsy grew, and by analogy, how nonlinear acoustics grew.

Review of Progress in Quantitative Nondestructive Evaluation, Vol. 11
Edited by D.O. Thompson and D.E. Chimenti, Plenum Press, New York, 1992

One morning, while Miss Ophelia was busy in some of her domestic cares, St. Clare's voice was heard, calling her at the foot of the stairs.

"Come down here, cousin; I've something to show you."

"What is it?", said Miss Ophelia, coming down, with her sewing in hand.

"I've made a purchase for your department, -- see here," said St. Clare; and, with the word, he pulled along a little Negro girl, about eight or nine years of age.

- - - - - -

Sitting down before her, she began to question her.

"How old are you, Topsy?"

"Dunno, Missis," said the image, with a grin that showed all her teeth.

"Don't know how old you are? Did n't anybody ever tell you? Who was your mother?"

"Never had none!" said the child, with another grin.

"Never had any mother? What do you mean? Where were you born?"

"Never was born!" persisted Topsy, with another grin, that looked so goblin-like, that, if Miss Ophelia had been at all nervous, she might have fancied that she had got hold of some sooty gnome from the land of Diablerie; but Miss Ophelia was not nervous, but plain and business-like, and she said, with some sternness, --

"You mus n't answer me in that way, child; I 'm not playing with you. Tell me where you were born, and who your father and mother were."

"Never was born reiterated the creature, more emphatically; 'never had no father nor mother, nor nothin'. I was raised by a speculator, with lots of others. Old Aunt Sue used to take car on us."

The child was evidently sincere; and Jane, breaking into a short laugh, said, --

"Laws, Missis, there 's heaps of 'em. Speculators buys 'em up cheap, when they's little, and gets 'em raised for market."

"How long have you lived with your master or mistress?"

"Dunno, Missis."

"Is it a year, or more, or less?"

"Dunno, Missis."

"Laws, Missis, those low Negros, -- they can't tell; they don't know anything about time," said Jane; "they don't know what a year is; they don't know their own ages."

"Have you ever heard anything about God, Topsy?"

The child looked bewildered, but grinned as usual.

"Do you know who made you?"

"Nobody, as I knows on," said the child, with a short laugh.

The idea appeared to amuse here considerably; for her eyes twinkled, and she added, --

"I spect I grow'd. Don't think nobody never made me."

This is my impression of the subject of nonlinear acoustics. I have yet to find somebody who claims to be the father of the subject, and I doubt that I will meet the mother. The subject "just grow'd." Almost twenty years ago I made some observations for the International Journal of Nondestructive Testing.[10] The conclusion written at that time bears repeating, for I think it will set the tone for this entire session.

> Nonlinear behavior of solids in which finite amplitude ultrasonic waves propagate can be demonstrated. It can also be predicted from an extension of elasticity theory. It is hoped that some of the phenomena observed can serve as the basis of new, exceptionally sensitive nondestructive testing techniques.

Since that time major changes have taken place in the subject. Nondestructive Testing has become nondestructive Evaluation. In addition correlation is being observed between nonlinearity and work hardening, for example, or nonlinearity and hardness of steels. Such efforts are of fundamental importance to nondestructive evaluation and to development of nondestructive evaluation techniques. There is another aspect of the development of a science that cannot be ignored. That is the basic knowledge of nonlinear material interactions and the mathematical description of them. This is the reason we introduced third order elastic constants in the early sixties. At the time they were introduced we didn't have the foggiest notion about their meaning. We didn't even know that third order elastic constants are almost always negative and have a magnitude of the order of ten times the magnitude of the second order constants. We still are trying to understand them, but we know more about them than we did then. Nowadays we know enough to make measurement of the nonlinear behavior of a solid and try to correlate the measurement with intrinsic properties. This can succeed, but it will succeed only to the extent that we thoroughly understand that some approximations and assumptions are involved, and recognize them at the time we are interpreting data. For example, there are such things as intrinsic nonlinearities and then there are nonlinearities arising from the characteristics of individual samples. The intrinsic nonlinearities arise from interatomic forces in the crystalline lattice, and can correctly be described by third order elastic constants. The other nonlinearities can arise from strains, dislocations or other imperfections in the sample. Sometimes our measurement techniques will separate the two, and sometimes not. It is up to us to make a correct interpretation of the data. Only then can we develop genuinely dependable techniques for NDE based on sample nonlinearity.

Some of the early experiments are illustrative of what we have to be aware of if we are to make sense of nonlinearity measurements, so I would like to turn back history for more than a quarter-century and present measurements made at that time, to show how much we have progressed in measurement--even of samples we measured initially, and to end with recent, very provocative measurements on piezoelectric ceramics, and even high T_c superconductors.

ARCHAEOLOGY OF NONLINEARITY

If we start digging we can discover that one participant in the early prehistory of nonlinear acoustics was my colleague Don Thompson. He and I will reminisce while the others can marvel that we had any inkling of the meaning of nonlinearity so far back in history. In order to facilitate discussion, it is necessary to write down the basic form of the nonlinear equation and of its solution. Near the end of the discussion I want to point out some implications about the form of the nonlinear equation that comes from our analysis of PZT.

THEORY

To correctly derive the equation describing propagation of an ultrasonic wave in a nonlinear crystalline lattice we begin with the definition of the elastic potential energy in terms of strains by writing an expansion in the form:

$$\phi(\eta) = \frac{1}{2!} \sum_{ijkl} C_{ijkl}\, \eta_{ij}\, \eta_{kl} + \frac{1}{3!} \sum_{ijklmn} C_{ijklmn}\, \eta_{ij}\eta_{kl}\eta_{mn} + \cdots \qquad (1)$$

The Cijkl are the elastic constants that appear in the linear approximation. The Cikjlmn are the third order elastic constants. They are the set of coefficients that make the use of the

first nonlinear terms meaningful. At this point one can introduce the effect of any additional strain, such as piezoelectricity, etc., by adding appropriate terms. Once we proceed beyond this point, however, the correct introduction of additional strains becomes increasingly difficult. One favorite technique for forcing nonlinear acoustics to grow (like Topsy, to be sure), is to include only the elastic terms given in Eq. 1 and to proceed with the derivation of the wave equation in which one defines a nonlinearity parameter. The next step is to see whether this wave equation agrees with experiment in various solids by determining whether the nonlinearity parameter has in it effects that the theory does not account for. If it does, one should begin again and account for the newly discovered strains in Eq. 1 and rederive everything. This is the point at which many physicists behave as speculators. They try to market their results rather than to correctly rederive them. To a certain extent, the authors of this treatise will behave as a speculator, as it develops. To compensate, there is an implied promise to complete the job at some further date. Thus, the speculator has integrity after all.

There are several ways to proceed once Eq. 1 has been written. The most direct is to define the Lagrangian function and use Lagrange's equation to derive the nonlinear wave equation. By using the appropriate form of Lagrange's equations and specializing to a specific orientation of the coordinates with respect to the ultrasonic wave propagation direction one can write the nonlinear wave equation in the form

$$\rho \ddot{x}_i = \frac{\partial}{\partial a_1} \sum_{k=1}^{3} J_{ik} \left(\frac{\partial \phi(\eta)}{\partial \eta_{1k}} \right) \tag{2}$$

which shows exactly how the strain energy with the elastic constants enters the nonlinear wave equation. If the strain energy correctly accounts for action of all of the forces in the sample, then the derived nonlinear equation correctly describes the propagation of an ultrasonic wave in the sample. Aye, there's the rub. I am not sure that always the averaging effect of all of the molecules propagating the wave is adequately described by the intrinsic third order elastic constants. But we have no alternative at the moment but to assume that it does and proceed with our analysis.

The thing that pleased us back in the dark ages, and the thing that made possible much of the progress in nonlinear acoustics, was the fact that when one specializes Eq. 2 to pure mode directions one finds that the equations are separable and that the longitudinal wave is described by an equation of the form

$$\rho_0 \frac{\partial^2 U}{\partial t^2} = K_2 \frac{\partial^2 U}{\partial a^2} + (3K_2 + K_3) \frac{\partial U}{\partial a} \frac{\partial^2 U}{\partial a^2} \tag{3}$$

in all three principal directions in a cubic lattice, and in an isotropic medium as well. We wrote the equation in this form to emphasize the fact that it applies in all principal directions, then defined K_2 and K_3 as shown in Table I so one could see the role played by the third order elastic constants. The definitions of the nonlinearity parameter

$$\beta = -\frac{3K_2 + K_3}{K_2} \tag{4}$$

emphasizes the fact that it is the ratio of the coefficients of the nonlinear term to the linear term in the nonlinear wave equation. This nonlinearity parameter, with the definitions given in Table I, only accounts for elastic nonlinearities. To account for other effects, the expressions for the nonlinearity parameters would be more complicated.

If one derived the nonlinear wave equation in a slightly different way he could define the analogous nonlinearity parameter for fluids. It was interesting to discover that the nonlinearity parameter for solids is of the same order of magnitude as the nonlinearity

Table 1 K_2 and K_3 for (100), (110), and (111) Directions in Cubic Crystals

Direction	K_2	K_3
(100)	c_{11}	C_{111}
(110)	$\frac{c_{11} + c_{12} + 2c_{44}}{2}$	$\frac{C_{111} + 3C_{112} + 12C_{166}}{4}$
(111)	$\frac{c_{11} + 2c_{12} + 4c_{44}}{3}$	$\frac{C_{111} + 6C_{112} + 12C_{144} + 24C_{166}}{9} + \frac{2C_{123} + 16C_{456}}{9}$

Table II Comparison of structure, bonding and acoustic nonlinearity parameters along the [100] direction of cubic crystals.

STRUCTURE	BONDING	RANGE OF β
Zincblende	Covalent	1.8 - 3.2
Flourite	Ionic	3.4 - 4.6
FCC	Metallic	4.0 - 7.0
FCC (inert gas)	Van der Waals	5.8 - 7.0
BCC	Metallic	5.0 - 8.8
NaCl	Ionic	13.5 -15.4

parameter for fluids. This can be confirmed by comparing Tables II and III. Table II gives nonlinearity parameters for a number of solids. Table III gives B/A and $\beta = B/A + 2$ for fluids. For solids the nonlinearity parameters range from 2 to 15. For fluids the range is from 6 to 14, approximately the same. This range can serve as reference for some data I will present later.

The solution of Eq. 3 allows one to show how nonlinearity parameters can be measured. A perturbation solution takes the form

$$U = A_1 \sin(ka - \omega t) - \beta A_1^2 k^2 a \cos 2(ka - \omega t) + \ldots \quad (5)$$

This solution shows that an initially sinusoidal ultrasonic wave in a solid will produce a second harmonic whose amplitude is proportional to the nonlinearity parameter. Thus, if we can measure the amplitude of the fundamental and the second harmonic after the ultrasonic wave has propagated through the sample, we can determine the nonlinearity parameter

$$\beta = \frac{A_2}{A_1^2 k^2 a} \quad (6)$$

since the propagation constant $k = \frac{\omega}{c}$, where c is the wave velocity. The sample length is a. Measurement of β as a function of temperature can be quite informative.

Table III Values of B/A and β for fluids at atmospheric pressure

Liquid	Temperature (°C)	B/A	β = B/A + 2
Water-Distilled	0	4.16	6.16
	20	4.96	6.96
	40	5.38	7.38
	60	5.67	7.67
	80	5.96	7.96
	100	6.11	8.11
Acetone	30	9.44	11.44
Benzene	30	9.03	11.03
Benzyl Alcohol	30	10.19	12.19
CCl4	30	11.54	13.54

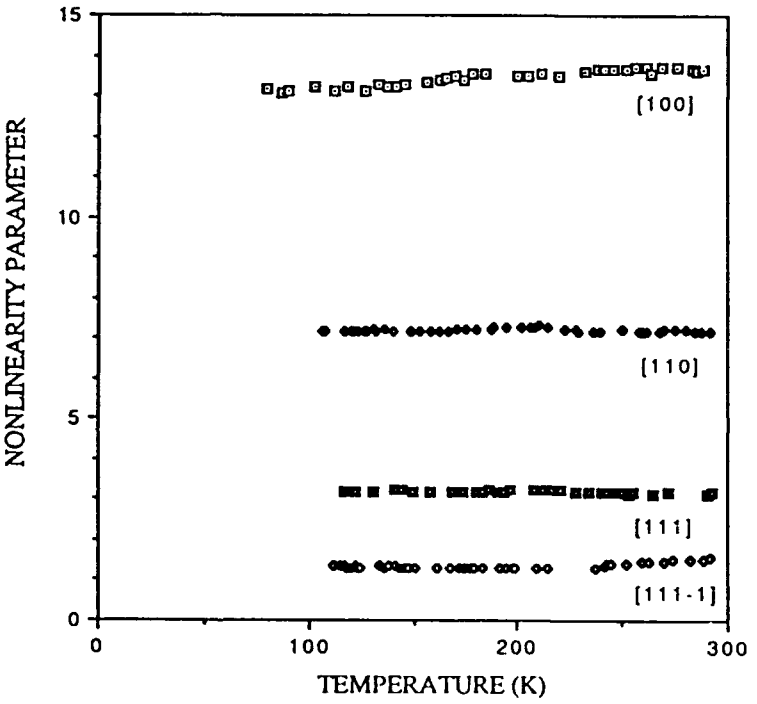

Figure 1. Temperature variation of the nonlinearity parameters in the principal directions of NaCl.

COMPARISON OF THE NONLINEARITY PARAMETERS OF NaCl, PZT and $YBa_2Cu_3O_{7-\delta}$

Recently we measured the nonlinear behavior of NaCl. The nonlinearity parameters for the principal directions in NaCl covered a wide range of values, but each did not change much with temperature between room temperature and liquid nitrogen temperature. Measured nonlinearity parameter values in the three principal directions in NaCl are given in Fig. 1. Different samples were used for each direction; however, measured values differed only in the [111] direction. The origin of the discrepancy is not known, even though it originally was thought to be the effect of OH^- ions. It is clear that the nonlinearity parameter in the [111] direction is extremely sensitive to sample difference, however.

The sample of NaCl is a single crystal, so there is variation in the magnitude of the nonlinearity parameter for different orientations. When one has a sample such as lead zirconate titanate (PZT) one has a ceramic which doesn't necessarily exhibit crystalline properties. We recently measured the nonlinearity parameters of two types of PZT both in the polarized state and in the unpolarized state. The nonlinearity parameter was measured along the direction of polarization. Results for the two samples of PZT are given in Figs. 2, 3, 4, and 5 as a function of temperature. In the cubic crystal NaCl, the magnitude of the nonlinearity parameter is 14 or less. Well below the Curie temperature T_c, the nonlinearity

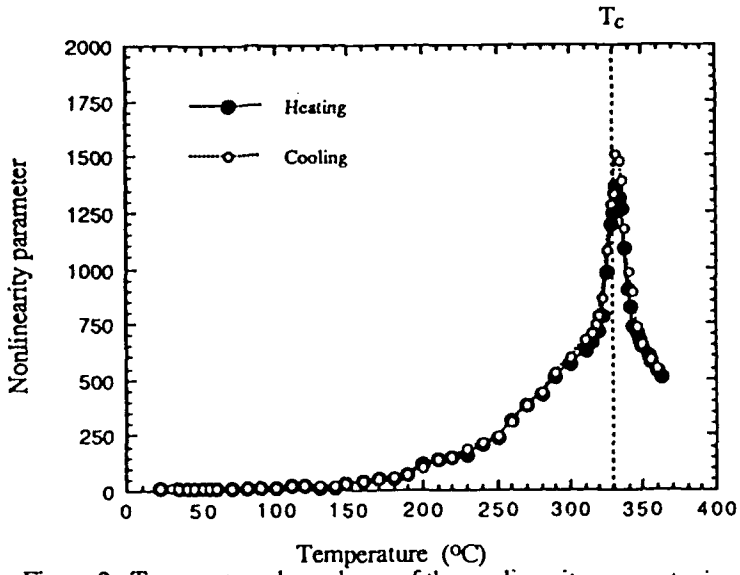

Figure 2. Temperature dependence of the nonlinearity parameter in K1-Unpolarized sample of PZT.

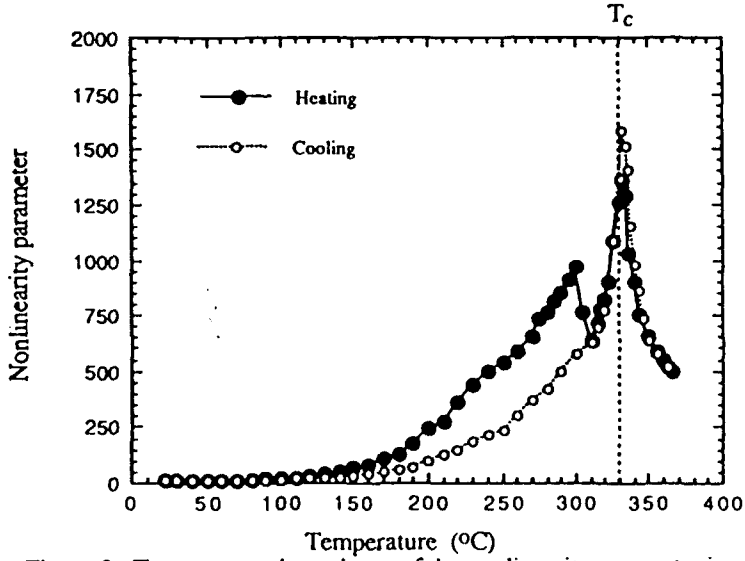

Figure 3. Temperature dependence of the nonlinearity parameter in K1-Polarized sample of PZT.

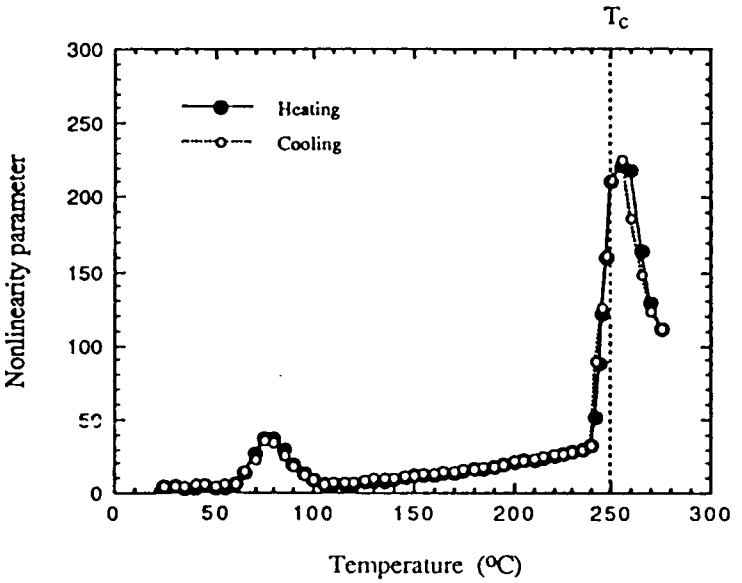

Figure 4. Temperature dependence of the nonlinearity parameter in S1-Unpolarized sample of PZT.

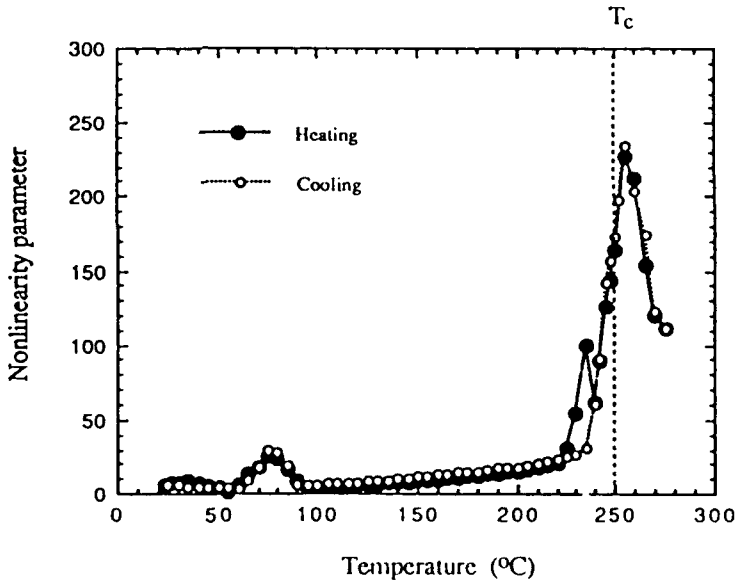

Figure 5. Temperature dependence of the nonlinearity parameter in S1-Polarized sample of PZT.

parameters in the samples of PZT are in this range. However, as the Curie temperature is approached the magnitude of the nonlinearity parameter becomes anomalously high, as high as 1500 in one case. The origin of this anomalously high nonlinearity parameter is not known at the moment. We assume that the large nonlinearity parameter is produced by effects other than elastic ones. Thus, it becomes necessary for this speculator to modify Eq. 1 by including other considerations. Once this is done, it will be necessary to rederive the nonlinear wave equation. Only then will one be certain whether the anomalously large magnitudes of the nonlinearity parameters of PZT really have meaning, or whether a completely new theory is necessary to explain this new development in the field of nonlinear acoustics.

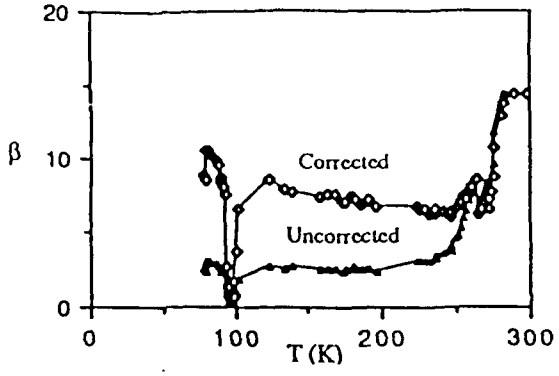

Figure 6. Temperature variation of β in the high T_c superconductor $YBa_2Cu_3O_{7-\delta}$ ($T_c \approx 94$°K).

The final example is the behavior of the nonlinearity parameter of the high T_c superconductor $YBa_2Cu_3O_{7-\delta}$. We measured the second harmonic as a function of temperature through the transition temperature T_c between the normal state and the superconducting state. When we interpreted the results in terms of the nonlinearity parameter β, we got the results shown in Fig. 6. At room temperature (30°C) the nonlinearity parameter had a large value, approximately 14. At lower temperatures the attenuation became noticeable, so we corrected for attenuation. The result is that both in the corrected data and in the uncorrected data the nonlinearity parameter appears to vanish at the transition temperature T_c, which is just below 100°K. This anomalous effect in the behavior of the ceramic $YBa_2Cu_3O_{7-\delta}$ is just opposite to that of PZT at the Curie Temperature. Considerable theoretical speculation now is desirable to explain the behavior of the nonlinearity parameters of ceramics near transition temperatures.

REFERENCES

1. M. A. Breazeale and J. Philip, in Physical Acoustics, edited by W. P. Mason and R. N. Thurston (Academic Press, New York, 1984), Vol. 17.
2. J. H. Cantrell, Proceedings of the IEEE Ultrasonics Symposium, Denver, Vol. 1, p. 425 (1987).
3. N. Dass and M. Kumari, Phys. Stat. Sol. (b) 124, 531 (1984).
4. R. K. Varshney and J. Shanker, Phys. Stat. Sol. (b) 122, 65 (1984).
5. A. L. Ruoff, J. Appl. Phys. 49, 197 (1978).
6. P. A. Lewin and L. Bjørnø in Ultrasound Tissue Characterization, edited by James Greenleaf, CRC Press, 141-162 (1986).
7. J. K. Na and M. A. Breazeale, in IEEE Ultrasonics Symposium Proceedings, Vol. 3, B. R. McAvoy, ed., IEEE Publishing Service, New York 1990, pp 1245-1248.
8. W. H. Jiang and M. A. Breazeale, in IEEE Ultrasonics Symposium Proceedings, Vol. 3, B. R. McAvoy, ed., IEEE Publishing Service, New York 1990, pp 1297-1200.
9. Harriet Beecher Stowe, Uncle Tom's Cabin, Penguin Books Ltd., Harmondsworth, England, 1981; First published 1852.
10. M. A. Breazeale, Int. J. Nondestr. Test. 4, 149-166 (1972).

Temperature dependence of elastic nonlinearities in single-crystal gallium arsenide

D. Joharapurkar,[a] D. Gerlich,[b] and M. A. Breazeale[c]
National Center for Physical Acoustics, University of Mississippi, University, Mississippi 38677

(Received 27 August 1991; accepted for publication 22 May 1992)

The six third-order elastic moduli (TOEM) of single-crystal gallium arsenide were determined by a combination of measurements of ultrasonic second-harmonic generation, and pressure dependence of the second-order elastic moduli, at room temperature. In the temperature range 77–300 K, the nonlinearity parameter for the propagation directions [100], [110], and [111] was measured. Utilizing the Keating model, these data were used in evaluating all six TOEM as a function of temperature. The TOEM C_{111}, C_{144}, and C_{456} turn out to be nearly constant in the above temperature range. The Cauchy relations seem to be obeyed somewhat better as 0 K is approached. The measured values of the TOEM have been employed in calculating a Murnaghan equation of state, which predicts a somewhat higher volume change than the measured one. The elastic Grüneisen constants deduced from the TOEM are in reasonable agreement with the thermal ones in the high-temperature limit.

I. INTRODUCTION

The nonlinear elastic properties of diamond and zinc-blende structure materials has been the subject of numerous studies.[1] In most of these studies only the room-temperature properties of the materials have been investigated, and only relatively few have been measured as function of temperature.[1–3] Several investigators have determined the third-order elastic moduli (TOEM) of GaAs in the past,[4–6] but all this work has been restricted to room temperature. Since the elastic nonlinearities are often correlated with various other anharmonic properties, knowing the temperature dependence of the elastic nonlinearities is quite vital in many instances. Due to the lack of more detailed information, researchers sometimes have assumed that the elastic nonlinearities in solids, specifically the TOEM, are temperature independent.[7] In order to clarify this question somewhat further, the present study was undertaken to measure the TOEM of single-crystal GaAs as a function of temperature. We have measured all six TOEM at room temperature by combining results of second-harmonic generation (SHG)[1] and hydrostatic pressure dependence of the second-order elastic moduli (SOEM).[8] In the temperature range 77–300 K, the three linear combinations of the TOEM available from SHG have been determined experimentally. Utilizing the Keating model,[9] and its extension to the zinc-blende structure,[10] all six TOEM have been determined. This is possible because the validity of the extended Keating model at room temperature can be verified by experimental data. Thus, this investigation presents all six TOEM of GaAs as a function of temperature in the range 77–300 K.

The Keating model[9] has been spectacularly successful in describing the linear and anharmonic elastic properties of the diamond structure materials germanium and silicon. Since the number of adjustable parameters in the model (two for the second order, three for the third order) is smaller than the number of elastic moduli in each case (three second order and six third order), the applicability of the model may be readily tested by comparing with experimental data. From measurement of SHG in the three longitudinal pure propagation modes ([100], [110], and [111]) in the temperature range 4–300 K, and utilizing the Keating model, all six TOEM as a function of temperature could be determined.[11] It should therefore be of interest to examine whether the Keating model[9] and its extension[10] are applicable to the zinc-blende structure as well, and whether all six TOEM as a function of temperature may be evaluated in the same way. These questions are examined in the present work.

II. EXPERIMENT

Single-crystal boules of GaAs, *n*-type, Si doped, having a room-temperature resistivity of $2.7\times10^{-3}\ \Omega$ cm, carrier concentration of $1.2\times10^{18}\ \mathrm{cm}^{-3}$, carrier mobility of 1990 $\mathrm{cm}^2\,\mathrm{V}^{-1}\,\mathrm{s}^{-1}$, were purchased from Crystal Specialties International. Two right parallelepipeds were cut from the above boules, the faces of one corresponding to crystalline planes (100), (110), and $(1\bar{1}0)$, the other one corresponding to (111), $(\bar{1}10)$, and $(11\bar{2})$ planes. Opposite faces were lapped flat and parallel. For the SHG measurements, longitudinal ultrasonic waves, fundamental frequency of 30 MHz, propagating in the [100], [110], and [111] crystalline directions were utilized. For the hydrostatic pressure runs, longitudinal and shear waves, 15 MHz frequency, propagating in the [110] and [111] directions were used. The waves were generated with quartz crystalline transducers, X and Y cut, bonded to the specimens for the room-temperature measurements with benzophenone, while for

[a] Present address: Department of Physics, Sindhu Mahavidyalaya, Nagpur 440017, India.
[b] Permanent address: School of Physics and Astronomy, Raymond and Beverly Sackler Faculty of Exact Science, Tel Aviv University, Tel Aviv 69978, Israel
[c] On assignment from Department of Physics and Astronomy, University of Tennessee, Knoxville, Tennessee 37996-1200

 0021-8979/92/182202-07$04.00

the low-temperature measurements the backing of scotch tape was used as a bonding agent.

The room-temperature ultrasonic velocity as well as its change under hydrostatic pressure were determined by the gated double-pulse superposition method,[12] which provided a resolution of 10^{-5}. The hydrostatic pressure was generated by means of a small manual hydraulic pump, using light weight oil as the pressurizing fluid, generating a pressure range of 0–0.2 GPa. The sample was placed inside a stainless-steel pressure vessel which was connected to the pump and a Bourdon gauge, which served for measuring the pressure in the system. These measurements yield the values of the three SOEM, c_{11}, c_{12}, and c_{44}, as well as the three linear combinations of the TOEM,[13]

$$\begin{aligned} C_1 &= C_{111}+2C_{112}, \\ C_2 &= C_{144}+2C_{155}, \\ C_3 &= C_{111}-C_{123}. \end{aligned} \tag{1}$$

In the SHG measurements, one determines the amplitudes of the fundamental and second-harmonic wave, A_1 and A_2, and these are directly related to the nonlinearity parameter β, which is given by

$$\beta = 8\left(\frac{A_2}{A_1^2}\right)\frac{1}{k^2 a} = -\frac{3K_2+K_3}{K_2}, \tag{2}$$

where k is the wave vector, a the length of the sample. K_2 and K_3 are the second- and third-order coupling constants. These constants are linear combinations of the SOEM and TOEM, respectively, e.g., in the cubic system (Laue group CI), for the three pure propagation modes, [100], [110], and [111], they are given by[1]

$$\begin{aligned} K_2[100] &= c_{11}, \\ K_2[110] &= (c_{11}+c_{12}+2c_{44})/2, \\ K_2[111] &= (c_{11}+2c_{12}+4c_{44})/3, \end{aligned} \tag{3}$$

and

$$\begin{aligned} K_3[100] &= C_{111}, \\ K_3[110] &= (C_{111}+3C_{112}+12C_{155})/4, \\ K_3[111] &= (C_{111}+6C_{112}+2C_{123}+12C_{144}+24C_{155} \\ &\quad +16C_{456})/9. \end{aligned} \tag{4}$$

As can be seen from Eqs. (1) and (4), measuring the pressure derivatives of the SOEM together with SHG measurements for the [100], [110], and [111] direction enables one to determine of all six TOEM with their propagated errors. The six TOEM are as follows:

$$C_{111} = K_3[100],$$

$$C_{123} = K_3[100] - C_3,$$

$$C_{112} = \frac{C_1}{2} - \frac{K_3[100]}{2},$$

$$C_{155} = \frac{K_3[110]}{3} + \frac{K_3[100]}{24} - \frac{C_1}{8},$$

$$C_{144} = C_2 - \frac{2K_3[110]}{3} - \frac{K_3[100]}{12} + \frac{C_1}{4},$$

and

$$C_{456} = \frac{9K_3[111]}{16} - \frac{3C_1}{16} - \frac{3C_2}{4} + \frac{C_3}{8}.$$

The corresponding errors are as follows:

$$|\Delta C_{111}| = |\Delta K_3[100]|,$$

$$|\Delta C_{123}| < |\Delta K_3[100]| + |\Delta C_3|,$$

$$|\Delta C_{112}| < \frac{|\Delta C_1|}{2} + \frac{|\Delta K_3[100]|}{2},$$

$$|\Delta C_{155}| < \frac{|\Delta K_3[110]|}{3} + \frac{|\Delta K_3[100]|}{24} + \frac{|\Delta C_1|}{8},$$

$$|\Delta C_{144}| < |\Delta C_2| + \frac{2|\Delta K_3[110]|}{3} + \frac{|\Delta K_3[100]|}{12} + \frac{|\Delta C_1|}{4},$$

and

$$|\Delta C_{456}| < \frac{9|\Delta K_3[111]|}{16} + \frac{3|\Delta C_1|}{16} + \frac{3|\Delta C_2|}{4} + \frac{|\Delta C_3|}{8}.$$

In the present investigation, at room temperature the values of K_3 for the three directions were evaluated by measuring the absolute values of A_1 and A_2. In the low-temperature run, a relative measurement of β was carried out. This was effected by keeping both values of A_1 and A_2 constant during the temperature run. A_1 was kept constant by varying the intensity of the sound energy delivered to the transducer, while A_2 was kept constant by changing the bias voltage V_b on the capacitive transducer. As can be shown,[1] the following relation is obtained for relative values of β:

$$\frac{\beta(T)}{\beta(T_R)} = \frac{V_b(T_R)C_D(T_R)K_2(T)}{V_b(T)C_D(T)K_2(T_R)}. \tag{5}$$

Here, T is the temperature, T_R a reference temperature (normally room temperature), and C_D is the capacity of the capacitive detector utilized in the determination of A_1 and A_2.[14] The temperature dependence of the SOEM, required for deducing the values of K_3 from β, was taken from the work of Cottam and Saunders.[15] We measured sound velocities in the three principal directions and found that our values agree within experimental uncertainty with those of Cottam and Saunders.

III. RESULTS

For the pressure dependence of the SOEM, five independent propagation modes were available: one longitudinal and two shear modes in the [110] direction, and a longitudinal and shear mode in the [111] direction. The experimental setup yields a resonant frequency f, as a function of pressure P. In Fig. 1 we present the changes in

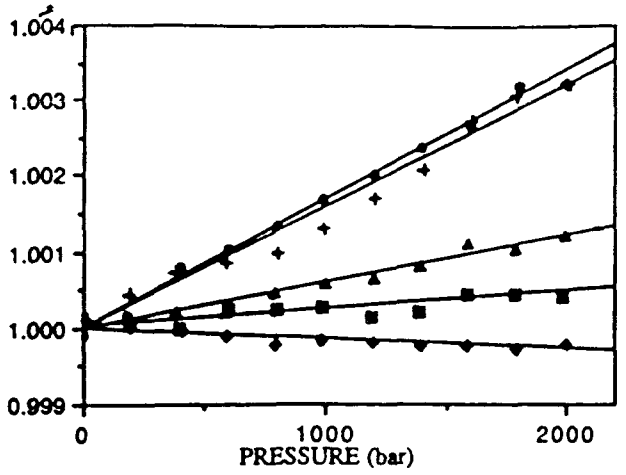

G. 1. Normalized resonance frequency as a function of pressure for ious propagation modes at room temperature: ● [110], [110]; +[111], 1]; ▲ [110], [001]; ■ [111], [01$\bar{1}$]; ♦ [110], [1$\bar{1}$0].

: normalized resonant frequency f_r/f_0 as a function of P, iere f_0 is the resonant frequency at $P=0$. The dots are : experimentally measured data points, while the straight es are a least-squares fit to these points. The slopes of se lines, $\partial(f_r/f_0)/\partial P$, are directly related to the pres- re derivatives of the natural modulus, $\rho_0 W^2$, where ρ_0 is : equilibrium density and W is the natural velocity,[11]

$$\frac{1}{(\rho_0 W^2)_0}(\rho_0 W^2)_0' = 2\left(\frac{\partial(f_r/f_0)}{\partial P}\right)_0. \tag{6}$$

re, the subscript 0 denotes the equilibrium state, while : prime denotes the pressure derivative, $(\rho_0 W^2)_0$ is the EM for the specified direction and is denoted by w. The ues of $(\rho_0 W^2)_0'$, as deduced from the slopes of Fig. 1, ether with their associated errors, are shown in Table I. e error bars for the individual data points in Fig. 1 are nificantly smaller than the statistical scatter. Hence the tistical scatter of the least-squares fit to the straight line ised as the probable error. In Table II, the values of the ear combination of the TOEM, C_1, C_2, and C_3, together h their errors, are shown, as well as the analogous quan- es derived from the work of McSkimin and Andreatch.[5] ure 2 presents plots of A_2 vs A_1^2 for the three SHG pagation directions [100], [110], and [111] at room tem- ature. The dots are the data points, while the straight s are least-squares fits to the points. For these data at st seven measurements of each sample showed that the roducibility is better than 6%. The slopes of these lines, $\partial/\partial A_1^2$, are presented in Table III. From the slopes K_3 is culated for the principal directions and the results are

BLE I. Values of $(\rho_0 W^2)_0'$ for various propagation modes.

le	[110] long	[110] shear [1$\bar{1}$0] pol	[110] shear [001] pol	[111] long	[111] shear
$W^2)_0'$	4.98 ±0.050	−0.090 ±0.016	0.750 ±0.038	4.90 ±0.29	0.130 ±0.049

TABLE II. Values of the linear combinations of the TOEM, C_1, C_2, and C_3 (units are GPa).

	C_1	C_2	C_3
Present work	−1401 ± 1	−512 ± 8	−538 ± 8
McSkimin and Andreatch[a]	−1396	−536	−565

[a]Reference 5.

shown in Table IV, together with similar data derived from the work of McSkimin and Andreatch.[5] As can be seen, the agreement of both sets of data with the results of McSkimin and Andreatch is very good. From the data shown in Tables II and IV, the six room-temperature TOEM may now be determined, and the results are shown in Table V. Also shown in the same table are analogous results obtained by other investigators.[4–6] As can be seen, the agreement among the different results for all six room-temperature TOEM is very reasonable.

In Figs. 3 and 4, the nonlinearity parameter β and K_3 are shown as a function of temperature in the range 77–300 K. As can be seen, both β and K_3 vary less than 25% over this temperature range, although a temperature dependence is obvious. For every sample the experiment was repeated at least three times for temperature runs to produce the data plotted.

IV. DISCUSSION

A. Keating model

The Keating model[9] has been very successful in describing the elastic properties of diamond structure materials. The theory is very plausible, physically intuitive, requires a minimal number of adjustable parameters, and is cast in a rotationally invariant form. It expresses the quadratic part of the strain energy in terms of two second-order force constants: a bond-stretch constant α, and an angle-bend constant β. The cubic part is expressed in terms of three third-order force constants: a bond-stretch constant γ, an angle-bend constant δ, and a mixed bond-

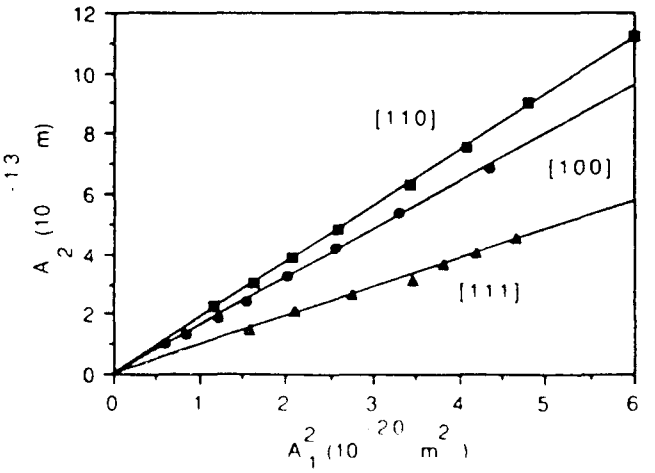

FIG. 2. A_2 as a function of A_1^2 from the room-temperature SHG measurements.

TABLE III. Values of the slopes $\partial A_2/\partial A_1^2$ for different propagation directions (units are 10^7 m^{-1}).

[100]	[110]	[111]
1.591 ± 0.025	1.865 ± 0.016	0.958 ± 0.035

stretch angle-bend constant ϵ. The model has been extended to the zinc-blende structure,[10] and in this case the three SOEM and the six TOEM are given by the following expressions:

$$c_{11}=\frac{\alpha+3\beta}{a}-4.053\,\frac{Z^2q^2}{a^4},$$

$$c_{12}=\frac{\alpha-\beta}{a}-5.538\,\frac{Z^2q^2}{a^4},$$

$$c_{44}=\frac{4\alpha\beta}{a(\alpha+\beta)}-(5.538-4.189\zeta^2)\frac{Z^2q^2}{a^4},$$

$$C_{111}=\gamma-\delta+9\epsilon+17.207(Z^2q^2/a^4),$$

$$C_{112}=\gamma-\delta+\epsilon+1.531(Z^2q^2/a^4),$$

$$C_{123}=\gamma+3\delta-3\epsilon+24.663(Z^2q^2/a^4),$$

$$C_{144}=\gamma(1-\zeta^2)+\delta(1+\zeta^2)+\epsilon(1+\zeta)(3\zeta-1)+\frac{\alpha-\beta}{a}\zeta^2-(24.663-33.526\zeta-0.820\zeta^2)\frac{Z^2q^2}{a^4},$$

$$C_{155}=\gamma(1-\zeta)^2-\delta(1+\zeta^2)+\epsilon(1+\zeta)(3-\zeta)+\frac{\alpha-\beta}{a}\zeta^2+(1.531-33.526\zeta+10.062\zeta^2)\frac{Z^2q^2}{a^4},$$

$$C_{456}=\gamma(1-\zeta)^3+(24.663-50.288\zeta+42.753\zeta^2-19.203\zeta^3)\frac{Z^2q^2}{a^4},$$

$$\zeta=\frac{[(\alpha-\beta)/a]-10.058(Z^2q^2/a^4)}{[(\alpha+\beta)/a]-4.189(Z^2q^2/a^4)}. \qquad (7)$$

Here, a is the lattice constant of the unit cell, Z the effective charge number,[16] and q the electronic charge. The terms containing Z^2q^2/a^4 are the corrections due to the Coulombic long-range interaction. In Table VI the short-range and Coulombic contributions to the various TOEM at room temperature are shown. As can be seen, except for C_{144} and C_{155} and possibly C_{123}, the long-range Coulombic contribution is completely negligible.

TABLE IV. The room-temperature values of β, K_2, and K_3 deduced from SHG measurements (K_2 and K_3 are in units of GPa).

Propagation direction	K_2	β	K_3	K_3[a]
[100]	118.4	2.3	-628 ± 54	-622
[110]	145.2	5.62	-1251 ± 7	-1252
[111]	154.2	4.19	-1108 ± 23	-1124

[a]Reference 5.

Since there are only three adjustable parameters for the six TOEM in the Keating model, from the three measured values of K_3 one may determine all three third-order force constants γ, δ, and ϵ, and thus calculate all six TOEM. In Fig. 5, the values of γ, δ, and ϵ as a function of temperature are shown as calculated from the data of Fig. 4. It is interesting to note that while δ and ϵ are nearly constant over the whole temperature range, γ exhibits a considerable variation. In Figs. 6 and 7, the values of the TOEM as calculated from the third-order force constants δ, ϵ, and γ in Fig. 5 are shown. The curves are a fifth-order polynomial fit of the data. The TOEM C_{112}, C_{123}, and C_{155} show considerable variation over the temperature range measured. The other three TOEM are nearly linear functions of temperature in the range 77–300 K. A comparison of the values of the TOEM in Table V and those read from Figs. 6 and 7 is a good test of the validity of the Keating model at room temperature. Such a comparison shows that all of the TOEM in Figs. 6 and 7 except C_{144} are within the errors stated in Table V. Closer examination of the values for C_{144} given by the different authors listed in Table V shows a wide range of measured values. C_{144} appears to be the most uncertain of the TOEM.

B. Cauchy relations

If all lattice interactions are of central force type, and each atom is a center of symmetry, the elastic moduli should obey the Cauchy relations. For the SOEM and TOEM, these relations are as follows:

TABLE V. Room-temperature values of the TOEM (units are GPa)

	C_{111}	C_{112}	C_{123}	C_{144}	C_{155}	C_{456}
Present work	-628 ± 54	-387 ± 27	-90 ± 62	24 ± 17	-269 ± 5	-44 ± 20
McSkimin and Andreatch[a]	-627	-387	-57	2	-269	-39
Drabble and Brammer[b]	-675	-400	4	70	320	69
Abe and Imai[c]	-620	384	59	14	282	44

[a]Reference 5.
[b]Reference 4.
[c]Reference 6.

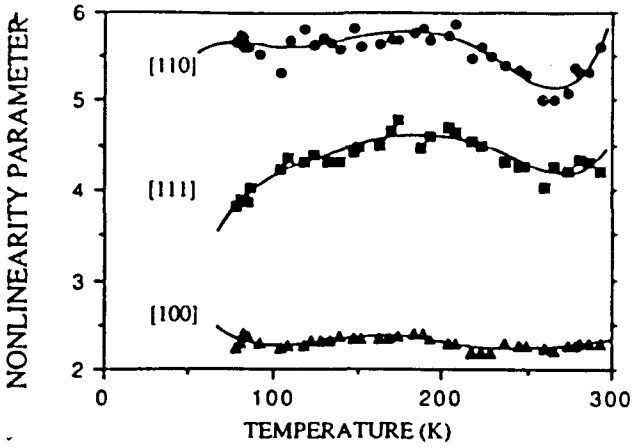

FIG. 3. Nonlinearity parameter β as a function of temperature.

$$c_{12}=c_{44}, \quad C_{112}=C_{155}, \quad C_{123}=C_{144}=C_{456}. \tag{8}$$

If, in addition to the above conditions, the short-range repulsive interaction is the dominant one, there are additional relations between the elastic moduli,[17] the so-called "strong Cauchy relations," which are

$$\begin{aligned} &c_{11}=2c_{12}=2c_{44}, \\ &C_{111}=2C_{112}=2C_{155}, \\ &C_{123}=C_{144}=C_{456}=0. \end{aligned} \tag{9}$$

From Eqs. (8) and (9), one obtains the following expressions among the TOEM:

$$C_{112}+4C_{155}=\tfrac{5}{2}C_{111}, \quad C_{123}+6C_{155}+8C_{456}=0. \tag{10}$$

In order to examine the validity of the "strong Cauchy relations" for GaAs, the values of $\frac{5}{2}C_{111}$, $C_{112}+4C_{155}$, and $C_{123}+6C_{144}+8C_{456}$ as a function of temperature, evaluated from the data shown in Fig. 4, are presented in Fig. 8. As can be seen, there is a tendency for a better agreement with the Cauchy relations as 0 K is approached, although there appears to be reasonable agreement at room temperature. Since both the Keating model and the Cauchy relations should strictly apply only at 0 K, this may indicate that the lattice interaction in GaAs is basically of the central type,

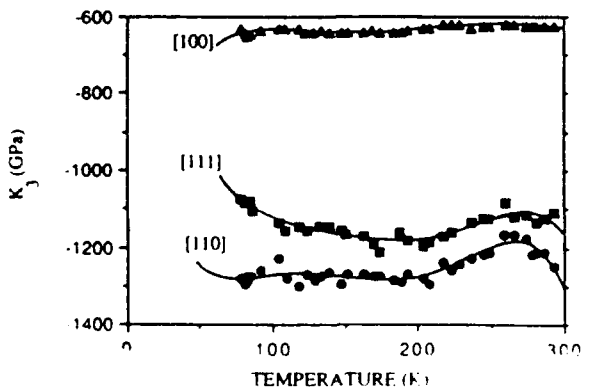

FIG. 4. Third-order coupling constant K_3 as a function of temperature

TABLE VI. Short- and long-range interaction contribution to the room-temperature TOEM (units are GPa).

	C_{111}	C_{112}	C_{123}	C_{144}	C_{155}	C_{456}
Short range	−627	−386	−79	42	−219	−41
Long range	−1	−1	−11	−18	−50	−3

and the deviations from the Cauchy relations are due to thermal effects. An analogous observation has also been made for germanium and silicon.[1]

C. Equation of state

By using the measured values of the TOEM, an equation of state (pressure-volume relation) for the material may be constructed. One of the simplest and most straightforward is the Murnaghan equation of state,[18]

$$\frac{V}{V_0}=\left(1+B_0'\frac{P}{B_0}\right)^{-(1/B_0')}, \tag{11}$$

where B_0 is the bulk modulus and B_0' its pressure derivative, both at $P=0$. B_0' is given by

$$B_0'=-(1/3B_0)(C_1-\tfrac{1}{3}C_3). \tag{12}$$

The Murnaghan equation of state for GaAs, Eq. (11), is shown in Fig. 9. The dot on the figure is the experimentally determined volume at the onset of 17.2 GPa phase transition. As can be seen, the Murnaghan equation of state predicts a somewhat higher compressibility than the measured one.

D. Mode Grüneisen gamma and Grüneisen constant

The TOEM are closely related to the mode Grüneisen gammas and the Grüneisen constant.[7] Within the framework of the anisotropic continuum model,[7] the mode Grüneisen gammas may be expressed as

$$\gamma(p,\mathrm{N})=(B_0/2w)(\rho_0 W^2)_0'. \tag{13}$$

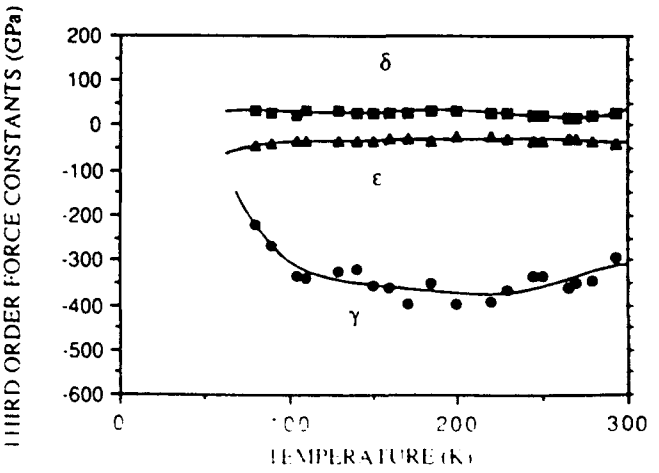

FIG. 5. The third-order force constants γ, δ, and ϵ as a function of temperature

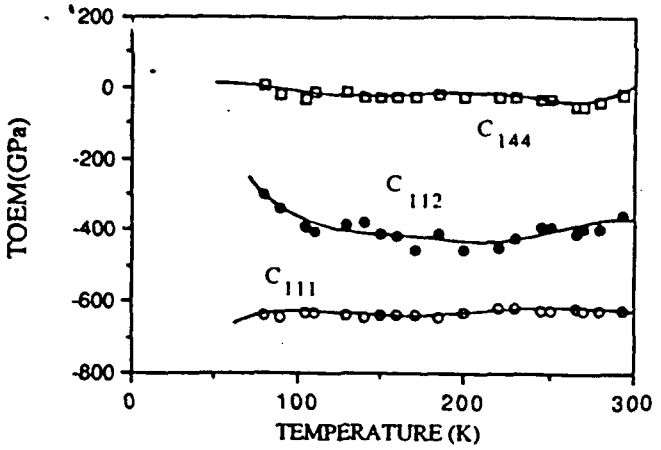

FIG. 6. The three TOEM, C_{111}, C_{112}, and C_{144} as a function of temperature.

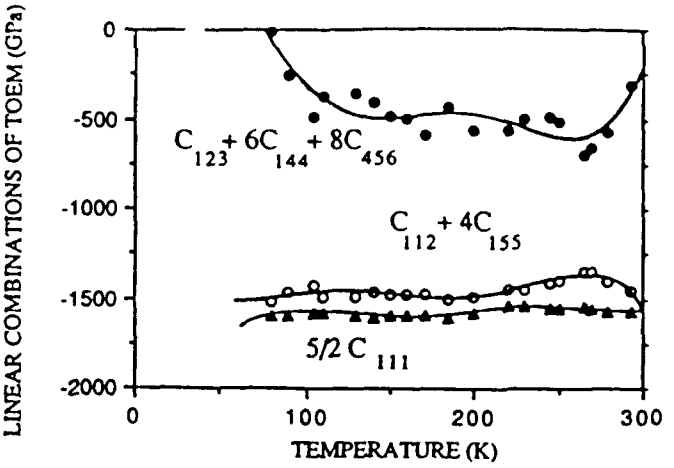

FIG. 8. Measured combinations of the TOEM compared with those derived from the Cauchy relations, as a function of temperature.

Here, N is a unit vector in the propagation direction and p the polarization index ($p=1,2,3$). For a cubic material $\gamma(p,\mathrm{N})$ may be expressed as

$$\gamma(p,\mathrm{N})=-(1/6w)(3B_0+2w+k), \tag{14}$$

where

$$w(p,\mathrm{N})=c_{11}K_1+c_{44}K_2+c_{12}K_3, \tag{15}$$

$$k(p,\mathrm{N})=C_1K_1+C_2K_2+(C_1-C_3)K_3, \tag{16}$$

and

$$K_1(p,\mathrm{N})=N_1^2U_1^2+N_2^2U_2^2+N_3^2U_3^2,$$

$$K_2(p,\mathrm{N})=(N_2U_3+N_3U_2)^2+(N_3U_1+N_1U_3)^2+(N_1U_2+N_2U_1)^2, \tag{17}$$

$$K_3(p,\mathrm{N})=2(N_2N_3U_2U_3+N_3N_1U_3U_1+N_1N_2U_1U_2).$$

The mode Grüneisen gammas may be related to the Grüneisen constant,[7] γ_G,

$$\gamma_G=\sum_p \int d\Omega\, \gamma(p,\mathrm{N})C(p,\mathrm{N})\Big(\sum_p \int d\Omega\, \gamma(p,\mathrm{N})\Big)^{-1}. \tag{18}$$

In this expression, $C(p,\mathrm{N})$ is the heat capacity of the (p,N) mode, Ω the spherical angle, and the integration is carried out over the irreducible part of the Brillouin zone, i.e., the spherical triangle whose apexes are [100], [110], and [111].

The mode gammas for some crystalline directions of high symmetry are presented in Fig. 10. It is noteworthy that the mode gammas for the slow shear mode become negative for certain directions. This raises the possibility that the thermal expansion will become negative at low temperatures, since this is the lowest-energy mode, and since the lowest-energy modes are the ones excited at low temperatures. This is borne out by the observation that the thermal expansion[19–22] of GaAs becomes negative around 40 K.

In the limiting cases of low and high temperature Eq. (18) simplifies significantly, and the corresponding values of γ are given by

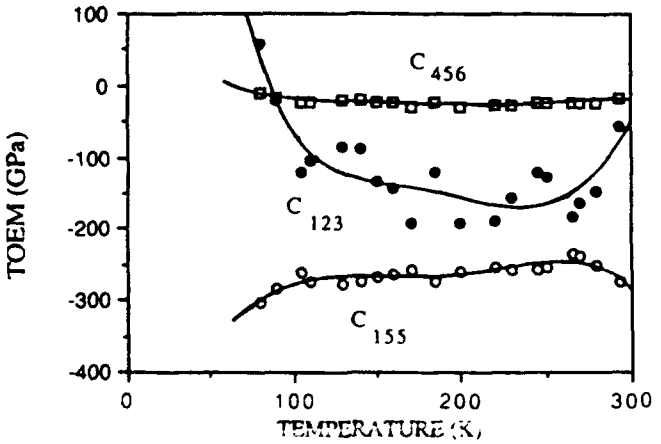

FIG. 7. The three TOEM, C_{123}, C_{155}, and C_{456} as a function of temperature.

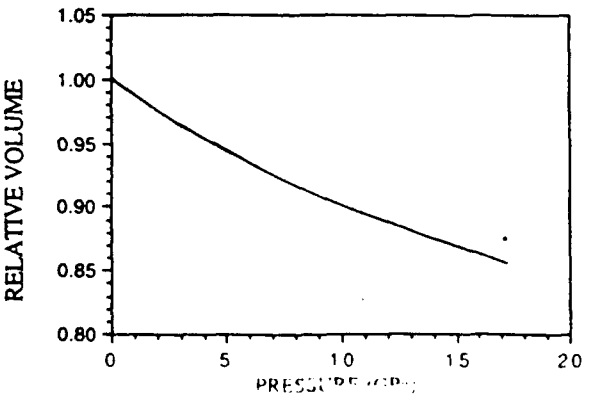

FIG. 9. Murnaghan equation of state for GaAs. The date point is an experimentally determined volume at the onset of the 17.2 GPa phase transition.

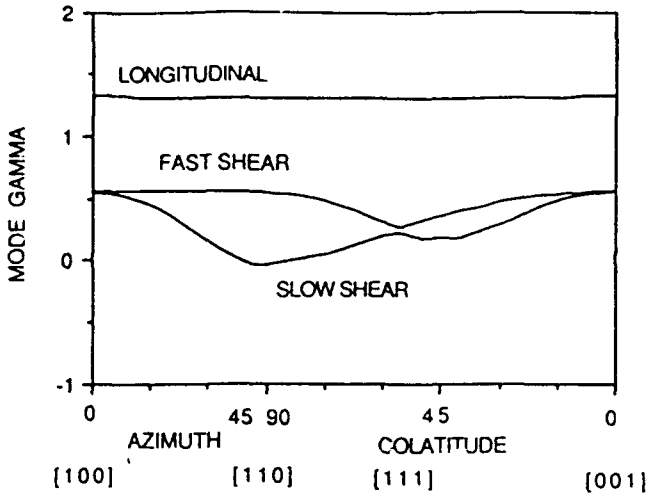

FIG. 10. GaAs mode Grüneisen gammas for some crystalline directions of high symmetry.

$$\gamma_L = \sum_{p,\mathrm{N}} S(p,\mathrm{N})^{-3}\gamma(p,\mathrm{N})\left(\sum_{p,\mathrm{N}} S(p,\mathrm{N})^{-3}\right)^{-1},$$

$$\gamma_H = \left(\sum_{p,\mathrm{N}} \gamma(p,\mathrm{N})\right)(N)^{-1}, \tag{19}$$

where the summation is to be carried out over all modes, N being the total number of modes, and $S(p,\mathrm{N})$ the sound velocity. In Table VII, the values of γ_L and γ_H as deduced from Eq. (19) are compared with the analogous values of the thermal Grüneisen constant, evaluated from the thermal expansion and specific heat. As can be seen, there is quite good agreement between the elastic and thermal γ_H, while for γ_L the elastic value is somewhat lower than the thermal one. But in this case the comparison is not very meaningful: At very low temperatures the thermal γ rises steeply as the temperature is lowered.

V. CONCLUSIONS

The present work demonstrates that the Keating model is useful in the evaluation of all six TOEM of GaAs at room temperature and shows how it and SHG results can be used to evaluate the temperature dependence of the TOEM. The agreement between experimentally measured TOEM at room temperature and the ones calculated by combining the Keating model and SHG results suggests that the Keating model, and its extension to include long-range Coulombic interactions, is applicable to all crystals having the zinc-blende structure. We suggest that the same procedure can be applied to other zinc-blende structure materials; especially the other III-V compounds. This produces the temperature dependence of the TOEM of III-V compounds even in the absence of direct measurements of all of them.

TABLE VII. Elastic and thermal values of the low- and high-temperature limits of the Grüneisen constant.

	γ_L	γ_H
Elastic	0.38	0.66
Thermal	0.60	0.70 (300 K)

ACKNOWLEDGMENTS

Research supported in part by the Office of Naval Research. The authors are grateful to Dehua Huang for statistical analysis of the data. D.J. is grateful to the National Center for Physical Acoustics for offering a Research Fellowship and to Dr. Powar and Sindhu Mahavidyalaya Authorities for sanction of his leave of absence. He also thanks Dr. Jiang and Dr. Na of NCPA for help and useful discussions. D.G. wishes to thank the National Center for Physical Acoustics for the award of a summer appointment, during the tenure of which this work was carried out.

[1] M. A. Breazeale and J. Philip, in *Physical Acoustics*, edited by W. P. Mason and R. N. Thurston (Academic, New York, 1984), Vol. XVII, p. 1.
[2] H. J. McSkimin and P. Andreatch, Jr., J. Appl. Phys. 34, 651 (1963).
[3] H. J. McSkimin and P. Andreatch, Jr., J. Appl. Phys. 35, 216 (1964).
[4] J. R. Drabble and A. J. Brammer, Solid State Commun. 4, 467 (1966).
[5] H. J. McSkimin and P. Andreatch, Jr., J. Appl. Phys. 38, 2610 (1967).
[6] Y. Abbe and K. Imai, in *Proceedings of the IEEE Ultrasonic Symposium*, San Francisco, edited by B. R. McAvoy (IEEE, New York, 1985), Vol. 2, p. 1109.
[7] K. Brugger and T. C. Fritz, Phys. Rev. 157, 524 (1967).
[8] D. Lazarus, Phys. Rev. 76, 545 (1949).
[9] P. N. Keating, Phys. Rev. 145, 637 (1966); 149, 674 (1966).
[10] D. Gerlich, in *Proceedings of the 6th Symposium on Thermophysical Properties*, Atlanta, GA, edited by P. E. Liley (ASME, New York, 1973).
[11] J. Philip and M. A. Breazeale, J. Appl. Phys. 54, 752 (1983).
[12] J. Williams and J. Lamb, J. Acoust. Soc. Am. 30, 308 (1958).
[13] R. Thurston and K. Brugger, Phys. Rev. 133, A1604 (1964).
[14] W. B. Gauster and M. A. Breazeale, Rev. Sci. Instrum. 37, 1544 (1966).
[15] R. I. Cottam and G. A. Saunders, J. Phys. C 6, 2105 (1973).
[16] R. M. Martin, Phys. B 1, 4005 (1970).
[17] Y. Hiki and A. V. Granato, Phys. Rev. 144, 411 (1966).
[18] O. L. Anderson, J. Phys. Chem. Solids 27, 547 (1966).
[19] S. Novikova, Sov. Phys. Solid State 3, 129 (1961).
[20] E. D. Pierron, D. I. Parker, and J. B. McNeely, J. Appl. Phys. 38, 4669 (1967).
[21] P. W. Sparks and C. A. Swenson, Phys. Rev. 163, 779 (1967).
[22] R. Feder and T. Light, J. Appl. Phys. 39, 4870 (1968).

ELECTRIC POTENTIAL IN PIEZOELECTRIC MEDIUM AND ITS INFLUENCE ON MEASUREMENT OF ULTRASONIC NONLINEARITY PARAMETER

Wenhua JIANG*, Gonghuan DU* and Mack A. BREAZEALE**

*The Institute of Acoustics, Nanjing University, Nanjing 210008, China
**The National Center for Physical Acoustics, Coliseum Drive, University, MS 38677, USA

INTRODUCTION

In the experiment of second harmonic generation (SHG), the capacitive detector is used to measure absolute amplitude of acoustic wave.[1] The assembly of the detector and sample can be simplified as shown by Fig.1. Usually the capacitive detector is mechanical displacement sensitive. When the sample is piezoelectric, however, it has been observed that capacitive detector gives output even there is no DC-bias applied to it.[2] In the present paper, the origin of the no DC-bias output is discussed and its influence on the measurement of ultrasonic nonlinearity parameter β is estimated. The calculation is compared with experiment. Although the analysis is done only for longitudinal wave along Z-axis of crystal $LiNbO_3$, the procedure of the analysis can be easily extended to any piezoelectric medium as long as there exists a piezoelectric-stiffened wave in certain direction.

ELECTRIC FIELD IN AIRGAP

Crystal $LiNbO_3$ has symmetry of 3m. The longitudinal wave along its crystallographic Z-axis is piezoelectric-stiffened. Without loss of generality one dimensional problem is treated here because most of SHG experiments are performed for pure longitudinal wave direction. Hence the coupling equation of particle displacement u and electric potential ϕ can be expressed as:

$$\rho_0\frac{\partial^2 u}{\partial t^2}-C_{33}\frac{\partial^2 u}{\partial z^2}-e_{33}\frac{\partial^2\phi}{\partial z^2}=\frac{\partial T_{33}^{NL}}{\partial Z} \qquad (1)$$

$$e_{33}\frac{\partial^2 u}{\partial t^2}-\epsilon_{33}\frac{\partial^2\phi}{\partial Z^2}=\frac{\partial D_3^{NL}}{\partial Z} \qquad (2)$$

Here T_{33}^{NL} and D_3^{NL} are the stress and electric displacement associated with nonlinear constants of the medium.

According to Fig.1. there is mechanical boundary condition of stress-free. The electric boundary conditions consist in continuity of ϕ or continuity of ϕ and D_3, depending on either the bottom surface of the sample is short or open circuited. Only the linear part of the solution is given here.

In the airgap between sample and detector button there exists only electric potential ϕ_g which satisfies Laplacian Equation:

$$\nabla^2\phi_g=0 \qquad (3)$$

Moreover, in addition to incident and reflected waves there should be a reflected evanescent wave ϕ_e in the piezoelectric medium in order to fulfill the boundary conditions.[3] ϕ_e satisfies Eqs.(1) and (2) with the solution of u=0, and $\phi_e\neq 0$.

OPEN-CIRCUIT

In open-circuit case, the bottom surface of sample is unmetallized. The solution for reflected evanescent wave is

$$\phi_e=A_e(z+h) \qquad (4)$$

here h is penetration depth of ϕ_e i.e. $\phi_e\to 0$ when $z\to -h$. The solution of one-dimensional Laplacian equation is

$$\phi_g=A'_e(Z-d)+\phi_c \qquad (5)$$

which also satisfies that $\phi_g=\phi_c$ when z=d. ϕ_c is the potential developed at load Y. Use of boundary conditions gives:

$$-jk\bar{C}_{33}A_s+jk\bar{C}_{33}B_s+e_{33}A_e=0 \qquad (6.a)$$

$$\frac{e_{33}}{\epsilon_{33}}A_s+\frac{e_{33}}{\epsilon_{33}}B_s+A_eh=\phi_c-A'_ed \qquad (6.b)$$

$$-e_{33}A_e=-\epsilon_0A'_e \qquad (6.c)$$

In addition, the circuit equation

$$\phi_cY+\frac{\partial(D_3S)}{\partial t}=0$$

should be applied. Here, A_s and B_s are amplitude of incident and reflected waves, respectively, s is top surface area of detector button. By solving Eqs(6) the following results are obtained:

$$\frac{B_s}{A_s}=1-\frac{2K_s^2e^{jkh}}{[(k_s^2-kdx_1)^2+(kdx_r)^2]^{1/2}} \qquad (7)$$

$$\phi_c=\frac{2j\omega}{Y}\frac{2Ke_{33}e^{j(\frac{\pi}{2}-\theta)}}{[(k_s^2-kdx_1)^2+(kdx_r)^2]^{1/2}}A_s \qquad (8)$$

Here

$$\theta=tg^{-1}\left(\frac{kdx_r}{K_s^2-kdx_1}\right),\ K=2\omega\left(\frac{\epsilon_{33}S}{d}\right)\frac{Y_r}{Y^2}$$

$$x_r=\frac{\epsilon_{33}}{\epsilon_0}+\frac{h}{d}-2\omega\left(\frac{\epsilon_{33}S}{d}\right)\frac{Y_1}{Y^2},\ Y^2=Y_r^2+Y_1^2$$

$$K_s^2=\frac{K_t^2}{1+K_t^2},\ K_t^2=\frac{e_{33}^2}{C_{33}\epsilon_{33}}$$

K_t^2 is the electromechanical coupling factor.

SHORT-CIRCUIT

In the case of short-circuit, the bottom surface of sample is coated with good conductor film and grounded.

the airgap electric potential is equal to zero because grounded bottom surface shields electric field in the sample. Under this condition, the measurement of ultrasonic nonlinearity parameter β for piezoelectric sample the same as for nonpiezoelectric one.

HE EFFECT OF PIEZOELECTRIC POTENTIAL

In the case of open-circuit, the vibration of bottom surface caused by incident acoustic wave cannot be detected by capacitive detector no matter whether there ... bias applied to it or not because the circuit is ... the output of the capacitive detector is ... airgap potential. The detector ... tive in this case. It can be ... detector is proportional ... wave.

... ence of penetrating ... measurement of ultrasonic ... a crystal z-$LiNbO_3$ sample is ... procedure in [1] when ... erent metallization extent ... the surface has different ... measured results. The ... value ... when DC-resistance of the ... very small(indicated by o in the table), which ... agreement with the previous one[4]. The measured ... of β decreases with the metallization extent of the ... tom surface becoming worse. Obviously, this is due to ... effect of penetrating potential.

In a practical experiment the metallization extent of ... bottom surface may be between completely short and ... circuited. "thin coated films" in Table 1 is corresponding to this situation. The capacitive detector ... sensitive to both mechanical displacement and electric charge. The experimental manifestation of ... is that the capacitive detector ... DC-bias applied ... DC-bias ... In the present experiment ... with DC-bias is 1.4 ... fundamental and 1.91 times ... of the calibration procedure in ... calculated amplitude of acoustic wave, the ... will be 1.71 times as high as that ... fundamental (A_1) and 1.53 times for second harmonic (A_2) ... the procedure in (1) take ... displacement contribution to the output ... ultrasonic nonlinearity parameter ... the ratio of β' measured ... under DC-resistance ... 0.5 ... good ... with the result indicated in ... where the ratio ... 0.5. Therefore the ... potential in piezoelectric medium could affect ... measured result of ultrasonic nonlinearity parameter ... metallization ... of bottom surface is not good enough ... completely screen it. On the other hand, the fact ... that the capacitive detector can also be used to ... the ... potential. Especially ... nonlinear acoustic field ... by nonlinear ... second ... detected by ...

... experiment shows that ... capacitive detector ... sensitive to electric charge than to mechanical ... Hence, a new approach to determine nonlinear ... of piezoelectric media through direct ... of nonlinear electric potential may be presented.

REFERENCES

(1) M.A.Breazeale and ..., in Physical Acoustics edited by W.P.Mason and R.N.Thurston XVII(Academic, New York 1981)

(2) Paul.J.Latimer and M.A.Breazeale, Tech.Rep.No. ... Physics Department, The University of Tennessee U.S.A. (1981)

(3) B.A.Auld, Acoustic Field and Waves in Solids II (John Wiley & Sons 1973)

(4) D.F. ..., J.Appl.Phys., 44 (1966) 1007-10..

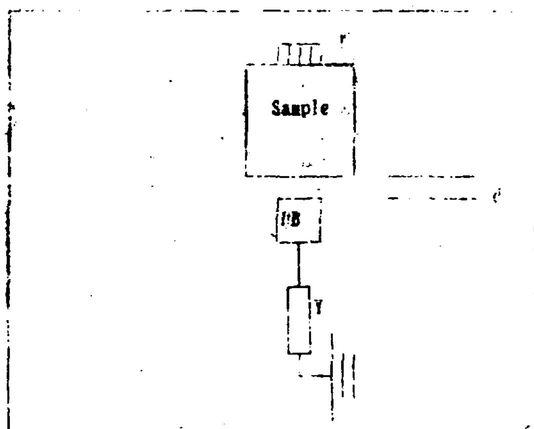

Figure 1.simplified assembly of capacitive detector and sample.

Table 1.Measured values of β and C_{333} under different metallization extent.

DC resistance of coated film	β	C_{333} (10^{11} N/...)
0	..95	15
1	2.45	1..73
3	2.4	..81
thin film	1.14	..43

317

Nonlinear Techniques for Nondestructive Evaluation of Composites

Mack A. Breazeale
National Center for Physical Acoustics
Coliseum Drive
University, MS 38677

ABSTRACT

Over the past quarter-century we have developed techniques for evaluation of the nonlinear properties of solids. In crystalline solids we can evaluate third order elastic constants in reliable fashion. Our technique makes use of harmonics generated by the nonlinearity of the medium as finite amplitude ultrasonic waves propagate. Some of our recent measurements with silicon and germanium, two diamond lattice solids, are mentioned by way of illustration.

Recently we studied the nonlinear behavior of PZT which exhibits a very large nonlinearity parameter. These results are described in more detail, and the implication of them for development of nonlinear techniques for nondestructive evaluation of composites is stressed.

To be published in the Proceedings of the US Navy Conference on Characterization and NDE of Heat Damage in Graphite Epoxy Composites, April 27-28 1993, Orlando FL

I. INTRODUCTION

There are many types of nonlinearity. In both plasma physics, and optics one can find electromagnetic nonlinearities. The nonlinearity we are interested in, however, is thermodynamical or mechanical. The first thermodynamical (or acoustical) nonlinearity studied probably was that of Poisson in 1808. Poisson[1] studied the propagation of sound waves of finite amplitude in an ideal gas. The first study of the propagation of ultrasonic waves of finite amplitude in liquids probably was that of Fox and Wallace[2]. Subsequently Keck and Beyer developed a theory for fluids[3], and many people have done useful experiments[4], often under funding of the Navy. The foundation of the study of the nonlinear properties of solids by ultrasonic techniques was laid by the definition of third order elastic (TOE) constants in the 1960's. Since that time in my laboratory we have done a number of experiments that suggest to us that nonlinear properties of composites might provide the basis of their nondestructive evaluation, and possibly even nondestructive evaluation of heat damage in them.

In this paper I propose to describe pertinent aspects of what we have done in the past, define the relationship between our past experience and characterization of the nonlinear behavior of composites, and finally, to give some recent results obtained in our laboratory with graphite epoxy composites.

II. THEORY

A. Linear approximation-Hexagonal Symmetry

In order to derive the linear wave equation one can simply define the elastic potential energy in terms of the elastic constants:

$$\phi(\eta) = \frac{1}{2!} \sum_{ijkl} C_{ijkl} \eta_{ij} \eta_{kl} \quad . \tag{1}$$

This strain energy substituted into Lagrange's equations gives the linear wave equation for principal directions a:

$$\rho_o \frac{\partial^2 U}{\partial t^2} = K_2 \frac{\partial^2 U}{\partial a^2} \qquad (2)$$

where K_2 is a linear combination of elastic constants. Our experience leads us to assume that epoxy composites will be describable in terms of equations appropriate to hexagonal symmetry. To evaluate the elastic constants of composites we propagate ultrasonic waves along the x3 axis. In this case

$$\rho v^2(001) = C_{33} \text{ for longitudinal waves} \qquad (3)$$

and

$$\rho v^2(100) = C_{44} \qquad \text{for transverse waves.} \qquad (4)$$

For propagation along any direction perpendicular to the x3 axis

$$\rho v^2(100) = C_{11} \text{ for longitudinal waves} \qquad (5)$$

and

$$\rho v^2(100) = C_{44} \text{ for transverse waves polarized in the (001) direction} \qquad (6)$$

$$\rho v^2(100) = \frac{1}{2}(C_{11} - C_{12}) \text{ for transverse waves polarized in the (010) direction} \qquad (7)$$

B. Nonlinear approximation - Cubic Symmetry

Most of our experiments on the propagation of finite amplitude ultrasonic waves have been done with solids of cubic symmetry, although we have worked out the nonlinear theory for any symmetry[5]. To describe our experiments, then, it is necessary only to state theoretical background for cubic symmetry. We begin again with the elastic potential energy, but now keep higher order terms:

$$\phi(\eta) = \frac{1}{2!}\sum_{ijkl} \eta_{ij}\eta_{kl} + \frac{1}{3!}\sum_{ijklmn}' C_{ijklmn}\,\eta_{ij}\eta_{kl}\eta_{mn} + \cdots \qquad (8)$$

Now we define the Lagrangian function

$$L = \frac{1}{2}\sum_{i=1}^{3} \rho\left(\frac{\partial x_i}{\partial t}\right)^2 - \phi(\eta) \tag{9}$$

and substitute into Lagrange's equations:

$$\frac{d}{dt}\left(\frac{\partial L}{\partial x_i}\right) + \sum_{k=1}^{3} \frac{d}{da_k}\left(\frac{\partial L}{\partial\left(\frac{\partial x_i}{\partial a_k}\right)}\right) = 0 \tag{10}$$

The result is that for principal directions in a cubic crystal we can write the nonlinear wave equation in the form

$$\rho_o \frac{\partial^2 U}{\partial t^2} = K_2\left(\frac{\partial^2 U}{\partial a^2}\right) + (3K_2 + K_3)\frac{\partial U}{\partial a}\frac{\partial^2 U}{\partial a^2} \tag{11}$$

where expressions for K_2 and K_3 for a cubic lattice are given in Table I.

Table I. K_2 and K_3 for principal directions in a cubic crystal

Direction	K_2	K_3
[100]	C_{11}	C_{111}
[110]	$\frac{C_{11} + C_{12} + 2C_{44}}{2}$	$\frac{C_{111} + 3C_{112} + 12C_{166}}{4}$
[111]	$\frac{C_{11} + 2C_{12} + 4C_{44}}{3}$	$\frac{C_{111} + 6C_{112} + 12C_{144} + 24C_{166} + 2C_{123} + 16C_{456}}{9}$

The solution of Eq. (11) pertinent to the present discussion is obtained under the assumption that a sinusoidal disturbance is generated at a = o. At a distance a from the sinusoidal driver the solution takes the form

$$U = A_1 \sin(ka - \omega t) - \left[\frac{3K_2 + K_3}{K_2}\right] A_1^2 k^2 a \cos 2(ka - \omega t) + \cdots \tag{12}$$

Our procedure involves the measurement of the amplitude of the fundamental A_1 and the amplitude of the second harmonic

$$A_2 = -\frac{3K_2 + K_3}{K_2} A_1^2 k^2 a \tag{13}$$

The nonlinearity parameter is defined as

$$\beta = -\frac{3K_2 + K_3}{K_2} \tag{14}$$

From Eqs. (13) and (14) we can define the nonlinearity parameter in terms of measured quantities as

$$\beta = \frac{A_2}{A_1^2 k^2 a} \tag{15}$$

In order to determine the nonlinearity parameter, then, we need only to measure the amplitudes of the fundamental and that of the second harmonic A_2. The propagation constant $k = \frac{2\pi}{\lambda}$ can be determined from the frequency and the sound velocity. The quantity a is the sample length.

III. MEASUREMENT TECHNIQUE

Measurement of the amplitudes of the fundamental and the second harmonic can be made with a variation of the capacitive microphone as shown in Fig. 1. The detector button produces an air gap of the order of 10μ between the button and the end of the sample. This

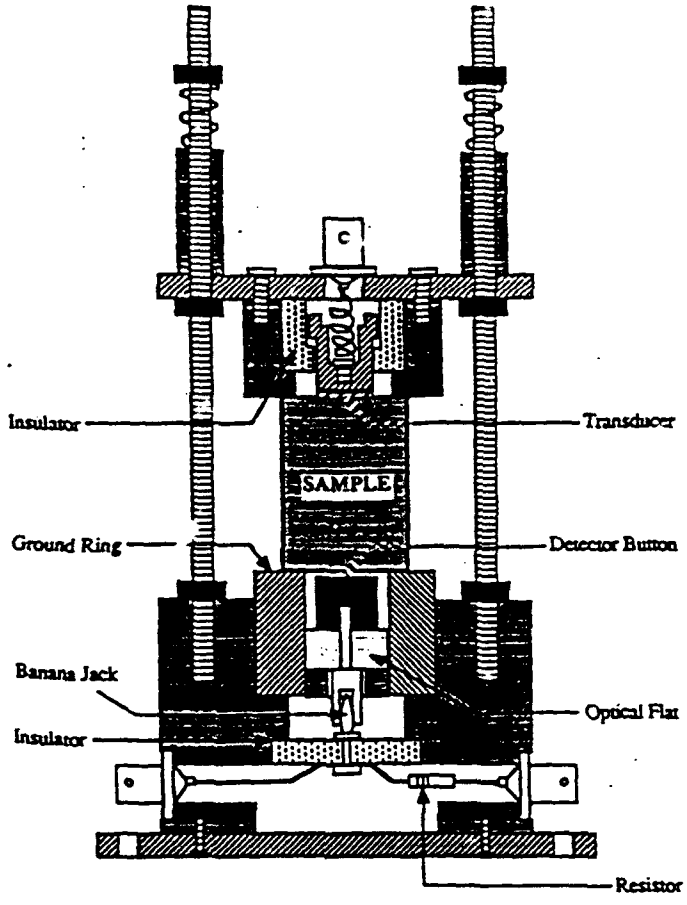

Figure 1. Capacitive detector for measurement at room temperature.

parallel plate capacitor is very sensitive. It allows us to measure amplitudes as small as 10^{-4} Angstroms. The detector is used in the apparatus shown in Fig. 2 for the measurement of fundamental and second harmonic amplitudes.

IV. RESULTS

Measured nonlinearity parameters as a function of temperature are shown in Fig. 3. The temperature dependence is relatively small so one can correlate different crystalline structures and bonding with the magnitudes of the nonlinearity parameters. In most materials the magnitudes of the nonlinearity parameters are between 2 and 15. Table II

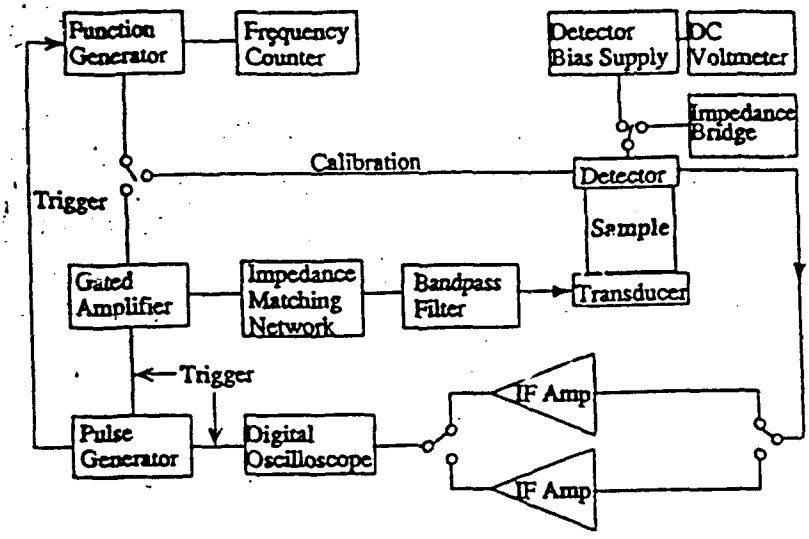

Figure 2. Experimental arrangement for measurement of the nonlinearity parameter.

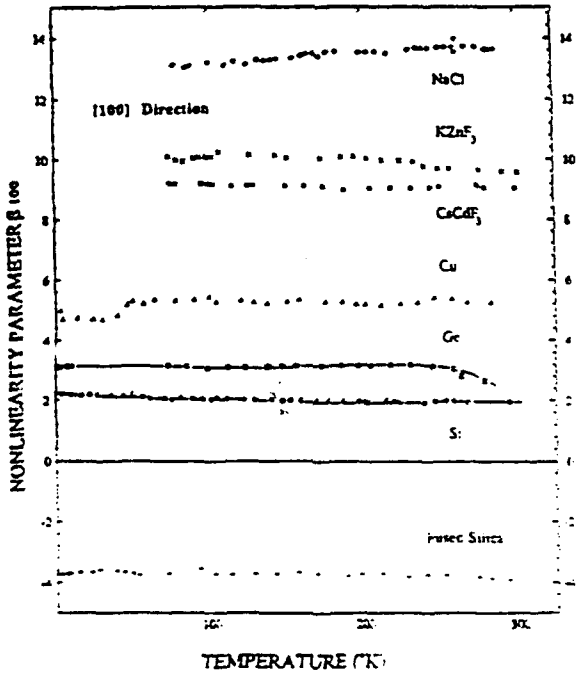

Figure 3. Measured temperature dependence of nonlinearity parameters.

Table II. Comparison of ultrasonic nonlinearity parameters

MATERIAL OR STRUCTURE	BONDING	β_{av}
Zincblend	Covalent	2.2
Fluorite	Ionic	3.8
FCC	Metallic	5.6
FCC (Inert gas)	Van der Waals	6.4
BCC	Metallic	8.2
NaCl	Ionic	14.6
Fused Silica	Isotropic	-3.4
$YBa_2Cu_3O_{7-\delta}$ Ceramic	Isotropic	14.3

gives a correlation between average nonlinearity parameters and crystalline structure. Zincblend, or diamond lattice solids with covalent bonding, have the smallest nonlinearity parameters of about 2, and NaCl with ionic bonding has the largest nonlinearity parameter, 14.6. The difference between nonlinearity parameters is real. Therefore variations of nonlinearity parameter may be correlated with material behavior and ultimately may serve as basis of a nondestructive evaluation technique for these materials, and possibly others such as composites.

A. Correlation of results for diamond lattice solids

In order to test specific results on diamond lattice solids we evaluated nonlinearity parameters of silicon and germanium. From Table I we were able to isolate specific combinations of third order elastic constants. The combinations we could isolate are shown in Figs. 4 and 5. The fact that the temperature behavior of these two diamond lattice solids is similar indicates that our data are meaningful. In addition, we were able to evaluate the behavior of the third order elastic constants of a central forces, nearest-neighbor model. For such crystals $C_{112} + 4\,C_{166} = 5/2\,C_{111}$ and $C_{123} = C_{144} = C_{456} = 0$. Examination of Figs. 4 and 5 reveals that such relationships are approached at absolute zero of temperature for both

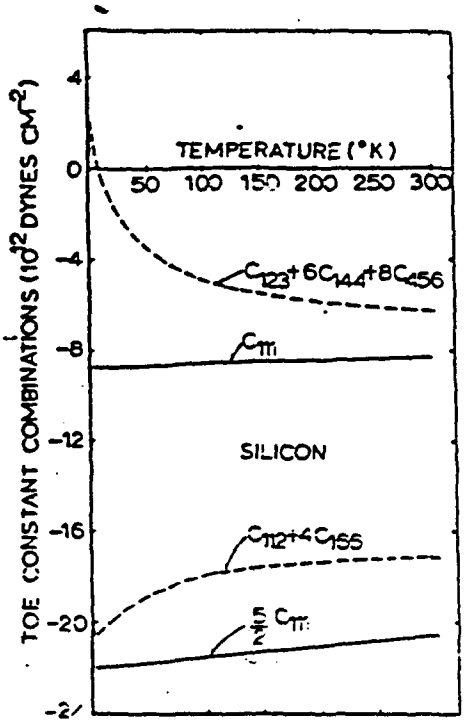

Figure 4. Third order elastic constants of silicon.

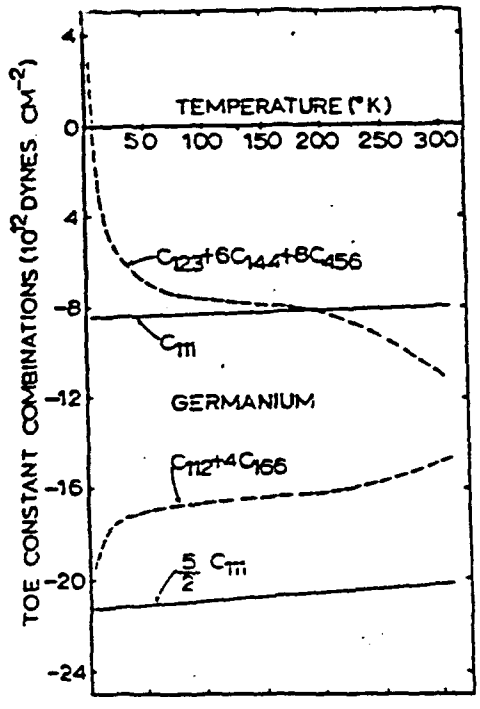

Figure 5. Third order elastic constants of germanium.

silicon and germanium . This is consistent with independent information about the two crystals.

A further test of the validity of the data can be made if all six third order elastic constants can be isolated from the data. We isolated all six third order elastic constants, then used them to calculate the Grüneisen parameter which can be determined independently from thermal expansion data. The comparisons are shown in Figs. 6 and 7. The minimum that shows up in the thermal experiment at approximately 0.1 θ (where θ is the Debye temperature) is reproduced by our data at the proper temperature. Note that our data are better than those of other experimenters in this respect. One can conclude, therefore, that the magnitudes of the nonlinearity parameters can be correlated with real physical behavior of silicon and germanium.

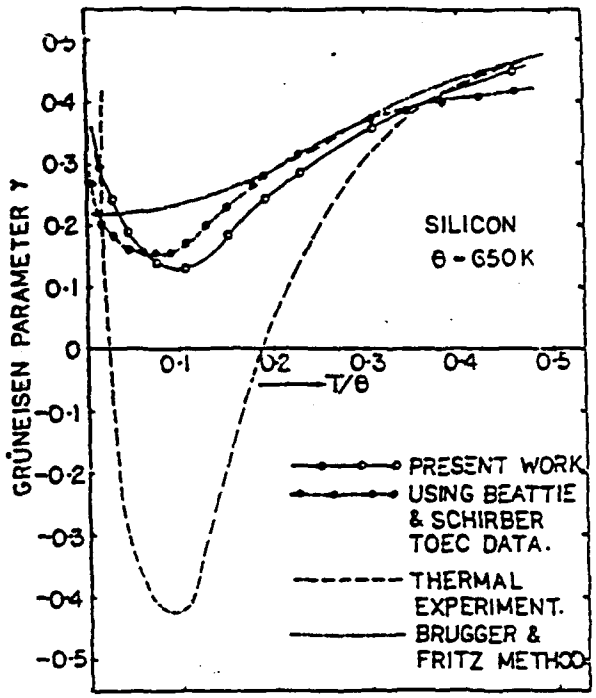

Figure 6. Grüneisen parameter of silicon.

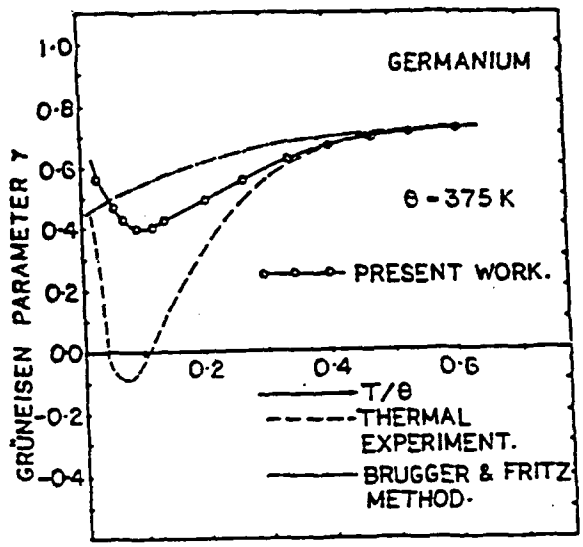

Figure 7. .Grüneisen parameter of germanium.

B. Effect of Material Behavior on Nonlinearity Parameter

The effect of material behavior on measured values of the nonlinearity parameter can be illustrated by recent measurements in PZT. As is well-known near the Curie temperature PZT goes from the room-temperature symmetry (which can be either rhombohedral or tetragonal, depending on the ratio of $PbTiO_3$ to $PbZrO_3$) to cubic symmetry. This atomic rearrangement is somewhat analogous to what happens in metals during work-hardening.

Measured values of the nonlinearity parameters of two samples of PZT are shown in Figures 8 and 9. In Fig. 8 the S1 sample goes from rhombohedral to cubic at the Curie temperature. In this case the nonlinearity parameter goes from $\beta \approx 4$ at room temperature to $\beta \approx 250$ at the Curie temperature. In Fig. 9 the nonlinearity parameter of K1 PZT is shown to go from its room temperature value of $\beta \approx 8$ to $\beta \approx 1500$ at the Curie temperature as the

sample goes from tetragonal to cubic symmetry. Such large variations in the nonlinearity parameter are associated with molecular rearrangements in the materials themselves. Such rearrangements also may take place in Heat damage to composites. This hypothesis suggests that measurement of the nonlinearity parameter of composites might be a very useful experimental program. It could result in a completely new nondestructive evaluation technique. Such a technique would depend on variation in nonlinear properties of composites, information that heretofore has been ignored.

C. Experimental results with composites.

As a preliminary set of experiments we have measured the velocity of ultrasonic waves in graphite epoxy rods. The results are shown in Table III. It is to be noted that the velocity of ultrasonic waves along the fiber direction (axial velocity) is three times the velocity along a perpendicular direction (radial velocity). If one assumes that the hexagonal model is appropriate, then this velocity difference translates into a factor of 10 in the ratio of the elastic constants, since

$$C_{ij} = \rho V^2 \ .$$

Such velocities should be measured with samples that actually are subjected to heat damage. A first test of the value of the hexagonal model of graphite composites would be to determine the result of heat damage on this ratio of velocities.

Table III. Measured ultrasonic velocities and elastic constants of graphite-epoxy composites.

PROPAGATION DIRECTION	COMPRESSIONAL VELOCITY (M/S)	ELASTIC CONSTANT (DYN/CM^2)
AXIAL	8088 89	$C_{33} = (1.074 \pm 0.031) \times 10^{12}$
RADIAL	2535 ± 59	$C_{11} = (0.1046 \pm 0.0056) \times 10^{12}$

$$\rho = 1.627 \pm 0.011 \text{ g / cm}^3$$

D. Nonlinear measurements in composites

Although experimental research is yet to be done on the nonlinear properties of composites, a theoretical basis for it exists. We have calculated the behavior of contributions to the nonlinear behavior of crystals of all symmetries. For hexagonal symmetry we find that the velocity is the same in all directions in the basal plane. In contrast, our calculations show the behavior of the third order elastic constants in the basal plane given in Fig. 10. For the [100] direction the appropriate third order elastic constant is C_{111}. For the [010] direction it is C_{222}. Since in general $C_{222} \neq C_{111}$ for hexagonal symmetry, the six-fold symmetry is in evidence in the nonlinear behavior of a hexagonal crystal even though it may be unobservable in the velocity, a linear phenomenon.

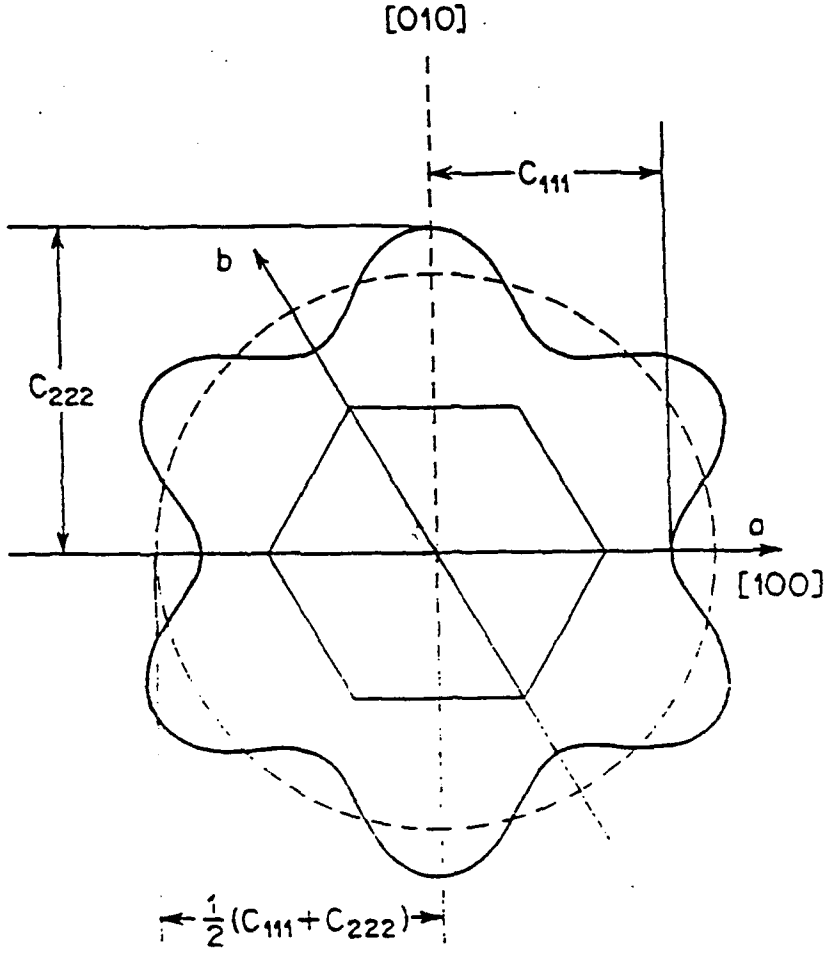

Figure 10. Third order elastic constants in the basal plane of a hexagonal crystal.

V. CONCLUSION

Variations in the nonlinearity parameter already have been correlated with ultimate yield strength of cubic solids, with hardness in steels, with crystalline structure and bonding, and with thermal expansion coefficient. Some experimental results taken in our laboratory are discussed and are shown to indicate that measurement of the nonlinear properties of composites could result in a very sensitive technique for nondestructive evaluation of composites. Such a technique might be sensitive enough to detect heat damage in composites long before it can be detected by other techniques.

VI. REFERENCES

1. S.D. Poisson, J. école polytech. (Paris) 7, 364-370 (1808).
2. F.E. Fox and W.A. Wallace, J. Acoust. Soc. Am. 26, 994 (1954).
3. W. Keck and R.T. Beyer, Physics of Fluids, 3, 346 (1960).
4. M.A. Breazeale, in Review of Progress in Quantitative Nondestructive Evaluation, Vol. II, D.O. Thompson and D.E. Chimenti, eds., Plenum Press, New York (1992), pp. 2015-2023; Jeong K. Na and M.A. Breazeale, in Frontiers of Nonlinear Acoustics: Proceedings of 12th ISNA; M.F. Hamilton and D.T. Blackstock, eds., Elsevier Science Publishers, London, (1990), pp. 571-576; Wenhwa Jiang and M.A. Breazeale, J. Appl. Phys. 68, 5472-5477 (1990); W. Cao, G.R. Barsch, W. Jiang and M.A. Breazeale, Phys. Rev. B 38, 10244-10255 (1988).
5. D. Gerlich and M.A. Breazeale, J. Appl. Phys. 63, 5712-5717 (1988).

VII. ACKNOWLEDGEMENT

Research supported by the Office of Naval Research. The author thanks Paul Elmore for the contents of Table III.

Graduate Fellowships

Principal Investigator: Lawrence A. Crum

Research Accomplished in 1992:

The National Center for Physical Acoustics is an integral part of the University of Mississippi, which as a strong reputation for its graduate programs in physics, mathematics, and engineering. Recruiting qualified US students into a Ph.D. program with research emphasis in acoustics is a high priority for NCPA. The NCPA fellowship program was developed with the hope that outstanding undergraduates would be identified and attracted to the University for specialized training in acoustics at NCPA. By offering these young scientists hands-on experience in this discipline, they would upon graduation be capable of filling positions in Navy Laboratories and/or facilities that conduct work relevant to acoustics.

In FY 91 and 92, NCPA received funds from the Office of Naval Research to administer a graduate fellowship program in acoustics. A limited number of applicants were awarded fellowships because of the high criteria we set for admission to this program and due to the limited number of available awards. The criteria for admission were revised further in 1993. We believe that this program has given more visibility to acoustics as a specialization in physics, and that visibility is in the best interests of the Navy.

Six NCPA Fellows were supported by these funds in the past year. These were:

Adam Calabrese. Mr. Calabrese is continuing his work in transient microcavitation under the direction of Professor Crum at the University of Washington. He remains a student in the University of Mississippi graduate program. Mr. Calabrese expects to graduate in 1993.

Paul Elmore. Mr. Elmore's Ph.D. research involves studies of nonlinearities in crystal structures. His research is directed by Dr. Mack Breazeale. Mr. Elmore successfully completed the comprehensive examinations in the fall of 1992 and expects to graduate in December 1994.

Jay Lightfoot. As a freshman graduate student, Mr. Lightfoot performed extraordinarily well in freshman graduate courses in physics. His research in the area of active noise control was directed by Dr. Shields from January through July. Mr. Lightfoot changes research areas in August 1992. He is now performing research in the general are of thermoacoustics under the guidance of Dr. Henry Bass and Dr. Richard Raspet. Mr. Lightfoot will take the comprehensive exams in the fall of 1993.

Keith Olree. Mr. Olree has also proven to be an outstanding graduate student. He is also doing research in active noise control under the direction of Dr. Shields and will take the comprehensive exams next fall.

Daniel Warren. Mr. Warren has successfully passed the comprehensive examination and has defended his

Distribution List

Dr Logan E Hargrove
Office of Naval Research
Physics Division ONR 312
800 North Quincy Street
Arlington VA 22217-5660

Defense Technical Information Center
Building 5 Cameron Station
Alexandria VA 22314

Administrative Grants Officer
Office of naval Research
Resident Representative N00014-92-J-1563
Administrative Contracting Officer

Naval Research Laboratory
Technical Library Code 5226
4555 Overlook Avenue SW
Washington DC 20375-5320

Professor W Patrick Arnott
Atmospheric Sciences Center
Desert Research Institute
P O Box 60220
Reno NV 89506

Professor Anthony A Atchley
Department of Physics
Code PH/AY
Naval Postgraduate School
Monterey CA 94943-5000

Professor Yves H Berthelot
School of Mechanical Engineering
Georgia Institute of Technology
Atlanta GA 30332

Professor David T Blackstock
Applied Research Laboratories
The University of Texas at Austin
P O Box 8029
Austin TX 78713-8029

Professor Andrea Prosperetti
Department of Mechanical Engineering
Johns Hopkins University
Baltimore MD 21218

Professor Steven L Garrett
Department of Physics
Code PH/GX
Naval Postgraduate School
Monterey CA 94943-5000

Professor Mark F Hamilton
Department of Mechanical Engineering
University of Texas at Austin
Austin TX 78712-1063

Professor Thomas J Hofler
Department of Physics
Code PH/HF
Naval Postgraduate School
Monterey CA 93943-5000

Professor Robert M Keolian
Department of Physics
Code PH/KN
Naval Postgraduate School
Monterey CA 93943-5000

Professor Andres Larraza
Department of Physics
Code PH/LA
Naval Postgraduate School
Monterey CA 94943-5000

Professor Moises Levy
Department of Physics
University of Wisconsin at Milwaukee
Milwaukee WI 53201

Professor Walter G Mayer
Department of Physics
Georgetown University
Washington DC 20057

Professor Julian D Maynard
Department of Physics
Pennsylvania State University
University Park PA 16802

Professor Wolfgang H Sachse
Theoretical and Applied Mechanics
Cornell University
Ithaca NY 14853-1503